Development of a Microfluidic Based Portable Analyzer for Continuous Monitoring of Glutamate and other Amino Acid Neurotransmitters

By

Nathan J. Oborny

B.S., Computer Engineering, University of Kansas, 2002

B.S., Genetics, University of Kansas, 2010

Submitted to the graduate degree program in Bioengineering and the Graduate Faculty of the University of Kansas in partial fulfillment of the requirements for the degree of Doctor of Philosophy.

_____

Chairperson: Dr. Susan Lunte

_____

Dr. Prajna Dhar

_____

Dr. Lisa Friis

_____

Dr. Karen Nordheden

_____

Dr. Yong Zeng

Dissertation Defense: October 10, 2017

Date Defended: October 10th, 2017

The Dissertation Committee for Nathan J. Oborny certifies that this is the approved version of the following dissertation:

Development of a Microfluidic Based Portable Analyzer for Continuous Monitoring of Glutamate and other Amino Acid Neurotransmitters

Chairperson: Dr. Susan Lunte_____

Date approved:_____

Abstract

The amino acid glutamate (Glu) is one of the most ubiquitous neurotransmitters in the brain and the chief excitatory neurotransmitter. As a neurotransmitter, Glu is integral to the normal workings of the brain and is involved in many functions, such as memory formation and long-term potentiation, via action on multiple receptors. Two primary classes of Glu receptors, metabotropic and ionotropic respond to the concentration of Glu in the extracellular space of the brain in a dose dependent manner. Large excesses of Glu have been shown to produce an excitotoxic effect, which can lead to the long-term neuronal damage seen in many neurological disorders including stroke and traumatic brain injury (TBI). Following an event such as these, methods for continuous monitoring of Glu concentrations in the brain can be very useful to clinicians for determining the best timing for pharmacological intervention, provided the acquisition of that information can itself be performed in a timely manner. With that in mind, this thesis focuses on the development of analytical methods that will provide information on the extracellular concentration of glutamate and other amino acids in a timely manner and thereby providing actionable information for a clinician.

Microdialysis (MD) is an *in vivo* sampling method that can be used to monitor multiple analytes simultaneously while also enabling the delivery of a pharmaceutical intervention directly to the site of the probe This technique can provide a powerful window into tissue function and health when combined with a separation-based analytical method. However, due to the need for very low flow rates, a trade off exists with regard to sample concentration and time. In order to maximize the concentration and minimize the time required, sensitive methods of detection must be used such as laser induced fluorescence (LIF) detection.

To minimize the time required for sample analysis (and make point of care analysis possible), a portable fluorescence detection system for use with microchip electrophoresis was developed. With this system, six neuroactive amines commonly found in brain dialysate (arginine, citrulline, taurine, histamine, glutamate, and aspartate) were derivatized offline with naphthalene-2,3-dicarboxaldehyde/cyanide, separated electrophoretic ally, and detected by fluorescence. It was found that this system was able to detect these analytes of interest within a range of 250 nM – 1.3 μM, which was adequate for subsequent detection in a microdialysis sample collected from the brain of an anesthetized rat.

Finally, the design and evaluation of a microfluidic device for coupling microdialysis to microchip electrophoresis with on-line derivatization (MD-ME) is discussed. By coupling sampling directly to the microchip, elements that would otherwise delay analysis such as the need to transport volumes to the analysis system or the wait for the generation of larger sample volumes can be avoided. The MD-ME device was modeled first using COMSOL Multiphysics™ in an effort to optimize the device geometry, allowing on-line sampling with minimal back pressure, but with complete sample derivatization prior to analysis. Following this, the device was evaluated experimentally to detect Glu samples collected via microdialysis over an extended time period. While the limits of detection for Glu were found to be slightly high for immediate use for *in vivo* brain sampling, it is hoped that modifications to materials used to construct the microchip may eliminate this problem.

Acknowledgements:

I have been extremely fortunate in my graduate career, and in life generally, to be surrounded by great people that have helped me along the way and I would like to thank you all here.

First and foremost, among those is my advisor and mentor, Dr. Susan Lunte. Like many members of the Lunte group, past and present, I feel extremely lucky to have joined Sue's lab. Over the years, she has given me guidance when I needed it and allowed me to search for the answer on my own when that was best. She's been there with a reassuring word when I haven't had any useful data for weeks (or even months) and could see the stress was getting to me, while understanding that sometimes some added pressure was what I needed to break through whatever the problem was. She's also made certain that I had every opportunity possible to further my grad career. Those opportunities have included attending multiple conferences, two of which were in South America. As a result of the efforts she makes to introduce her students to all of her academic and industry contacts, I've felt embedded in a network of excellent scientists across the world and have what may be the perfect job waiting for me.

I will also always look back fondly on the lab events the Lunte Lab(s) held every year. In particular, the BBQs in the summer and the Christmas parties with Craig's hilarious version of a white elephant exchange. He is missed.

I also want to thank my lab mates. In particular, I want to thank Dr. Rachel Saylor and Dr. Jessica Creamer. Rachel was always there to act as a sounding board for an idea or to help me find a way out of a problem. Despite the difficulties in her own project, she was always ready to help. Jess taught me how to run a CE, how to diagnose pressure leaks and current spikes and how to coordinate with other labs on campus. She also helped me to think about my project in a larger sense and I look forward to working with her again in my post-doc. Both of you taught me more than you know. Other lab mates, past and present, were of course instrumental in my development as a scientist. In particular I want to thank Dr. Tom Linz and Dr. David Scott. Tom, I listened to you give hour long presentations in group meetings every few weeks. At the time, they were exhausting. However, I learned a lot in those hours. For that, and for teaching me how to run microchips, thank you. Dave, thanks for taking it upon yourself to teach me how to make chips in the cleanroom. To Dr. Abdullah Al-Hossaini, thanks for being a sounding board for crazy ideas. To Shamal and Manjula, thanks for being constantly helpful, even when you were busy. To Amanda, thank you for all your help with the rats. And to everyone else, Kelci, Joe, Mike, Dhanushka, Anne, Richard, Simon, Amanda, Ryan, Nhan, Emily, Dulan, Giuseppe, Claudia and all the others, thanks. You've all made an impact. To Cady Bush, thank you for you your tireless work keeping everything running behind the scenes!

To Galina and Vince, the two group members I was lucky enough to mentor. They say you don't actually know anything until you can teach it and until the two of you I hadn't put that to the test. Mentoring you both has really helped me. I hope you've learned a lot from me and, having spent many hours working with you, I know that you'll both be great scientists.

Outside of school I've also been very fortunate to have great friends and family supporting me. To all of you that helped keep me sane, thank you. To my parents and brothers, you've supported my going back to school and changing careers, and continued to be supportive even as it became evident just what that entailed. Mom and Dad, I couldn't have gotten to this point in my life without your guidance and support. To everyone else I haven't mentioned directly by name, thank you.

Finally, to Rachel (and Pete), you've been with me every step of the way from the undergrad classes to this final step. You were by my side when things didn't work for months and you were there when I finally had reasonable data. You stuck around when I worked repeated weekends for months at a time, you made sure that I still had a social life and forced me out of the house knowing that ultimately it was what I needed, not more work. I know this was a lot to put you through, thank you for putting up with me during it. I love you and I can't wait for the next phase of our lives to begin!

Table of Contents

List of Figures

List of Tables

List of Equations

1. Dissertation Overview

This thesis, throughout the following chapters, represents an iterative process of design and experimentation. This process evolved from the rationale for monitoring glutamate (Glu) as a biomarker of traumatic brain injury (TBI) and neurodegeneration, an explanation of how *in vivo* measurements of Glu are acquired, through the construction of microchip electrophoresis devices, the development and evaluation of a portable detection system, and finally the development of an online system for monitoring Glu levels in near real time.

In chapter two, I discuss the role of Glu as an excitatory amino acid neurotransmitter. Glu is ubiquitous throughout the brain and is required for many vital functions playing a role in virtually all *excitatory* events such intercell signaling, memory formation and learning. Three major types of glutamate receptors involved in ion transport exist in the brain: AMPA, NMDA, and Kainate. Each of these has a specific function which are discussed in chapter 2. In addition, several metabotropic receptors are mentioned that control the intracellular environment through the activation of G-protein coupled receptors, that in turn control pathways within the cell. The overall function of glutamate-glutamine cycle is also discussed as well as how this system operates to maintain homeostasis in the brain. Particular attention is paid to the maintenance of intracellular Ca^{2+} in neurons. Finally, because Glu plays such an important role in the development of secondary damage following TBI, the consequences of the breakdown of this system is discussed.

Monitoring Glu in the living brain under the conditions of TBI can be challenging. A common method, and the method of choice for the studies covered here, is microdialysis sampling.

Microdialysis has many advantages over other sampling techniques. These are elaborated in chapter two and include the ability to sample multiple analytes simultaneously and to do so continuously for an extended period of time.

In chapter three, the use of the electrophoresis for the analysis of biological samples is discussed and how this technique can be used with microdialysis sampling. Two methods in particular, capillary electrophoresis (CE) and microchip electrophoresis (ME), are elaborated, focusing primarily on ME. These methods are uniquely suited for the analysis of complex biological samples such as brain dialysate samples containing Glu as well as other amino acids. They are compatible with limited sample volumes and a requirement of high temporal resolution with low overall time lag. The basis for analyte separations via electrophoresis is discussed. Because the detection of analytes, of opposite as well as neutral charges, simultaneously relies on the generation of an electroosmotic flow (EOF) at the surface of the separation channel, the nature of the EOF is discussed as well as its dependency on material choice. The ability of CE to analyze exceedingly small sample volumes (on the order of 100nL) was very important to this work and this chapter presents a rationale specifically for the use of microchip electrophoresis as the ideal method of analysis for these ultralow volumes of complex samples especially when time constraints are of the essence and multiple analytes are of interest. The advantages of CE based analyses in comparison to other approaches, such biosensors and liquid chromatography, is discussed. The manipulation of such low volumes (on the order of 100nL) can be problematic however and the use of electrokinetic gating for sample injection methods with electrophoretic techniques is discussed.

Finally, ME is introduced beginning with the similarities to capillary electrophoresis and the differences that are beneficial to this application. Methods for detection that can be combined with ME, the materials and methods used in chip construction, and modeling approaches to streamline ME design are also covered. Fabrication processes used for the construction of three different types of microchip electrophoresis (ME) devices is elaborated including devices made entirely from poly-dimethylsiloxane (PDMS) polymer, all glass substrates, and hybrid devices made with both.

Two issues with the use of ME for monitoring TBI are the need for a fluidic connection from the microdialysis probe implanted in the patient's brain to the ME assay that can simultaneously sample and derivatize a sample, addressed in chapter five, and the need to minimize lag time between sample acquisition and analysis by placing the detection system as near the patient as possible. This later concern was the subject of chapter four. The portable detection system discussed in chapter 4 consisted of a light emitting diode (LED), a photodiode based detector, and an inexpensive custom amplifier based on an Arduino microcontroller. Focusing of the excitation light and subsequent collection of the emitted light was performed using an inverted optical arrangement consisting of a dichroic beam splitter, which directed collimated excitation light to the detection point through an objective lens while allowing emission light to be focused on a photodiode. This light was converted into an electrical signal, amplified and then filtered, before being further processed by the microcontroller and connected laptop. As noted in chapter 4, the portable system was shown to be adequate for the detection of a series of clinically relevant bioactive amines in brain dialysate samples including those of primary interest for this work, Glu and aspartate (Asp).

Finally, in chapter five, a microfluidic device is described that allows an online dialysate sample collected from an *in vivo* model and to be continuously monitored using microchip electrophoresis with fluorescence detection. This device was modeled using Comsol Multiphysics and then evaluated experimentally. This demonstrated that continuous sampling via microdialysis at 1uL per minute was possible for extended periods and with minimal time lag.

As with all research, the work presented here has opened many unexplored avenues and presented unresolved problems. Therefore, in the final chapter, near and long-term directions for future researchers to pursue are presented.

2. Introduction to Glutamate Pharmacology and Microdialysis Sampling

Modified, with permission from the book chapter:

"Separation-based Sensors using Microchip Electrophoresis with Microdialysis for Monitoring Glutamate and Other Bioactive Amines" published in "Biochemical Approaches for Glutamatergic Neurotransmission" [1]

Nathan Oborny[1,3,4], Michael Hogard[2,3,4], and Susan Lunte[1,2,3,4]

Department of Bioengineering

Department of Chemistry

Department of Pharmaceutical Chemistry

Ralph N. Adams Institute for Bioanalytical Chemistry

University of Kansas, Lawrence, KS

2.1 Glutamate as a Neurotransmitter

Glutamate (Glu) is among the most abundant amino acids in the human body making up both a largest percentage of the amino acids we ingest [2] as well as a large portion of other amino acids produced via the citric acid cycle (TCA). It is also the most ubiquitous neurotransmitter in the mammalian brain [3] and is critical to the normal function of the brain and is present in virtually every sub region. Despite the fact that Glu is ubiquitous in the brain, for many years it was thought that its only role was as a component of the TCA cycle. During the last quarter century however, it has become clear that this viewpoint was incorrect. It has been shown that Glu is be found throughout the brain, is a signaling molecule for many important processes, and is controlled by a complex array of receptors, transporters, and control mechanisms [4, 5]. Not surprisingly, the disruption of these control mechanisms is a common thread underlying many neurological diseases including epilepsy, psychosis, Huntington's, Parkinson's, and the secondary effects of stroke and traumatic brain injury (TBI) [2, 6].

2.1.1 Normal Glutamatergic Function

Almost all of the neurotransmitter functions of Glu in the brain are excitatory in nature, including such important functions as memory formation and neural plasticity. Because Glu's important role in these functions it is not surprising that, while Glu is found in all regions of the brain, local concentrations and receptors for Glu are at their highest concentration in regions that specialize in memory formation such as the hippocampus, stress responses such as the amygdala, and higher-level thought such as the cerebrum. Glu is released by neurons into the synapse in response to an action potential. When Glu concentrations in the synapse spike as a result of this release, receptors sensitive to Glu in nearby post synaptic neurons are triggered. If this triggering event is of sufficient intensity, that neuron will, in turn, undergo an action potential. Briefly, an action potential is the passage of an electrical impulse along the membrane of a neuron. As this impulse occurs, ionic gradients along the cell are rapidly altered in succession down the cell body. As this happens, the impulse can travel the length of the neuron until reaching another synapse where it results in the release of Glu. If sufficient Glu is released, the action potential begins anew in the neuron on the opposite side of the synapse.

Once an action potential has occurred, the remaining Glu at the initial synapse must be quickly removed from the synaptic cleft. In contrast to other neurotransmitters there is no enzyme that degrades Glu in the extracellular space. Therefore its concentration is entirely determined via uptake and release [3]. This process is accomplished via transporters that are present on both the pre and post synaptic neurons, as well as on the nearby specialized glial cells called astrocytes.

Uptake via these transporters returns the synaptic concentration to be baseline level, leaving the neuron ready to fire once again.

2.1.2 Synthesis, Release and Uptake of Glu

The synthesis, release, and uptake of Glu in the brain occur in a biochemical pathway referred to as the Glutamine-Glutamate cycle. This cycle is not completely closed to outside sources of Glu (that from dietary sources for instance), however, because Glu cannot cross the blood brain barrier without active transport, the vast majority of Glu is synthesized within the neurons themselves [7].

In the neurons, Glu is initially synthesized from α-ketoglutarate, which itself is synthesized from pyruvate as a component of the TCA cycle. Pyruvate is in turn synthesized during the glycolysis of glucose. Studies of brain metabolism have shown that virtually all the glucose entering the brain is ultimately converted to Glu [4]. In addition, glutamine (Gln) within the neuron can be converted to Glu via the enzyme glutaminase. As is explained in the following paragraphs, the majority of Glu is removed from the extracellular space and recycled in this manner.

Glu is transported via vesicular glutamate transporters and stored in vesicles within the presynaptic neuron. The release of Glu from these vesicles into the synapse occurs in a Ca^{2+} dependent manner as the neuron depolarizes in response to an action potential and Ca^{2+} levels rise.

Upon release of the Glu from the presynaptic neuron into the synaptic cleft Glu can diffuse to several possible destinations, including receptors on the post synaptic neuron. Additionally, to maintain low extracellular concentrations of Glu in the synapse, additional transporters on neighboring cells remove the remaining Glu from the synapse. Three glutamate transporters are found throughout the mammalian brain, with two additional transporters being localized to certain regions. The three major transporters are referred to as the *excitatory amino acid transporters* (EAAT 1-5). EAAT1 and EAAT2 are primarily expressed in astrocytes located near the synaptic cleft. EAAT3 is expressed in the neuron itself, and EAAT4 and EAAT5 are found in purkingje neurons and the retinal neurons respectively [4, 6]. The relative positions of these transporters can be seen in Figure 2.2. The EAAT transporters are arrayed around the synapse in such a way as to prevent synaptic Glu from leaking into the extra-synaptic space. This is an important detail with regard to Glu levels during pathological events [8].

When Glu is removed from the extracellular space via the EAAT's, it is taken up into the neuron is resequestered into vesicles. The remaining Glu is removed via uptake through EAAT1 or EAAT2 and passes into the cytosol of neighboring astrocytes. Here, Glu is converted to Gln via the enzyme glutamine synthase. The process from uptake to synthesis is an energetically costly one. A sodium (Na^+) gradient in the astrocytes is exploited to uptake Glu into the cell. For each molecule of Glu that is transported into the cell, three Na^+ ions and one hydrogen ion (H^+) are co-transported in exchange for potassium (K^+) ions. It is important following this process to reestablish the Na^+ and H^+ gradient across the cell membrane. Both the reestablishment of this gradient and the synthesis of Gln from Glu require energy in the form of adenosine triphosphate (ATP). For each molecule of Glu converted to Gln via glutamine synthase, a single ATP is used.

Within the astrocyte, this ATP is produced via the glycolysis of glucose into lactate resulting in two molecules of ATP from the recycling of two molecules of adenosine diphosphate (ADP). One of these ATP's is used in the conversion of Glu to Gln, the other is used to expel three Na^+ in exchange for two K^+ [9].

The conversion of glucose into lactate also has the added benefit of providing the nearby neuron with a molecule of lactate to use in the TCA cycle, producing an additional 34 ATP molecules. Finally, the Gln is transported into the neuron where a mitochondrial specific enzyme, glutaminase converts the Gln to Glu. The Glu is then packaged into vesicles for future release into the synapse [4]. This process is shown in Figure 2.1.

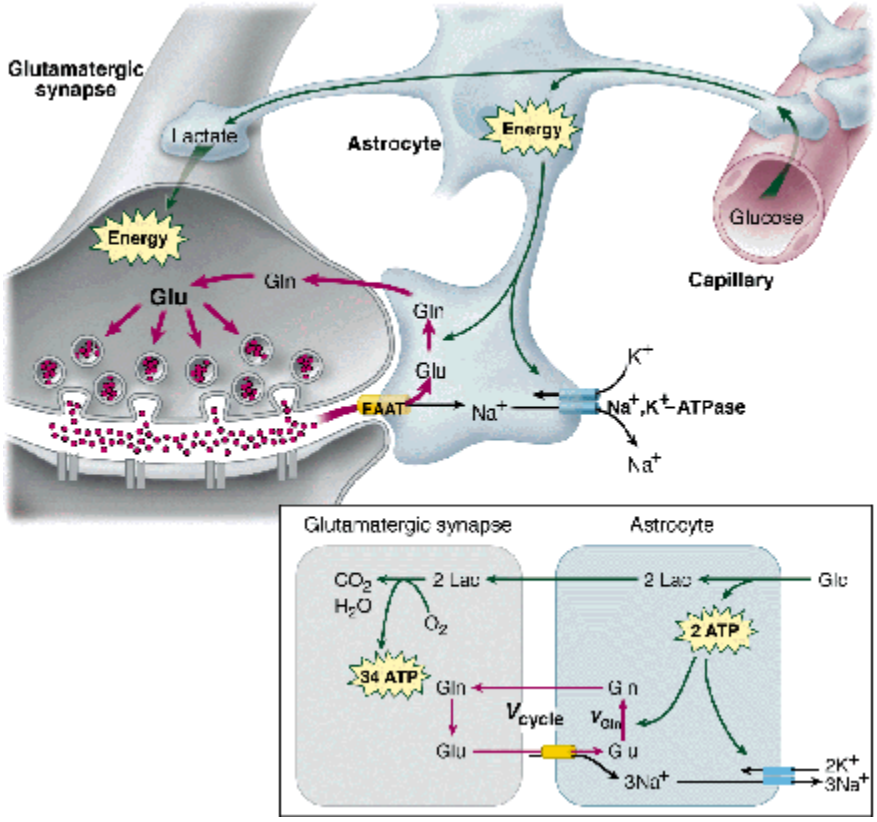

Figure 2.1: The release of Glu from the neuron into the synaptic cleft results in postsynaptic activation of Glu receptors as well as the activation of nearby transporters on astrocytes (glial cells). These transporters remove Glu into the astrocyte body where it is converted to Gln before transport back to the neuron where conversion in the opposite direction occurs. Each conversion step requires ATP (inset). Reproduced with permission from[9]

2.1.3 Glutamate Receptors

Multiple receptors are activated by Glu at the postsynaptic neuron. Among these are three ligand activated ion channels that are named for ligands known to bind them specifically, and multiple metabotropic Glu receptors (mGluR). Among this later group, the mGluR receptors, are -coupled receptors effecting intracellular metabolic processes. This broad generalization of function however is somewhat misleading as the processes influenced by these receptors, of which three families and many subtypes exist, vary widely in function from control of protein phosphorylation to regulation of synaptic transmission [7]. Although extremely important, this thesis focuses on the second class of Glu receptors, those controlling ion channels.

The ligand gated ion channels to which Glu is an agonist include α-amino-3-hydroxy-5-methylisoxazole-4-proionic acid (AMPA), Kainate, and N-methyl-D-aspartic acid (NMDA). As with the mGluR receptors, several subclasses of these receptors (iGluRs) exist with varying local distributions throughout the brain. Each receptor type consists of multiple subunits conferring slightly different behaviors, such as the enhancement or attenuation of their respective reaction kinetics [2]. AMPA, for instance, consists of 4 subunits (GluR1-4); Kainate of 5 subunits (GluR5-7 as well as KA1 and KA2); and NMDA of 7 subunits (NR1, NR2A-D, and NR3A-B) [10]. While the precise function of each of these subunits is beyond the scope of this thesis, what is common to all iGluRs is the fact that, once triggered by Glu, these receptors respond in an extremely rapid manner, becoming permeable to specific ions including to Na^{+}, K^{+}, and Ca^{2+} [10].

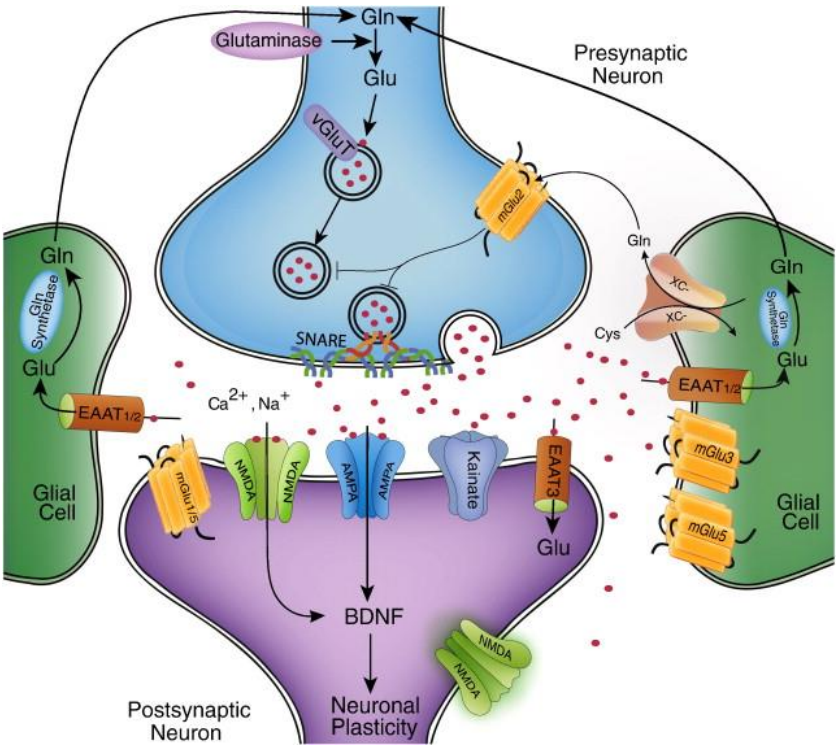

Figure 2.2: Glu is packaged into vesicles in the pre-synaptic neuron. Upon release into the synapse, Glu activates a variety of receptors on the post-synaptic neuron including metabotropic receptors (mGlu1/3) and ionotropic receptors (NMDA, AMPA and Kainate). The removal of Glu from the synapse by transporters into the neuron (EAAT3) and nearby astrocytes (glial cells) maintains tight control over Glu concentrations following stimulation. Finally, Glu is converted to Gln for transport back to the neuron from the astrocyte (glial cell). Reproduced with permission from.[4]

2.1.4 Non-NMDA Receptors: AMPA and Kainate

The three types of iGluRs are commonly separated into the Non-NMDA receptors and the NMDA receptor indicating the importance of the NMDA receptor physiologically as well as pathologically. Recent evidence however has shown that the AMPA receptor plays a significant role in initiating neural plasticity and the long-term potentiation (LTP) needed for memory formation. Additionally, while less is known about the function of the Kainate receptor, it too appears to play a significant moderating effect on neuronal function.

AMPA receptors (AMPAR) are ubiquitous throughout the brain and are the primary receptors involved in fast synaptic signaling [11]. AMPAR, as mentioned, consist of assemblies of heterodimer subunits GluA1-A4. The AMPAR, once formed, is a transmembrane receptor with 4 ligand binding sites, specific for Glu. These binding sites show extremely fast reaction kinetics, responding to a spike in synaptic Glu concentrations in < 1ms. The opening of the AMPAR occurs when 2 of the binding sites are occupied, with the channel opening further as the remaining binding sites are occupied [12]. What the open receptor channel allows into the cell, however, depends on the subunit composition of the AMPAR. For AMPAR lacking the GluA2 subunit, an open channel will allow Na^+, K^+, and Ca^{2+} into the cytoplasm of the cell. However, if the GluA2 subunit is present, as is the case for the majority of AMPAR, Ca^{2+} will be prevented from entering the cell. Whether GluA2 is present or not, AMPAR once saturated will quickly become desensitized within 4-8 ms after activation, resulting in a closing of the ion channel [13]. The effect of this 1-8 ms influx of positive ions on the neuron is significant, particularly with respect to the function of the NMDA receptor, covered in the next section.

Less is known regarding the function of Kainate receptors (KARs), as compared with the other two iGluRs. Like the APMA and NMDA, KARs consist of subunits that can be assembled to result in specific responses to Glu binding. However, KARs appear to have both a pre and post synaptic function in regulating neuronal excitability. KARs exhibit reaction kinetics slower than AMPARs and a permeability primarily to Ca^{2+} ions. KARs appear to play an important role in neuropsychiatric disorders. However, research into the precise function of these receptors is ongoing [14].

Both AMPARs and KARs are active components of the excitatory response to Glu within the mammalian brain and each appears to play a role in both the normal functioning of the system as well in related chronic disease states. However, more acute disease states, such stroke or traumatic brain injury, tend to directly involve the third iGluR, the NMDA receptor.

2.1.5 The NMDA Receptor

The NMDA receptor (NMDAR), as mentioned above, is a ligand gated iGluR, like the AMPA and Kainate receptors. Similar to those receptors, NMDAR consists of multiple subunits, each conveying specific functions. Unlike AMPA and Kainate receptors however, NMDARs possess sites to bind multiple different ligands, as well as a binding site for Mg^{2+} that is blocked by default, providing a much higher level of regulation than for any other GluR. No fewer than 6 binding sites exist on NMDARs. These include binding sites for polyamines and cations, such as zinc (Zn^{2+}), Mg^{2+} and H^{+}. The polyamines include spermidine. Zn^{2+} and H^{+} have modulating effects on the permeability of NMDARs to Na^{+} or Ca^{2+}. In contrast, Mg^{2+} acts as a channel blocker, rendering the NMDAR impermeable to ion flow by default [4].

The two remaining binding sites, those for Glu (on the NR2 subunit) and glycine (Gly) (NR1 subunit) are obligatory. The NMDAR will remain impermeable to ion flow until these sites are occupied. Although their affinity for Glu and Gly is very high, other substrates including D/L-Aspartate (Asp) (although not D-Glu) can serve as a replacement for Glu ,as can D-Serine (D-Ser) for Gly [4]. The structure of the NMDAR can be seen in Figure 2.3

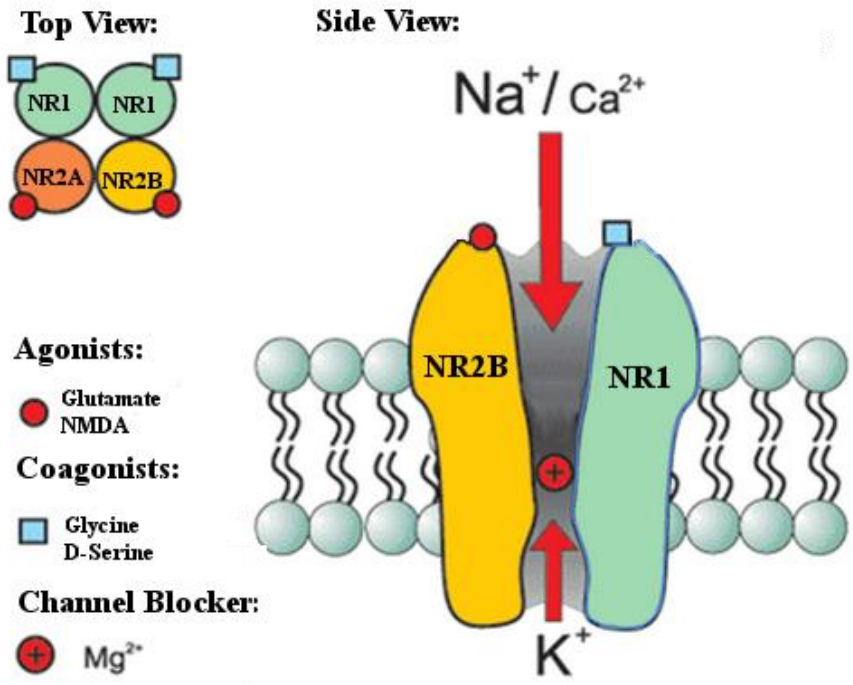

Figure 2.3: The NMDA receptor consists of multiple subunits including NR1, NR2A and NR2B each of which have specific functions. To open the NMDA ion channel, Glu must bind the NR2A or B subunit while a co-agonist such as Gly binds the NR1 subunit. Additionally, the Mg^{2+} channel block must be removed before ions can pass through the channel.

Because NMDARs are blocked by default, before activation a series of events must take place. When it is released into the extracellular space, molecules of Glu bind NMDARs as well as AMPARs and KARs. At this point, the AMPAR and KAR are activated. However, the NMDAR remains inactive until both the Mg^{2+} ion has been dislodged and Gly has bound as a co-agonist. The removal of the Mg^{2+} block is accomplished through the activation of nearby AMPARs, which having faster kinetics than NMDARs, rapidly respond to the increased Glu concentration, becoming permeable to ion transport. As these ions (Na^+ and K^+) enter the cytoplasm, the voltage dependent block of Mg^{2+} is weakened, allowing its removal, and opening the NMDAR.

This relationship between fast acting AMPARs and the slower responding NMDAR is the origin of the long term potentiation that is necessary for memory formation and neural plasticity [15]. Once the NMDAR is activated, Na^+ and Ca^{2+} enter the cell. This process continues until, like AMPARs, NMDARs become desensitized to the Glu through a Ca^{2+} dependent feedback as one of the subunits (NR1) is deactivated [16, 17].

2.1.6 Calcium and the Neuron

As Ca^{2+} enters the neuron, it's effects vary widely. Changes in Ca^{2+} concentrations are one of the most common cell signaling mechanisms. The use of Ca^{2+} as a signal can be found in virtually all cell types. Consequently, the cytoplasmic concentration of Ca^{2+} is under tight control and kept to a concentration of approximately 100 nM depending on the cell type [18]. This internal concentration is maintained in the presence of extracellular concentrations that can range from 1-2.5 mM. The maintenance of this concentration gradient is accomplished via Ca^{2+} dependent ATPases.

Within the cell, Ca^{2+} is stored primarily within the endoplasmic reticulum (ER) where it is bound to the storage protein calsequestrin (CSQ), each of which can bind 50 Ca^{2+} ions. In addition to what is storied in the ER, Ca^{2+} plays a vital role in the electron transport chain used during the production of ATP in the mitochondria. Enumerating the many functions of Ca^{2+} in neurons, much less each cell type, is beyond the scope of this thesis. However, three broad functions within neurons require mention. The first is that within the neuron, signaling is initiated via the release of Ca^{2+} from the ER, which extends virtually the entire length of the neuron body. This release can

modify the excitability of the neuron, altering its ability to respond to an action potential [19]. Secondly, uniporters allow the passage of Ca^{2+} into the mitochondria where they are involved in the production of ATP. Specifically, as Ca^{2+} enters the mitochondria, it allows the exclusion of H^{+} ions, having the net effect of increasing ATP synthesis [20]. Lastly, at high concentrations Ca^{2+} begins to have more deleterious effects. These effects result from a poisoning of the mitochondria due to the production of reactive oxygen species (ROS) that can lead to lipid peroxidation. This in turn can cause the activation of phospholipases, proteases, and pathways responsible for cellular apoptosis [2, 21, 22].

2.1.7 Summary of Glu Signaling Pathways

In summary, the release of Glu from the presynaptic neuron into the synaptic cleft produces a momentary spike in Glu concentration. A variety of nearby transporters and receptors immediately respond to the presence of this signal. AMPAR and KARs react rapidly to Glu by becoming permeable to ions. Metabotropic receptors are triggered, modifying the action of complex pathways within the cell. While these signals are being transmitted into the postsynaptic neuron, transporters located on nearby astrocytes have already begun the removal of the Glu from the synaptic cleft using the Na^{+} gradient to aid in transport. Once inside the astrocyte, that Glu is converted to Gln (via glutamine synthase) and the Na+ gradient is reestablished, both via glycolysis of a glucose molecule. The resulting lactate and Gln are transported back to the neuron where the subsequent respiration of the lactate molecule is used to produce enough ATP for normal cell function as well as the conversion of Gln, back to Glu (via glutaminase). If sufficient Glu is released, the depolarization of the membrane caused by activation of AMPAR and KARs will

allow the Mg^{2+} block of the NMDAR ion channel to be released. In conjunction with the co-agonist Gly, Glu binding the NMDAR will cause the ion channel to become permeable to Na^{+} and Ca^{2+}. Once this occurs, the resulting cascade of signals will result in a variety of changes to the cell.

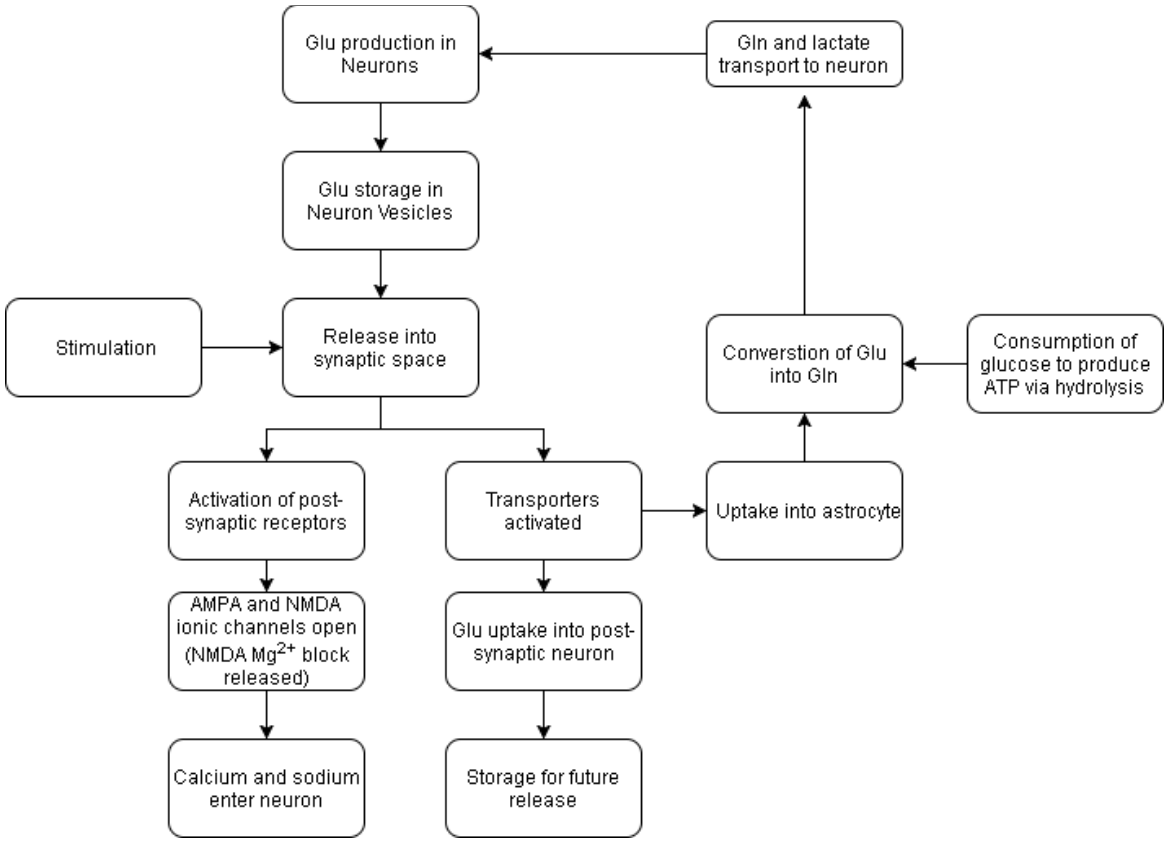

Figure 2.4: A summary of the actions and cycling of Glu in the brain.

2.2 Glutamate and Calcium Under Neurological Stress

Given the intricate the relationships between Glu receptors and transporters, as well as the strict control of Glu concentrations in the brain, it should come as no surprise that damage to any part of the system can result in a breakdown of the glutamatergic signaling system. This is especially true in traumatic brain injury (TBI) and ischemic stroke (IS). These conditions not only cause local cellular damage but also lead to a disruption of ATP production due to tissue hypoxia. As mentioned above, the cycling of Glu and maintenance of ion gradients are energy intensive processes without which signaling networks rapidly fail.

Changes in Glu concentrations in the brain following TBI and hypoxia also play a critical role in *secondary injuries*, and subsequently affect long-term patient outcome [23]. The currently accepted hypothesis as to how continuing damage occurs after TBI or IS is that damaged neurons release Glu into the extracellular spaces following the injury at a concentration significantly above basal levels. The large excess of Glu overwhelms the Glu transporters that normally maintain low micromolar (1–3 μM) [24] concentrations in the extracellular space, resulting in rapid uptake by surrounding healthy neurons. This leads to an increased uptake of calcium (Ca^{2+}) [25-28] into the cells, causing a cascade of events and culminating in the activation of apoptotic pathways due to ROS production and lipid peroxidation. Simultaneously, a disruption of the respiratory pathway results in a decrease in ATP production in the surrounding tissue including the neurons and astrocytes at precisely the moment it is required. In both cell types, this causes a failure in the maintenance of Ca^{2+} levels and the Na^{+} gradients required for removing Glu from the extracellular space. In astrocytes this situation is further complicated by the *efflux* of Glu as a response to

hypoosmotic conditions caused by the influx of Na^+ and consequent swelling of the cell [29]. The resulting cell death that happens as excess Glu results in cascades of damage to surrounding neurons is referred to as excitotoxicity [30] and is among the chief causes of secondary damage following TBI or stroke.

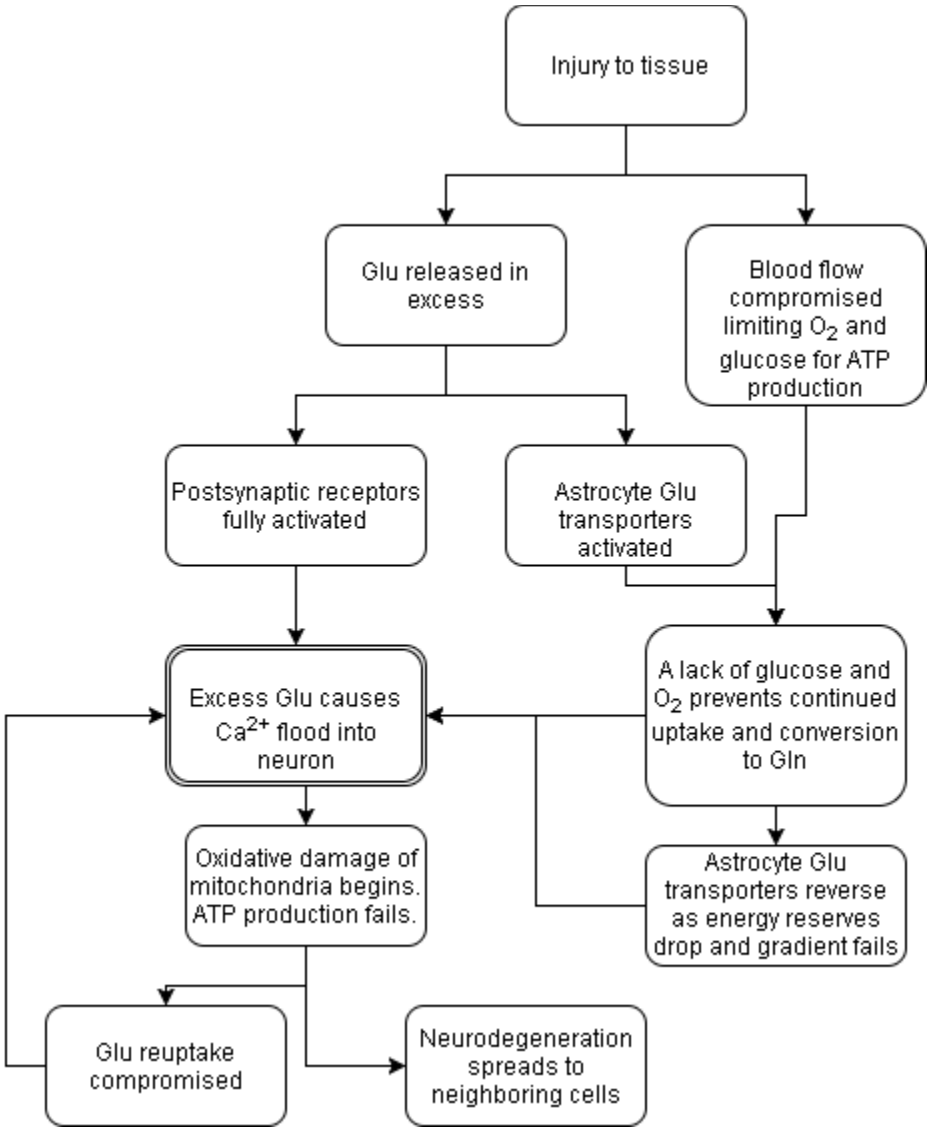

Figure 2.5: A flow chart of secondary damage following TBI. Tissue damage results in a surge in excess Glu in the extracellular space. This excess immediately results in activation of receptors and transporters as in the healthy system. However, the compromised delivery of glucose and oxygen necessary for ATP production combined with the overwhelming of Glu transporters results in NMDA receptors remaining open for an extended period. As calcium floods into the cell, mitochondrial dysfunction results in oxidation and cell death.

Since elevated Glu concentrations are the proximal cause of this excitotoxicity, the desire for methods to monitor extracellular Glu in a clinical setting has grown in recent years. The hope is that by monitoring changes in Glu concentration in the brain, rapid intervention that would prevent continued excitotoxicity and tissue damage may be possible. With this in mind, two methods for monitoring Glu *in vivo* have been developed: electrochemical biosensors and microchip electrophoresis (ME).

2.3 Biosensors for the Glutamate Detection

Biosensors can be broadly defined as devices that convert the recognition of a biochemical species into an electrical or optical signal [31]. For this to be useful, not only must the recognition be specific to the analyte of interest, but the sensor must be able to detect it at biologically relevant concentrations.

The most commonly used Glu biosensors in a clinical setting are based on amperometric detection [28, 32]. These biosensors use an enzyme specific to Glu to generate electroactive species. These biosensors commonly incorporate glutamate oxidase [28] or glutamate dehydrogenase, which generate hydrogen peroxide or NADPH, respectively, in the presence of Glu [32].

These enzyme-based biosensors have many advantages for monitoring Glu in the brain. The biggest of these is their high temporal resolution. Biosensors can respond to changes in Glu

concentration on time scales from 5–10 seconds. Additionally, due to their small diameter (10–100 µm), they exhibit excellent spatial resolution in heterogenous tissues, such as the brain [33]. The excellent temporal and spatial resolution offered by Glu biosensors makes them very useful for monitoring rapid, localized changes such as Glu release into the synaptic cleft [34]. However, these biosensors have the disadvantage that they can usually monitor only a single analyte at a time. This means that multiple biosensors with different biorecognition elements must be used to detect multiple species in a specific region of the brain.

2.4 Microdialysis Sampling

Microdialysis sampling (MD) allows for continuous sampling of both *in vivo* environments, such as the extracellular fluid (ECF) of the brain, and *in vitro* tissue cultures. Sampling is accomplished using a 100–500 µm probe containing a semi-porous membrane with a specific molecular weight cut-off. The probe is inserted at the biological site of interest and a perfusate solution, similar in composition to the ECF, is pumped through the probe at flow rates generally between 0.1 and 1 µL/min. Since the perfusate lacks any of the analytes of interest, a concentration-based diffusion gradient is created across the probe membrane. Analytes smaller than the membrane pore size, typically those with molecular weights between 20 kDa–60 kDa [35], diffuse through the membrane based on their concentration gradient into the perfusate, now referred to as the dialysate. Slower flow rates allow longer equilibration times and higher analyte recovery through the probe, but lead to much smaller sample volumes. Finally, the dialysate leaves the probe via the exit tubing [35]. Dialysate samples can then be analyzed offline or online for the compounds of interest, a distinction explained in the following sections.

Microdialysis is an ideal sampling method to couple to ME for several reasons. The first of these is that the sampling process exhibits no net fluid loss, allowing samples to be taken for extended periods of time [27]. Second, strategic selection of pore size can prevent interfering proteins and other large molecules from entering the perfusate, effectively eliminating the need for further sample preparation steps. Finally, as sampling is due entirely to analyte diffusion across a semipermeable membrane, virtually any small molecule can be sampled using the technique. However, this last point can also be problematic. Because sampling is diffusion limited, the ultimate concentration of analyte collected is dependent primarily on the flow rate of the perfusate [36]. While flow rates of around 1 µL/min are commonly used, only 20–40% of the analyte is recovered with such a high flow rate. Thus, to recover 100% of a target analyte, flow rates of approximately 100 nL/min are required [24].

Practically speaking, the trade-off between flow rate of the perfusate and analyte concentration in the dialysate, shown in Figure 2.6, dictates that any subsequent assay must either have a very low volume requirement, a very high mass sensitivity, or a low requirement for temporal resolution for analytes found at low concentrations in the ECF. An example of how perfusate flow rate can influence an assay can be envisioned by imagining a hypothetical assay requiring 4 µL of sample. If the microdialysis flow rate used to collect this sample is 1 µL/min, we can expect to recover only 20–40% of any target analyte present in the ECF due to the limited time available for analyte diffusion. If an analyte of interest—extracellular Glu at a concentration of 1 µM for instance—is collected at this flow rate, we can therefore expect to only recover 300–400 nM. Additionally, the assay could only be performed 15 times per hour. Therefore, this flow rate has dictated both the

temporal resolution and the minimum limits of detection our assay must have. Decreasing our flow rate to 100 nL/min would allow us to have higher limits of detection (with full recovery of 1 µM), but at the expense of worsening our temporal resolution to 40 minutes per assay [37].

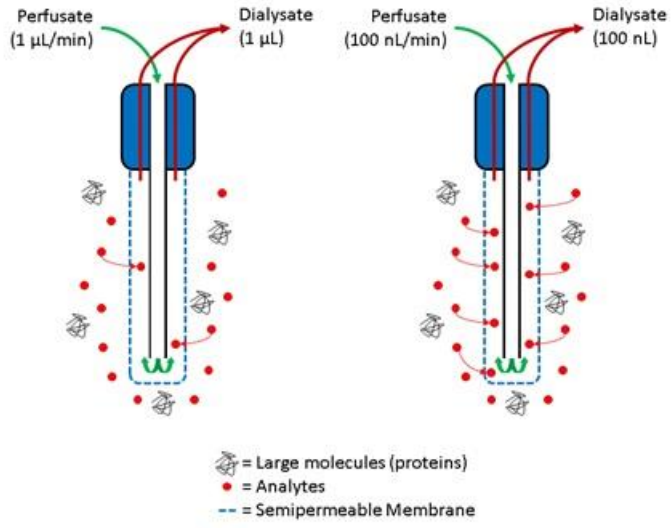

Figure 2.6: Schematic of a microdialysis brain probe with regard to flow-dependent recovery of an analyte. (Left) At faster flow rates, more sample volume can be collected, but fewer analytes will diffuse across the semipermeable membrane. (Right) At slower flow rates, more analytes can diffuse across the membrane, but at the cost of collecting much less sample. In both cases, compounds above the molecular weight cut-off of the membrane (such as proteins) are not collected.

The continuous sampling nature of MD makes it an extremely useful tool to evaluate the health of patients following traumatic brain injury or other neurotrauma. An example of this is the CMA Cerebral Tissue Monitoring System (CMA Microdialysis AB, Kista Sweden). The CMA system uses microdialysis to collect perfusate in microvials for offline analysis in a "microdialysis analyzer" such as the CMA 600, ISCUS or ISCUS^{Flex} model [38]. These microdialysis analyzers are capable of monitoring several compounds of neurological interest including glucose, lactate, pyruvate, glycerol, urea and Glu from multiple patients in an offline batch mode [39]. By collecting and analyzing samples in this manner, the ISCUS^{Flex} is able to make 30 discrete measurements per hour using sample volumes between 200 nL and 2 µL [40]. However, offline processing of samples

in this manner can be problematic, as evaporation from such small sample volumes can skew analysis, even when the system is designed to minimize such evaporation. The direct coupling of MD to ME (MD-ME) avoids both of these problems by enabling rapid, continuous sample analysis.

The combination of MD and ME for continuous monitoring of drugs and neurotransmitters *in vivo* has recently been reviewed [41]. By taking continuous, online sampling into consideration when designing a microchip-based analysis system, nanoliters of sample can be analyzed with high mass sensitivity, following rapid separations and analysis of complex samples. This chapter will discuss the principles of ME with a focus on design considerations, along with the fabrication and use of ME devices.

2.5 Derivatization for Fluorescence Detection

Many analytes, such as Glu, are not natively fluorescent and, consequently, require a derivatization reaction to produce a fluorescently active product that can be detected. When choosing a fluorogenic compound (or fluorophore, more generally), several parameters must be taken into consideration. The first is the selectivity of the reagent for specific functional groups on the analyte of interest. In the case of amino acid analysis, the most commonly used reagents are selective for the primary amine group. A reagent containing a fluorophore can complicate analysis and require additional work to separate the fluorescent reagent from the analytes of interest. Ideally then, a reagent will be fluorescently active only following derivatization of the target analyte (fluorogenic). Another consideration when selecting a reagent is that of high quantum efficiency

of the reaction product at the desired excitation wavelength. Finally, when performing online separations using ME or CE, the rate and yield of the derivatization reaction, and its reproducibility, are of utmost importance.

With these considerations in mind, two fluorogenic compounds that are typically used for the determination of amino acids are naphthalene-2,3-dicarboxaldehyde (NDA) and *o*-phthalaldehyde (OPA. This is due to their rapid reaction times, selectivity for primary amine groups, and compatibility with commercially available lasers. These reagents are non-fluorescent prior to reacting with a primary amine, eliminating additional fluorescent species that could complicate analysis [42]. The NDA reaction occurs in the presence of CN and takes 120–240 seconds to complete, while the OPA reaction occurs in the presence of 2-mercaptoethanol (2-ME) and takes 10–30 seconds to complete [42, 43]. These reactions are shown in Figure 2.7. It should be noted that NDA can react in presence of thiol compounds such as 2-ME and does so at a faster rate than it reacts with CN. However, the fluorescent products created via this reaction are less stable and have a lower fluorescence quantum efficiency than those created via the reaction with CN, undermining any gains to be had via the increased rate [44].

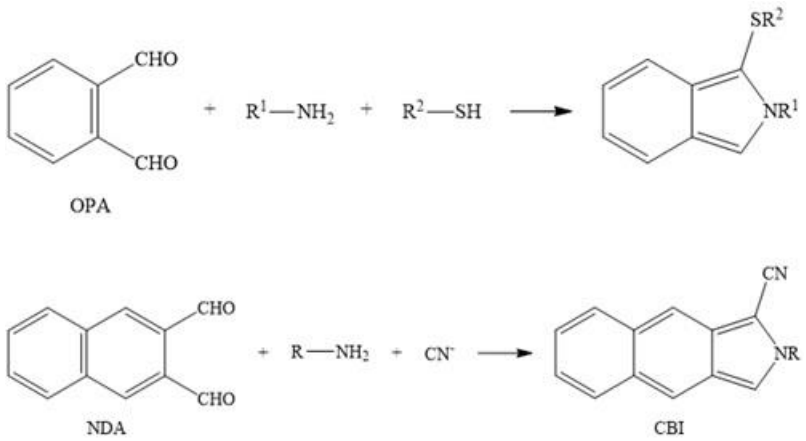

Figure 2.7: NDA and OPA Derivatization Reactions

In the case of an online assay, where the sample is derivatized between the microdialysis probe and the electrophoretic separation, the derivatization reaction does not always go to completion. Due to their rapid reaction rates, both NDA and OPA can be used for online derivatization. However, the instability of OPA can complicate the separation. Consequently, in further discussions here, we focus on the use of NDA.

When using NDA (or OPA) for derivatization, it should be noted that both CN and 2-ME are highly toxic and should be handled with care. NDA is optimally dissolved in 100% acetonitrile (ACN) to the desired stock concentration [45] and NaCN should be dissolved in water. Stock solutions of both NDA and NaCN should be stored in a refrigerator and protected from light and atmospheric conditions when not in use. Experience has shown that fresh stock solutions of NDA and NaCN should be made weekly. 2-ME is both flammable and toxic and should be handled

accordingly. In addition, it is easily oxidized and should be stored in a sealed container. Finally, 2-ME is extremely noisome, and should be used in a fume hood.

When using NDA (and OPA), the optimal derivatization yield for amino acids normally occurs at a pH that corresponds to the pKa of the analyte amine group [42] . This is typically around pH 9.2 for amino acid analytes. Whether performing offline or online derivatization, the reagents used should be prepared in 10–100-fold excess of the estimated concentration of primary amines in the sample. Derivatization of analytes of interest can be performed in either an offline manner or an online manner.

2.6 Offline Sample Derivatization

When performing off-line analysis with ME and fluorescence detection, samples must be derivatized before performing the separation. As mentioned in the derivatization section, a variety of fluorophores and fluorogenic compounds are available for this purpose. While NDA/CN and OPA/2-ME are popular due to their rapid reaction rate and ease of use for online derivatization, offline sample preparation allows the researcher more latitude with regard to derivatization. Selectivity and quantum efficiency should be the chief concerns in this case, and selection of a fluorophore/fluorogenic compound should be made to maximize both. That said, instability of the products of OPA derivatization can complicate offline analysis. For this reason, we recommend using NDA for offline derivatization.

Offline sample derivatization should be performed with at least a 10-fold excess of both NDA and NaCN compared to the analyte(s) of interest. A feature of using these compounds is that they are fluorogenic, that is, not fluorescently active prior to reacting with a primary amine. Fluorescent reagents that are not fluorogenic require better separations for the parent compound and side products that complicate analysis. However, care should be taken not to use too high a concentration of fluorogenic reagents since fluorescent side products can form. Typical reaction conditions for analyte concentrations ranging from 1–100 µM include equal volumes of NDA and NaCN at stock concentrations of 5 mM and 10 mM, respectively. An example of the derivatization of a solution containing 100 µM Glu and 100 µM aspartate (Asp) might be as follows:

2.1.5 Suggested Derivatization Conditions

2.1.5.1 Stock Concentrations:

1. Glu stock concentration: 2 mM in H_2O
2. Asp stock concentration: 2 mM in H_2O
3. NDA stock concentration (in 100% ACN): 5 mM
4. NaCN stock concentration (in 100% Water): 10 mM
5. Tetraborate buffer (BGE) concentration at pH 9.2: 15 mM

2.1.5.2 Volumes Used for Final Volume of 200 µL:

1. Glu: 10 µL for final concentration of 100 µM
2. Asp: 10 µL for final concentration of 100 µM
3. NDA: 2x the volume of all amino acids or 20 µL for a final concentration of 500 µM
4. NaCN: again, 2x the volume of all amino acids or 20 µL. Final concentration is 1 mM
5. BGE volume: 140 µL

Therefore, the limiting reagent in this hypothetical sample is the amino acids, *not* the derivatization agent. As mentioned above, high concentrations of NDA and NaCN alone can result in the formation of fluorescent side products. However, these are usually very low in concentration and do not typically complicate the assay.

One thing to note regarding this derivatization procedure is the final concentration of ACN in the sample. A total of 20 µL of ACN was added, resulting in a sample that is 10% ACN v/v. Experience has shown that, due to the hydrophobicity of NDA, injecting a sample containing NDA dissolved in ACN into a channel containing only borate buffer (for instance) will result in NDA precipitating out of solution and forming a clog. To prevent this from occurring, ACN or another similar hydrophobic solvent must be added to the BGE at a percentage greater than approximately 3%. Should a clog form, refer to Appendix C for more information and useful strategies.

2.7 Online Derivatization

The same principles are maintained for online derivatization as in offline. The differences between the two arise from differences in fluid mixing at the microscale and in the fact that reactions typically do not proceed to completion within the limited time frame available for mixing. In addition, it is difficult to mix laminar flows in microfluidic devices so the design of the MD-ME interface should take into account mixing architectures (passive or active) to ensure full mixing of sample inlet and derivatization agents. These are discussed in chapter 5.

As mentioned, NDA/CN and OPA/2-ME are used for many MD-ME systems because of their rapid derivatization reactions and the fact that they are fluorogenic. However, even these reagents can require several minutes to fully derivatize a sample. Consequently, when performing derivatization online, much lower levels of fluorescent product are likely to be created prior to detection, leading to relatively high limits of detection. A complication that should be anticipated.

2.8 References

1. Oborny, N.J., M. Hogard, and S.M. Lunte, *Separation-based Sensors using Microchip Electrophoresis with Microdialysis for Monitoring Glutamate and Other Bioactive Amines* in *Biochemical Approaches for Glutamatergic Neurotransmission*, S. Parrot and L. Denoroy, Editors. 2018, Humana Press.
2. Meldrum, B.S., *Glutamate as a neurotransmitter in the brain: review of physiology and pathology.* The Journal of nutrition, 2000. **130**(4): p. 1007S-1015S.
3. Zhou, Y. and N. Danbolt, *Glutamate as a neurotransmitter in the healthy brain.* Journal of neural transmission, 2014. **121**(8): p. 799-817.
4. Niciu, M.J., B. Kelmendi, and G. Sanacora, *Overview of glutamatergic neurotransmission in the nervous system.* Pharmacology Biochemistry and Behavior, 2012. **100**(4): p. 656-664.
5. Fonnum, F., *Glutamate: a neurotransmitter in mammalian brain.* Journal of neurochemistry, 1984. **42**(1): p. 1-11.
6. Tapiero, H., et al., *II. Glutamine and glutamate.* Biomedicine & pharmacotherapy, 2002. **56**(9): p. 446-457.
7. Cooper, J.R., F.E. Bloom, and R.H. Roth, *The biochemical basis of neuropharmacology*. 2003: Oxford University Press, USA.
8. Zheng, K., A. Scimemi, and D.A. Rusakov, *Receptor actions of synaptically released glutamate: the role of transporters on the scale from nanometers to microns.* Biophysical journal, 2008. **95**(10): p. 4584-4596.
9. Magistretti, P.J., et al., *Energy on demand.* Science, 1999. **283**(5401): p. 496-497.
10. Mayer, M.L., *Glutamate receptor ion channels.* Current opinion in neurobiology, 2005. **15**(3): p. 282-288.
11. Henley, J.M. and K.A. Wilkinson, *Synaptic AMPA receptor composition in development, plasticity and disease.* Nature Reviews Neuroscience, 2016. **17**(6): p. 337-351.
12. Rosenmund, C., Y. Stern-Bach, and C.F. Stevens, *The tetrameric structure of a glutamate receptor channel.* Science, 1998. **280**(5369): p. 1596-1599.
13. Armstrong, N., et al., *Measurement of conformational changes accompanying desensitization in an ionotropic glutamate receptor.* Cell, 2006. **127**(1): p. 85-97.
14. Contractor, A., C. Mulle, and G.T. Swanson, *Kainate receptors coming of age: milestones of two decades of research.* Trends in neurosciences, 2011. **34**(3): p. 154-163.
15. Watt, A.J., et al., *A proportional but slower NMDA potentiation follows AMPA potentiation in LTP*. Nature neuroscience, 2004. **7**(5): p. 518.
16. Ehlers, M.D., et al., *Synaptic targeting of glutamate receptors.* Current opinion in cell biology, 1996. **8**(4): p. 484-489.
17. Ehlers, M.D., et al., *Inactivation of NMDA receptors by direct interaction of calmodulin with the NR1 subunit.* Cell, 1996. **84**(5): p. 745-755.
18. Berridge, M.J., M.D. Bootman, and H.L. Roderick, *Calcium signalling: dynamics, homeostasis and remodelling.* Nature reviews. Molecular cell biology, 2003. **4**(7): p. 517.
19. Berridge, M.J., *Neuronal calcium signaling.* Neuron, 1998. **21**(1): p. 13-26.
20. Santo-Domingo, J. and N. Demaurex, *Calcium uptake mechanisms of mitochondria.* Biochimica et Biophysica Acta (BBA)-Bioenergetics, 2010. **1797**(6): p. 907-912.
21. Ermak, G. and K.J. Davies, *Calcium and oxidative stress: from cell signaling to cell death.* Molecular immunology, 2002. **38**(10): p. 713-721.

22. Xiong, Y., et al., *Mitochondrial dysfunction and calcium perturbation induced by traumatic brain injury.* Journal of neurotrauma, 1997. **14**(1): p. 23-34.
23. Maas, A.I., N. Stocchetti, and R. Bullock, *Moderate and severe traumatic brain injury in adults.* The Lancet Neurology, 2008. **7**(8): p. 728-741.
24. Benveniste, H., *Brain microdialysis.* Journal of neurochemistry, 1989. **52**(6): p. 1667-1679.
25. Sattler, R. and M. Tymianski, *Molecular mechanisms of calcium-dependent excitotoxicity.* Journal of molecular medicine, 2000. **78**(1): p. 3-13.
26. Kristián, T. and B.K. Siesjö, *Calcium in ischemic cell death.* Stroke, 1998. **29**(3): p. 705-718.
27. Chamoun, R., et al., *Role of extracellular glutamate measured by cerebral microdialysis in severe traumatic brain injury.* Journal of neurosurgery, 2010. **113**(3): p. 564.
28. Soldatkin, O., et al., *Monitoring of the velocity of high-affinity glutamate uptake by isolated brain nerve terminals using amperometric glutamate biosensor.* Talanta, 2015. **135**: p. 67-74.
29. Anderson, C.M. and R.A. Swanson, *Astrocyte glutamate transport: review of properties, regulation, and physiological functions.* Glia, 2000. **32**(1): p. 1-14.
30. Szydlowska, K. and M. Tymianski, *Calcium, ischemia and excitotoxicity.* Cell calcium, 2010. **47**(2): p. 122-129.
31. Dale, N., et al., *Listening to the brain: microelectrode biosensors for neurochemicals.* Trends in biotechnology, 2005. **23**(8): p. 420-428.
32. Zhang, M. and L. Mao, *Enzyme-based amperometric biosensors for continuous and on-line monitoring of cerebral extracellular microdialysate.* Front Biosci, 2005. **10**: p. 345-352.
33. van der Zeyden, M., et al., *Microdialysis of GABA and glutamate: analysis, interpretation and comparison with microsensors.* Pharmacology Biochemistry and Behavior, 2008. **90**(2): p. 135-147.
34. Khan, A.S. and A.C. Michael, *Invasive consequences of using micro-electrodes and microdialysis probes in the brain.* TrAC Trends in Analytical Chemistry, 2003. **22**(8): p. 503-508.
35. Nandi, P. and S.M. Lunte, *Recent trends in microdialysis sampling integrated with conventional and microanalytical systems for monitoring biological events: a review.* Analytica chimica acta, 2009. **651**(1): p. 1-14.
36. Stenken, J.A., *Methods and issues in microdialysis calibration.* Analytica chimica acta, 1999. **379**(3): p. 337-358.
37. Georganopoulou, D.G., et al., *Development and comparison of biosensors for in-vivo applications.* Faraday discussions, 2000. **116**: p. 291-303.
38. Cecil, S., et al., *Traumatic brain injury advanced multimodal neuromonitoring from theory to clinical practice.* Critical care nurse, 2011. **31**(2): p. 25-37.
39. *510(k) Summary for CMA Cerebral Tissue Monitoring System*. 2002, Food and Drug Administration: accessdata.fda.gov.
40. AB, M.D. *ISCUSflex Microdialysis Analyzer*. 2015; Available from: http://www.mdialysis.com/analyzers/iscusflex-for-point-of-care.
41. Saylor, R.A. and S.M. Lunte, *A review of microdialysis coupled to microchip electrophoresis for monitoring biological events.* Journal of Chromatography A, 2015. **1382**: p. 48-64.

42. De Montigny, P., et al., *Naphthalene-2, 3-dicarboxyaldehyde/cyanide ion: a rationally designed fluorogenic reagent for primary amines.* Analytical Chemistry, 1987. **59**(8): p. 1096-1101.
43. Chen, R.F., C. Scott, and E. Trepman, *Fluorescence properties of o-phthaldialdehyde derivatives of amino acids.* Biochimica et Biophysica Acta (BBA)-Protein Structure, 1979. **576**(2): p. 440-455.
44. Matuszewski, B.K., et al., *N-substituted 1-cyanobenz [f] isoindole: evaluation of fluorescence efficiencies of a new fluorogenic label for primary amines and amino acids.* Analytical chemistry, 1987. **59**(8): p. 1102-1105.
45. Bantan-Polak, T., M. Kassai, and K.B. Grant, *A comparison of fluorescamine and naphthalene-2, 3-dicarboxaldehyde fluorogenic reagents for microplate-based detection of amino acids.* Analytical biochemistry, 2001. **297**(2): p. 128-136.

3. Capillary and Microchip Electrophoretic Separations

3.1 An Introduction to Electrophoretic Separations

Electrophoresis is a separation technique whereby analytes with differing ratios of charge-to-hydrodynamic radius can be separated using an applied external electric field. The general technique of electrophoresis has been in use for many years [1-3]. Briefly, an electrophoretic separation begins with the application of an electric potential to a conductive electrolyte solution containing the analytes of interest. The application of this potential results in a force on all charged analytes toward the electrode of opposite charge, with positive analytes migrating toward the negatively charged cathode and negative analytes migrating toward the positively charged anode. The degree that an individual analyte responds to the electric field is known as its electrophoretic mobility. That mobility is given by the following equations beginning with the velocity of an analyte in an applied electric field:

$$\nu = \mu_E E$$

Equation 3.1: Analyte velocity due to an applied electric field

Where ν is the analyte velocity, $\mu_E$is the electrophoretic mobility of the analyte, and E is the applied electric filed in V/cm. The force applied to an analyte is found as a relationship between the force due to the applied electric field:

$$F_E = q\ E$$

Equation 3.2: The force applied to an analyte as a function of charge and applied electric field strength

With F_E is the force due to the applied field, q is the charge on the analyte, and E is the applied field strength. This force is balanced however against the forces of frictional drag given by:

$$F_F = -6\pi\eta r\nu$$

Equation 3.3: The frictional forces on an analyte

Which is Stokes law for frictional drag on a spherical object where F_F is the frictional force, η is the viscosity of the solution, ν is the velocity of the analyte, and r is the radius of the ion. Combining these equations and solving for the analyte mobility μ_E we arrive at:

$$\mu_E = \frac{q}{6\pi\eta r}$$

Equation 3.4: Analyte mobility as a function of analyte charge, size and solution viscosity.

It can be seen then that any differences in mobility between analytes is a function of the relative charge to size ratio of each analyte as well as their response to changes in solution viscosity. The problem of how to separate analytes of opposing charges or those having none at all is discussed in the next section.

The separation of analytes based on relative differences in their electrophoretic mobilities is a broadly applicable technique as many analytes either possess a charge or can be induced to process one via changes in pH. However, the migration of charged analytes toward opposite electrodes can be problematic in cases where both positive and negatively charged analytes are of interest. In addition, low separation efficiencies and inadequate resolution make the use of slab gel electrophoresis impractical for small molecules.

3.2 Capillary Electrophoresis

Like gel electrophoresis, capillary electrophoresis (CE) functions via the application of an electric potential to a conductive background electrolyte (BGE). In this case, the BGE is contained within a long capillary tube, typically made of fused silica and optionally coated with a polyimide coating that provides additional robustness. The capillary can range in length from 20 cm to over 100 cm, with an internal diameter between 10 μm and 100 μm. The outer diameter of the capillary generally ranges from 200 to 375 μm. These dimensions have important repercussions that have resulted in vastly improved performance of this system over gel-based electrophoresis for small molecules. First, the high ratio of surface area to volume allows substantial amounts of heat to be dissipated. This in turn allows the use of higher potentials (typically on the order of several hundred volts per centimeter), thereby increasing separation efficiency. Secondly, the small internal dimensions limit sample volume requirements. Injection volumes for CE are typically on the order of 100 nL, although they can be larger if desired. Finally, the charged groups on the inner surface of the capillary can create an electrical double layer and cause the production of electroosmotic flow (EOF) when an electric potential is applied. This EOF makes it possible to detect all compounds, regardless of charge, at one end of the capillary.

3.2.1 Electroosmotic Flow

Electroosmotic flow (EOF), shown in Figure 3.1, is generated in the capillary as a result of an electrical double layer that is formed on the surface of silica capillaries when using a BGE of pH

3 or greater. Above this pH, silanol groups on the surface of the capillary become ionized, resulting in a net negative surface charge. In response to the formation of this surface charge, a layer of cations from the BGE forms a compact layer of positive charges near the surface. This layer becomes more diffuse as the distance from the negative capillary surface increases. When a separation potential is applied to the capillary, these diffuse cations migrate toward the cathode, dragging the solvent with them. If the EOF is stronger than the attraction of the analytes of interest to the anode (electrophoretic mobility), then all analytes, regardless of charge, will migrate toward the cathode where the detector is placed.

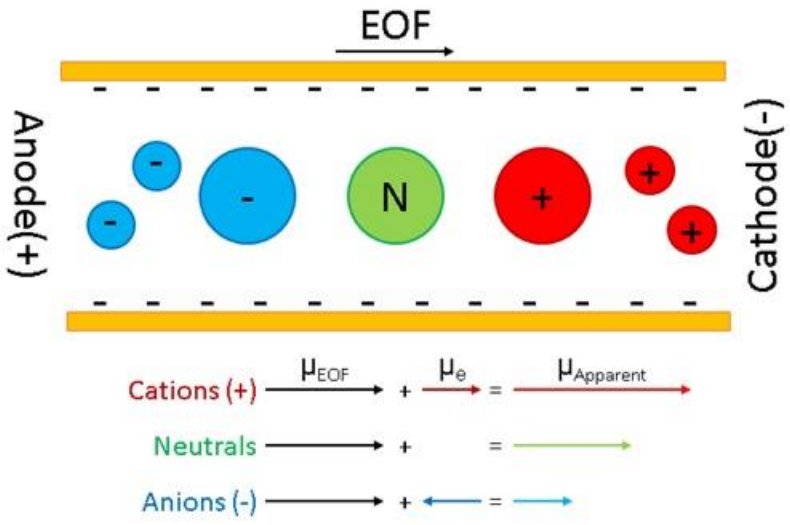

Figure 3.1: A negative charge is generated on the surface of silica capillaries due to the use of a BGE with pH of 3 or greater. As an external voltage is applied to the channel, a bulk flow (μ_{EOF}) is created from anode (+) to cathode (-). Simultaneously, analytes begin to migrate toward their respective opposite charge (negatively charged cations toward the anode, positively charged anions toward the cathode). This electrophoretic mobility (μ_e) of each analyte is governed by its individual charge-to-mass ratio. The overall apparent mobility of each analyte is the resulting sum of μ_{EOF} and μ_e.

Analyte mobility due to EOF is independent of charge and is given by:

$$\mu_E = \frac{\varepsilon\zeta}{\eta}$$

Equation 3.5: Analyte mobility due to EOF

Where ε is the dielectric constant of the solution, $\zeta$is the zeta potential, and η is the viscosity.

Many variables can affect the formation of an EOF, including channel dimensions (at greater than ~200 μm, viscous forces overwhelm the net motion of the BGE and Joule heating increases), viscosity and ionic strength of the BGE, pH, and applied potential. It is through the proper balancing of these variables and those concerning the interaction of each analyte with the BGE and resulting in their individual electrophoretic mobilities (μ_e) that a well-resolved separation is achieved.

Finally, the direction of the EOF can be reversed through the application of a surface coating of positive charge and a reversal of the polarity of the applied electric potential. Operating in reversed polarity can be beneficial when separating some charged species.

3.2.2 Sample Injection

The two primary methods by which samples are injected into a CE or ME system are electrokinetic and hydrodynamic injections. Electrokinetic injection uses control of the EOF and electroosmotic mobility generated by an applied potential difference to inject sample into the capillary. To accomplish this, the capillary is placed into a sample and a potential is applied for a prescribed amount of time. Analytes are introduced into the capillary using the same principles of migration that are used during a separation. Because analytes migrate at varying rates depending on their electrophoretic mobility, electrokinetic injection can therefore be biased toward smaller

analytes having opposite charge to the polarity of the separation voltage. In the extreme case where an EOF is not present, this bias will result in only analytes of a single charge being injected.

By contrast, hydrodynamic injections exhibit no such bias. In this injection scheme, a defined volume of sample is injected into the capillary by first placing the capillary in the sample and then applying a pressure differential to the sample itself. The result is fluid displacement into the capillary. Following this injection, a separation potential is applied and electrophoretic separation proceeds normally.

3.3 Microchip Electrophoresis

Like CE, microchip electrophoresis (ME) has many benefits over more common separation methods such as liquid chromatography, including the ability to analyze extremely small sample volumes, high separation efficiencies, and rapid analysis times. In addition to these advantages, ME has several added benefits. The first of these is that ME devices have a much smaller footprint than existing CE systems. The decrease in length from a 75-cm channel in CE to a 5-cm channel, along with the smaller dimensions of the channels (15 μm deep by 50 μm wide), allows a fraction of the voltages to be used while preserving the 333 V/cm separation potential. The smaller dimensions of a ME setup can be seen in Figure 3.2. The decrease in voltage needed as well as in the associated instrumentation can lead to a much smaller overall system. The separation efficiency, which is a function of field strength, is preserved, resulting in decreased analysis times as analytes travel shorter distances to the detection point.

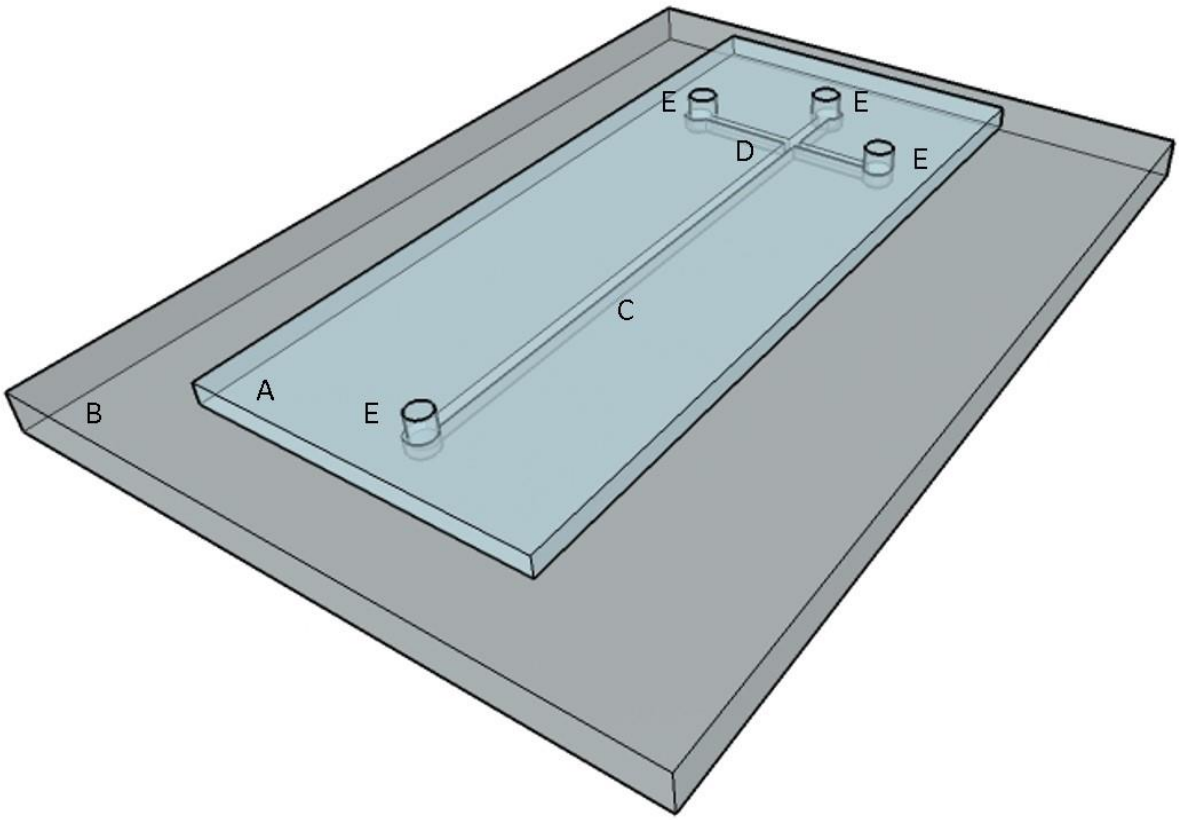

Figure 3.2: Schematic of a typical ME device with a simple-T design. The entire system is usually no bigger than 3 cm x 10 cm x 5 mm thick. (a) Channel substrate. The channel's dimensions can vary with application, but are usually on the order of 50 µm wide x 15 µm deep. (b) Base substrate. The channel substrate can be reversibly or irreversibly bound to the base, as discussed in Section 3. (c) Separation channel, which can vary in length from 2.5 cm to 15 cm depending on the device design. (d) Electrokinetic gate (e) Sample and buffer reservoirs. The exact conditions to perform an electrokinetic injection on a ME device are discussed further in Figure 3.7.

Another advantage of microchip electrophoresis is that modern micro-manufacturing techniques such as photolithography, hot embossing, injection molding, and casting make it possible to integrate multiple complex features into a single device [4]. These features, which can include gating for the introduction of sample to the separation channel, tapered geometries to improve separation efficiencies, the addition of electrodes for electrochemical detection, and

micromixers to facilitate on-chip derivatization of samples, add greatly to the utility of microchip systems. By integrating these functions directly into the microchip, it is also possible to radically decrease sample and reagent volume requirements. Finally, these techniques allow microchip designers to select materials based on properties such as optical clarity, surface chemistry, material expense, and ease of integration.

In light of the limitations placed on any analytical method by a sampling technique such as microdialysis, as mentioned in the previous section, microchip electrophoresis represents an ideal method for analyzing small sample volumes and enabling high temporal resolution. To take full advantage of the ability to handle small volumes, a detection strategy with sufficiently low limits of detection (mass sensitivity) must also be used.

3.4 Microchip Detection Strategies

Virtually all the detection strategies used in modern analytical chemistry have been successfully integrated with the microchip format. The most common methods include fluorescence, electrochemical, and contactless conductivity detection. Additionally, mass spectrometry has been interfaced with ME using methods such as electrospray ionization.

As with CE, the most common detection methods used with ME are optical in nature. However, unlike CE, in which absorbance detection is very common, the thick planar substrates used in the construction of microchips can make absorbance measurements difficult. Additionally, the short optical path length of the separation channel leads to a lack of sensitivity, although this can be

mitigated by the use of a specially designed detection cell [5]. Electrochemical and conductivity detection are popular methods of detection in the microchip format due to the ease of integrating electrodes directly into the microchip substrate. However, fluorescence detection is more often used due to its generally low limits of detection and the fact that it does not suffer from limitations due to pathlength, and that it exhibits a lower background than other detection methods. The additional ease of focusing an excitation light source such as a laser on the ME channel results in it being commonly used with ME. However, because the majority of compounds and, specifically, Glu are not inherently fluorescent, it is often necessary to first derivatize a sample with a fluorophore prior to separation using ME.

In this chapter and, in particular, the next section, we will discuss the types of materials used in the construction of an ME device, the methods used, and the relative pros and cons of each. Due to the advantages mentioned above, our detection method of choice for Glu is fluorescence. While the methods discussed reflect this preference, the design and construction principles are broadly applicable to other detection strategies.

3.5 Analysis of Complex Samples via Microchip Electrophoresis

Microchip electrophoresis (ME) is based on the same principles as capillary electrophoresis and, thus, separates compounds based on the ratio of their size and charge. This technique is therefore well-suited for the analysis of small, charged molecules such as Glu. In contrast to

biosensors, microchip electrophoresis permits the simultaneous analysis of multiple analytes in a single run.

Detection in ME can be accomplished using a variety of methods, the most common being electrochemistry, mass spectrometry, and fluorescence. Glutamate is most frequently measured using fluorescence detection following derivatization with a fluorescent (or fluorogenic) reagent. Using microchip electrophoresis, it is possible to separate Glu from other important biogenic amines in a brain microdialysate sample. In particular, the detection of Glu in conjunction with aspartate (Asp) and γ-aminobutyric acid (GABA) can provide particular insight into the status of the brain tissue being sampled. Arginine and citrulline are indicators of nitric oxide synthase activity in the brain and can be measured under the same conditions. As Figure 3.3 demonstrates, sample collection via microdialysis, derivatization, and separation using ME (all of which are described in detail later in this chapter) can provide a powerful view of multiple analytes within minutes of sample acquisition [6].

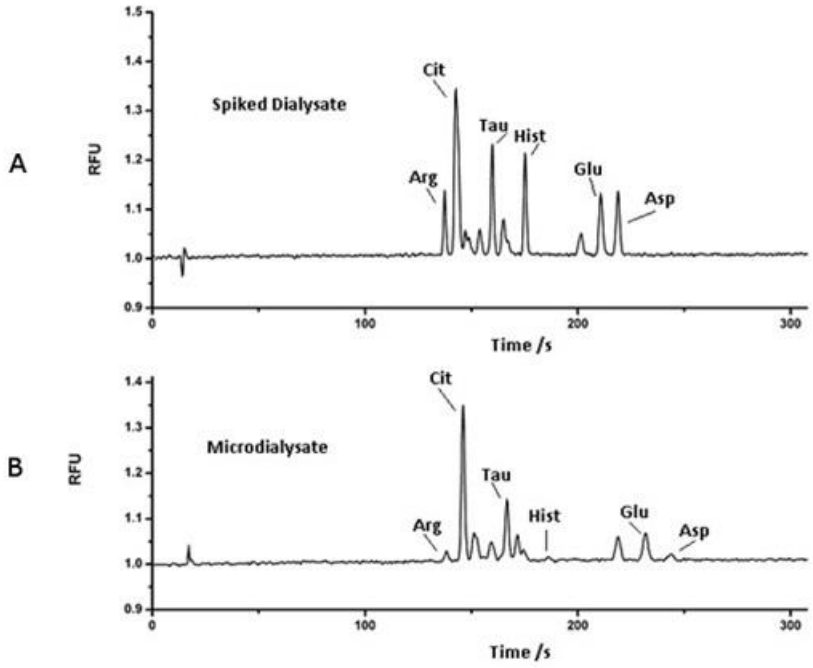

Figure 3.3: (A) An electropherogram of an NDA/CN-derivatized MD sample spiked with 5 µM arginine (Arg), citrulline (Cit), taurine (Tau), histamine (Hist), glutamate (Glu), and aspartate (Asp) for peak identification. Analysis performed offline using a 15-cm ME device.

(B) An electropherogram of a NDA/CN-derivatized MD sample from the striatum of a male Sprague Dawley rat. Sample was collected at 1 µL/minute^{-1} and derivatized offline prior to separation.

3.6 Microchip Electrophoresis with Fluorescence Detection

The construction and operation of ME devices, whether they are operated offline or online coupled to MD, is a multistep process involving photolithography, chemical etching, and high temperature bonding. These procedures are best performed in a cleanroom environment for the highest level of reproducibility, although it is possible to construct these devices in a laboratory setting if care is taken to maintain a clean environment. The materials, facilities and instrumentation listed below describe what is used in our laboratory for the fabrication of glass

and PDMS microfluidic devices. A detailed explanation of their use in the fabrication process is found in the methods section following this section.

3.7 Online MD Coupling

3.7.1 Required Equipment

Online sampling using MD requires the use of precision syringe pumps capable of maintaining a flow at 1µL/min. For the work discussed in thesis, a CMA Model 100 syringe pump was used with 1 mL syringes, also from CMA (CMA Microdialysis, Holliston, MA). Polyethylene tubing having an internal diameter of 0.39mm and an outer diameter of 1.09 mm was used. The method used to connect this tubing to a microchip can vary. For the work here though, bonded port connectors (model C360-400 from Labsmith, Livermore, CA) was used for glass-glass devices while 24 gauge coupling pins were used for PDMS-glass and PDMS-PDMS devices.

3.7.2 Sample Introduction

The development of a microfluidic devices begins with the design process. In designing an ME device, it is helpful to first determine what requirements will be placed on the function of the device itself. Four initial questions that must be asked: (1) Will the ME device interface directly to a microdialysis probe in an online manner or will samples be added to the device offline? (2) Will sample derivatization be performed on-chip or off? (3) How will sample be injected into the separation channel? (4) What length of separation channel will be required?

If sample acquisition is to be performed via online interface to microdialysis, pressure at the device inlet must be taken into account and channel widths adjusted accordingly. If derivatization will occur on-chip as well, multiple laminar flows must be mixed, either actively or passively, and the reactants must be given sufficient time following mixing for derivatization to occur. Sample injection, whether via pressure or performed electrokinetically, requires channel geometries that allow flow in one direction (down the separation channel) to be prevented.

Pressure injection is accomplished in ME devices by using additional PDMS membrane layers and the application of external positive and/or negative pressures to prevent fluid flow through channels. Unlike electrokinetic injection, which can result in biased injections of sample ions depending on their charges, pressure injection of sample is unbiased. However, due to the requirement of a flexible layer of PDMS, this approach is not typically used with all-glass ME devices. Providing a source of negative or positive pressure also further complicates the system design. For this reason, we focus primarily on the use of electrokinetic injection for all three types of ME devices described here.

When using electrokinetic injection, potentials are applied to each channel in order to establish a “gate”, with longer channels requiring higher potentials. Additionally, asymmetrical geometries (such as having channels of varying lengths) can necessitate multiple high voltage supplies.

Finally, the length and geometry of the separation channel itself will directly determine many performance characteristics of the ME device, including peak resolution, EOF magnitude, and the

separation voltage required. Separation channel widths greater than 200 µm should be avoided as viscous fluid properties begin to overwhelm those of the EOF beyond this point and Joule heating increases substantially. When comparing channel lengths, longer separation channels will result in greater separation efficiencies, assuming a comparable applied potential (measured in volts per centimeter). However, care should be taken when designing channels longer than 10 cm, since these necessitate serpentine channels that can result in a "racetrack" effect. This effect can be mitigated by tapering turns. Tapered turns themselves can be problematic, however, as the localized electric field strengths are increased. As the field strength increases, the current passing through that region of the channel also increases. This leads, in turn, to a resistive heating of the BGE termed Joule heating, which can bring about poor resolution. Despite the potential for this effect, optimal channel dimensions can greatly improve resolution when properly implemented for longer channel lengths if Joule heating is prevented [7, 8].

3.8 Modeling studies and chip design

Modeling of ME devices using software such as Comsol® prior to any production steps can be very advantageous. However, modeling entire geometries can be computationally intensive and time consuming. Unless it is necessary to model all parts of the chip simultaneously, the best practice is to model specific regions, such as the electrokinetic gate and turns, in order to optimize those particular geometries. The design of mixing and derivatization geometries can also benefit from modeling the device prior to construction to ensure that the chosen combination of mixing geometry and sample flow rate will result in a fully derivatized sample prior to injection and separation. Designs must typically be exported into a computer-aided drafting (CAD) format prior

to being made into a photomask, a process that may require additional review to ensure that the conversion of formats itself did not introduce errors.

Finally, printed photomasks must be of an extremely high resolution, and these are not attainable without the use of a specialized photomask printer. For that reason, professional services such as that provided by Infinite Graphics (Minneapolis, MN) are typically used. It is more cost-effective both in terms of printing photomasks and ultimately in terms of substrate usage to have multiple copies of devices on a single photomask. For reasons that will be explained in the following sections, these copies should be laid out in such a way that they can easily be separated into individual devices (*i.e.*, easy to cut the glass substrate without scratching a neighboring device) while fitting the maximum number of devices onto a single glass substrate. It is important that the photoresist is removed along a line between the devices, due to the fact that glass cutters will not cut through photoresist or chrome layers. Finally, if holes are to be drilled in the device following development, the diameter of the drill bit must be taken into account by providing an additional margin to prevent the destruction of neighboring features.

3.9 Material Selection

Selecting a material with which to construct an ME device must begin with consideration of the detection method used. In the case of optical detection, the optical clarity of the material, including any autofluorescence of the material itself at the target wavelength, is of paramount concern. This can be of particular importance with plastic substrates. When using electrochemical or conductivity detection, the ability to integrate an electrode into the substrate must be considered.

The surface chemistry of materials must also be taken into account, not only when considering the EOF generated by the electric field but also when determining whether or not analyte adsorption is likely to be a problem.

With this in mind, two materials have been widely evaluated and are commonly employed for ME: glass and polydimethylsiloxane (PDMS). A third option, which will also be discussed, is to combine these two materials in to a hybrid device in an effort to take advantage of aspects of each. These three options are by no means an exhaustive list of substrates for ME construction. Many other polymers, including poly (methyl methacrylate) (PMMA) and cyclic olefin copolymer (COC), are commonly used in device manufacture, each with their individual pros and cons. This chapter is focused on the use of glass, PDMS, and PDMS-glass hybrid devices because these substrates represent ideal material characteristics (glass) and ideal ease of use (PDMS). Their individual properties are described in the following sections.

3.9.1 Glass ME Devices

In many ways glass is an ideal substrate for an ME device. Its optical clarity is superb over a range of wavelengths, its surface chemistry is stable over range of pH values resulting in high reproducibility, and it has the ability to withstand high voltages (and subsequent Joule heating) associated with electrophoretic separations [9]. Additionally, because CE capillaries are typically glass, separation conditions can easily be transferred from CE to ME and vice versa.

The construction of glass-glass ME devices begins with the use of photolithography to transfer a device pattern to a borosilicate glass substrate pre-coated with chrome and photoresist. While it is possible to coat glass substrates manually, pre-coated substrates purchased from a company such as Telic (Valencia, CA) are inexpensive and consistent in performance. Following the transfer of the pattern, a multistep process to remove sections of the pattern followed by etching with a hydrofluoric acid solution is used to create the channels in the bottom glass substrate. Finally, holes are drilled, the glass is cut to size, and a two-step bonding process is used to permanently bond a blank glass piece to the etched glass. The result is an ME device that can withstand both the pressures of a microdialysis flow as well as the high voltages necessary for electrophoresis.

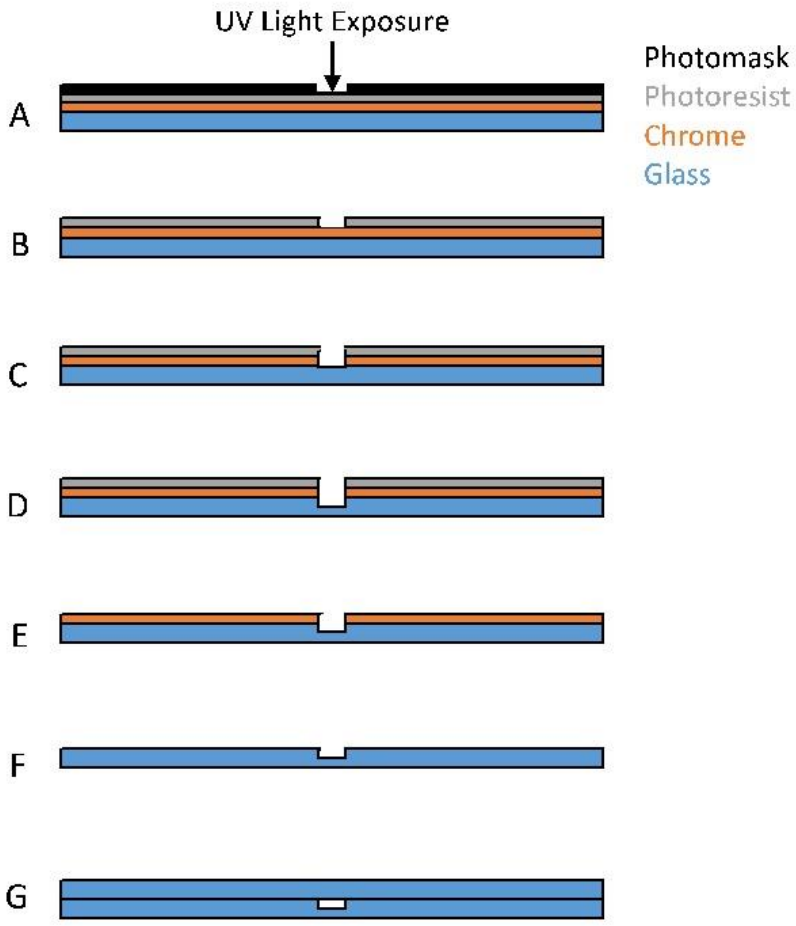

Figure 3.4: Schematic of glass-glass microchip fabrication. (a) Align photomask on coated glass and expose to UV light. (b) Remove photomask and soak in developer to remove exposed photoresist. (c) Remove exposed chrome using chrome etchant. (d) Etch exposed glass with hydrofluoric acid, then confirm channel depth with profilometer. (e) Remove remaining photoresist with acetone. (f) Remove remaining chrome with chrome etchant. (g) Bond to another piece of unmodified glass to form complete chip.

3.9.2 Polydimethylsiloxane (PMDS) ME Devices

Glass microchips permit highly reproducible separations and can last for extended periods of time if properly cared for. However, the fabrication process is lengthy and difficult and requires the use of dangerous and expensive materials. As these chips are irreversibly bonded, if there are

any issues with the construction of the separation channel or solution reservoirs (such as clogging or scratches), they must be disposed of and replaced. This makes all-glass microchips a poor choice for prototyping methods, in which multiple chip designs are studied before settling on a final pattern.

Polymeric substrates are often used for device development to avoid these complications and allow faster prototyping. A wide variety of polymeric substrates are used for microchip electrophoresis; however, polydimethylsiloxane (PDMS) is by far the most common and will be the only polymer described here. Its elastomeric properties (including the ability to seal to surfaces without distorting), optical transparency, low cost, and ease of fabrication make it an excellent candidate for microchip fabrication [10]. After a master mold with the desired microfeatures is made, multiple PDMS chips can be prepared using the same master for extended periods. This process is shown graphically in Figure 3.5. For a step by step set of instructions, please refer to Appendix B.

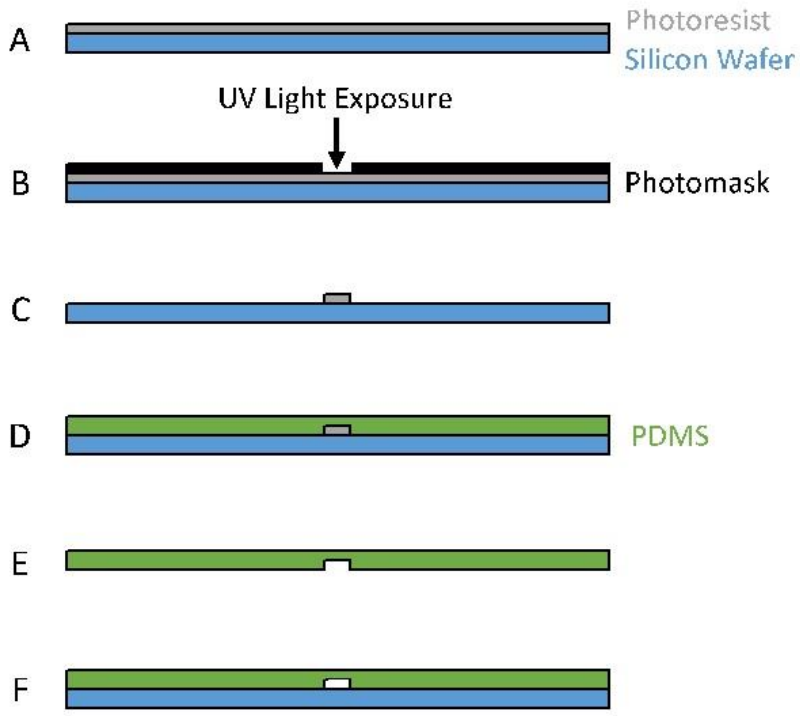

Figure 3.5: Schematic of PDMS-PDMS or hybrid microchip fabrication. (a) Spin-coat silicon wafer with negative photoresist. (b) Align photomask on coated wafer and expose to UV light. (c) Use developer to remove unexposed photoresist, then post-bake and confirm microfeature dimensions with profilometer. (d) Pour PDMS over master and cure in oven for at least two hours. (e) Peel PDMS off of master and cover with Parafilm^{TM} if not bonding immediately. (f) Punch holes for buffer reservoirs in PDMS, remove Parafilm^{TM} , if necessary, and bond to substrate of choice (PDMS or glass).

PDMS has only a very small surface charge, which means an EOF will not occur in PDMS channels. To achieve a separation, additives that will adhere to the walls and lend it their charge must be included in the BGE. The additive used depends on whether a normal or reverse polarity is applied. A common additive for normal polarity is sodium dodecyl sulfate (SDS), while a common additive for reverse polarity is tetradecyltrimethylammonium bromide (TTAB).

3.9.3 Hybrid ME Devices

Despite the ease of fabricating PDMS microchips, they suffer in terms of longevity and reproducibility. A PDMS chip can often be used for only a 6 to 8-hour period before a new one must be made. This is especially true if using high field strengths, which can cause the PDMS polymer to degrade or burn. This results in many different chips being required for even the simplest of studies, which can produce slight changes in separation efficiency and migration times for the analytes of interest. This variability in chips is further exacerbated because PDMS is not natively charged, which means additives must be added to the buffer in order to establish an EOF.

One solution to these reproducibility issues is the fabrication of PDMS-glass hybrid microchips. In this design, the microfeatures are prepared in either PDMS or glass; they can then be bonded to the opposite substrate to create the completed device. This method combines the strengths of glass and polymeric devices. The inclusion of glass as a substrate leads to more reproducible EOFs, while the inclusion of PDMS still allows rapid fabrication and easy cleaning of clogs [11].

When making a hybrid device, the main consideration is which substrate will contain the separation channel. This depends on the analytical needs of your method. If a reproducible EOF is required or higher field strengths are a necessity, having three walls of the channel made from glass will result in better separations. However, if there are no available facilities for etching and drilling glass or rapid prototyping of the channel design is required, a device with three walls of PDMS can be used.

The previous sections outlined methods of preparing microchannels in both glass (Section 3.3.) and PDMS (Section 3.4). These methods are unchanged; the only difference in constructing a hybrid device is the method of bonding. For most purposes, reversible bonding will suffice, as it is much faster and is compatible with most separations. Irreversible bonding is required only when there are concerns regarding the seal of the substrates, such as when incorporating a pressure-driven flow as the sample source. A step by step set of instructions can be found in Appendix C.

3.10 Device Use

As mentioned in the previous sections, the detection of Glu using ME can be performed either in an offline or online fashion. These two methods of operation differ primarily in terms of sample acquisition, derivatization and, in the case of online, the added complexity of integrating fluid handling into the ME device. Consequently, the following sections are divided into offline sample preparation and handling, online sample preparation and handling, and, finally, the sample injection, detection, and separation steps common to both. In either case however, as noted previously, ME devices have exceedingly small internal volumes on the order of 15 µm deep by 50 µm wide, making it easy for particles to block channels. This is of less concern for online microdialysis samples as the process of microdialysis itself prevents larger molecules from entering the dialysate. Samples, stock solutions and any other solution used in the device including cleaning solutions, should be filtered prior to use using a 0.22 µm filter. Additionally, care should be taken to prevent dust from collecting in the channel inlets of glass-glass devices between use. Two common methods for preventing dust accumulation are wrapping the chip in Parafilm™ and

storing the chip under water. The latter is a popular method used to maintain the chip overnight while the former is used for long-term storage. New PDMS-PDMS and PDMS/glass hybrid devices should be made between uses, preventing this problem.

3.10.1 Cleaning and Conditioning ME Devices

3.10.1.1 Glass-glass ME Devices

Prior to each use of a glass-glass ME device, the channels must be cleaned and conditioned (referred to from this point onward simply as conditioning) using a sequence of steps designed to remove any of a series of surface contaminants, finishing with the application of sodium hydroxide (NaOH) to leave the separation channel with a negatively charged surface. The following sequence should be applied for each full conditioning. For each step, the solution should be added to all wells but one, allowing the application of negative pressure at that well to pull the solutions through. Negative pressure can be generated using a pump or a vacuum aspirator. The sequence for full conditioning:

1. Deionized, Millipore™ filtered water for >5 minutes
2. 0.1 M HCl for >5 minutes
3. Deionized, Millipore™ filtered water for >5 minutes
4. 0.1 M NaOH for >5 minutes
5. Deionized, Millipore™ filtered water for >5 minutes
6. Background electrolyte (BGE) until channels are filled completely

Between individual uses of the device, it may be possible to skip steps 2 and 3. Care should be taken not to add acids or bases to the device without first cleaning with water as rapid changes in pH can result in the formation of precipitates within the channel. Additional information regarding chip cleaning can be found in Section 4.5 at the end of this chapter.

3.10.1.2 PDMS-PDMS and PDMS/Glass Hybrid ME Devices

Conditioning a PDMS-PDMS or PDMS/glass hybrid device requires a different procedure, primarily because using strong acids can lead to delamination of the PDMS. Therefore, a full conditioning for these devices consists of only the following sequence of flushing the chip:

1. Deionized, Millipore™ filtered water for >5 minutes
2. 0.1 M NaOH for >5 minutes
3. Deionized, Millipore™ filtered water for >5 minutes
4. Background electrolyte (BGE) (fill channels with BGE)

3.10.2 System Setup

Just as ME designs vary, the orientation of the supporting equipment (power supplies, detection equipment, associated optics, etc.) is often specific to the application or laboratory. Therefore, the description we offer here represents only one possible implementation. We have found this

implementation useful for a variety of ME devices and applications, including both online and offline analysis. A schematic diagram of the general system setup can be seen in Figure 3.6.

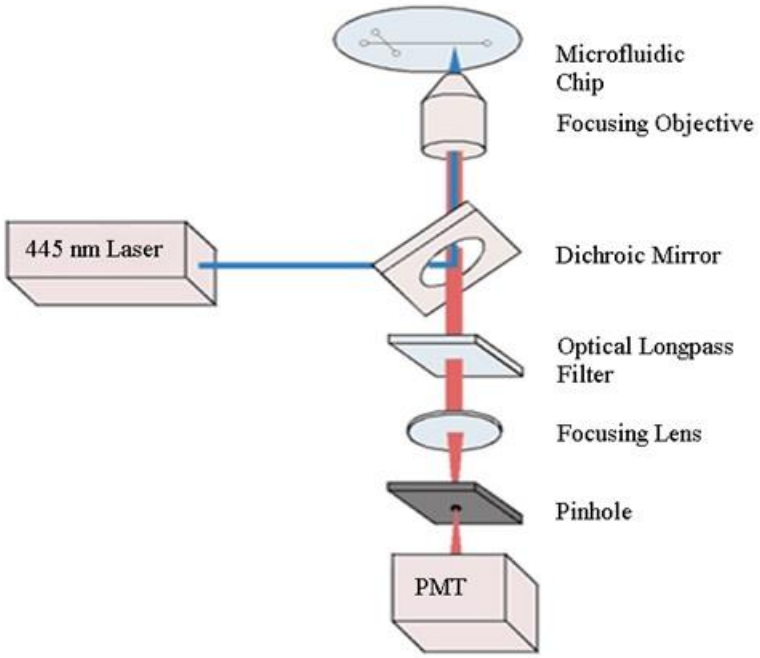

Figure 3.6: An excitation light source, here at 445 nm laser, is focused such that its output is reflected upward by a dichroic mirror mounted at 45º. The ME device is mounted so that the excitation light intersects the separation channel near the end of the channel. As fluorescent analytes pass through the beam, emitted light passes through the dichroic mirror due to its longer wavelength. Continuing along this path, an optical longpass filter is used to remove residual excitation light before the remaining light is focused onto a photomultiplier tube (PMT) for amplification and conversion to an electrical signal.

3.10.2.1 Materials List

Focusing an excitation light source on a small microfluidic channel can be challenging. For the work discussed here, this was accomplished using a Nikon Eclipse Ti Microscope which focused the beam of an Omicron PhoxX 445nm diode laser on the detection point. The emitted

light from the derivatized analyte was detected using a Hamamatsu PMT Model R1527 with Pacific Instruments Model 227 PMT Power Supply. The output of this PMT was subsequently amplified using a Stanford Research Labs Model SR570 Preamplifier before a USB-6229 data acquisition card from National Instruments converted the signal for display on a nearby PC.

3.10.2.2 Optical System

Briefly, a Nikon Eclipse Ti microscope is used as a stage upon which an ME device is placed. A 445 nm laser, specific for NDA excitation, is fired into a fiber optic cable, which is subsequently interfaced to the Nikon Eclipse Ti microscope. The incoming laser light passes through an excitation optical filter, attenuating any wavelengths of light other than 445 nm before being reflected upward using a dichroic mirror mounted at 45º. This dichroic mirror is chosen specifically to reflect wavelengths lower than that of the emitted light from the target fluorophore. The result is laser light reflected upward through a focusing objective lens, and intersecting the end of the ME device's separation channel, which has been placed on the microscope stage. As NDA-tagged analytes, such as Glu, migrate toward the end of the separation channel, they pass through the beam of 445 nm laser light. Encountering this results in fluorescent excitation and emission of light at approximately 490 nm. The emission of this light occurs in all directions, including back down through the focusing optics. As this emitted light continues along its path, it passes through the dichroic mirror due to its longer wavelength. A final emission filter is used to remove any light having a wavelength less than a cutoff of ~490 nm (chosen to prevent excitation laser light from striking the detector).

3.10.2.3 Signal Detection and Amplification

A photomultiplier tube (PMT) with an applied bias voltage of 1000 V was used to detect the light emitted by the analytes, converting the light into an electrical current. The current produced by the PMT during this process is typically on the order of 1 nA to 1 µA and requires subsequent amplification before being converted to a digital signal for analysis. This amplification step is performed by a current-to-voltage amplifier (Model SR570). This particular model of amplifier allows the user to specify a low noise, high gain setting, which we typically set to a gain of 200 µA/V, and a low pass filter set to attenuate high frequency noise over 3 Hz.

Finally, following amplification, a National Instruments data acquisition system, model USB-6229, was used to convert the analog output of the amplifier into a digital signal for display and analysis using custom Labview-based software.

3.10.3 Offline Injection and Separation

As mentioned in the previous sections, electrokinetic injection is our preferred method of sample injection due to the relative simplicity of the system. That said, the coordinated use of multiple high voltage (HV) potentials in a small area while maintaining optical alignment of microscale features can be nontrivial. Safety is a chief concern when using HV power supplies. Additionally, a HV supply should be chosen to have high stability over time, digital control

allowing potentials to be toggled on and off quickly, short circuit protection to protect both user and supply, and feedback to the user regarding the actual voltage and current output of the system. Feedback to the user is incredibly useful in diagnosing problems and is discussed in Section 4. With these requirements in mind, we typically use Ultravolt power supplies such as the HVRack-4-250. Finally, for the purposes of this example, we will assume a 'simple T' architecture such as the one in Figure 3.7 that uses two HV ports and two ground ports to create a gate and separation potential for offline sample analysis.

To begin, the chip should be mounted on the microscope platform such that the excitation light is focused on the gate of the chip to first determine the correct ratio of HV potentials to use to establish a gate. For the simple T with 2.5 cm side channels and a separation channel 5 cm in length such as the design in Figure 3.7, a ratio 3:4 is typically sufficient, meaning that applying 2000 V to the "Buffer" port as a separation voltage and *(2000*.75)* = 1500 V to the "Sample" port will create a gate. This ratio will differ depending on the chip geometry used. Once established, this gate can be seen through the microscope by adjusting the position of the chip such that the excitation light is focused on the gate region of the chip, a fact that can be useful for diagnosis. Wires should be attached and secured with HV applied to the sample and buffer ports and ground wires in the buffer waste and sample waste ports. Alligator clips should be soldered to the ends of both the HV and ground wires, and platinum wires should be placed in the wells themselves. Once the presence of a gate has been established, the detection point should be moved to the end of the separation channel. To inject a sample, the "Buffer" voltage will need to be turned off momentarily, allowing the potential to float. This is not to be confused with grounding the

potential, which would result in sample flowing into the buffer reservoir as the EOF reversed direction.

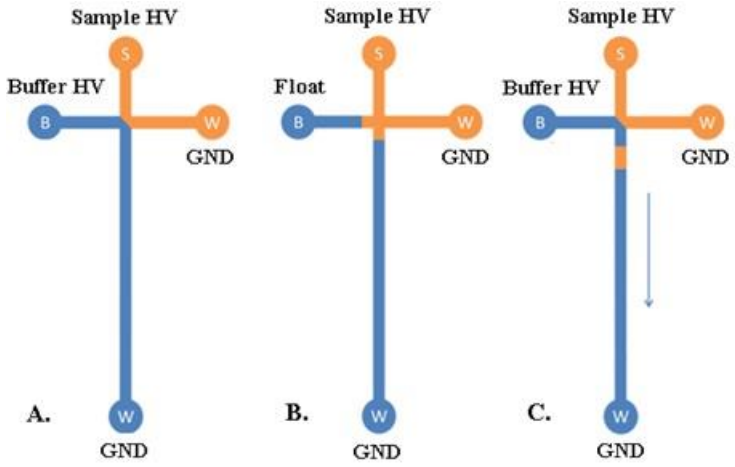

Figure 3.7: A) The microchip is loaded with sample (S) and buffer (B). A high voltage potential is applied, resulting in electroosmotic flow toward the waste ports (W). B) Buffer voltage is floated, allowing sample to be injected. C) Buffer voltage is reestablished and analyte separation proceeds.

After sample has been allowed to enter the separation channel (a one second injection time is typically more than sufficient), the voltage applied to the "Buffer" port is reapplied. This has the effect of both reestablishing the electrokinetic gate, preventing additional sample from entering the channel, and applying a potential to the separation channel. It is at this point in the process of analysis that analytes will begin to migrate with the EOF, separating according to their individual electrophoretic mobilities, toward the end of the separation channel.

3.10.4 Online (MD-ME) Injection and Separation

The operation of an integrated MD-ME system is very similar in function to the offline example described above. As with offline analysis, the ME device is mounted over the detection system with the excitation light focused on the end of the separation channel. Integrating an MD flow to an ME device, however, requires that ports first be bonded to the surface of the device. As mentioned previously, UV glue is typically used in conjunction with bonded port connectors to create an interface capable of withstanding the pressure produced by the microdialysis flow.

Once the ports have been attached, polyethylene tubing can be used to connect the syringes containing NDA in ACN, NaCN in H_2O, and the output of the microdialysis probe to the ME device. The fluids from these three inlets must be given sufficient time to mix on-chip, allowing analytes in the dialysate to form fluorescent products.

As in offline analysis, an electrokinetic gate is established at the inlet to the separation channel to prevent sample from continuously entering the channel. However, in the case of a coupled MD-ME system, the *MD interface must be grounded* in order to prevent damage to equipment or test subjects. If, however, the port is grounded near the gate, a counter-flowing EOF can be created. Therefore, the MD flow should be grounded as far from the separation channel as possible. Once a grounded pressure flow has been established, a separation voltage can be applied. An example of this can be seen in Figure 3.8.

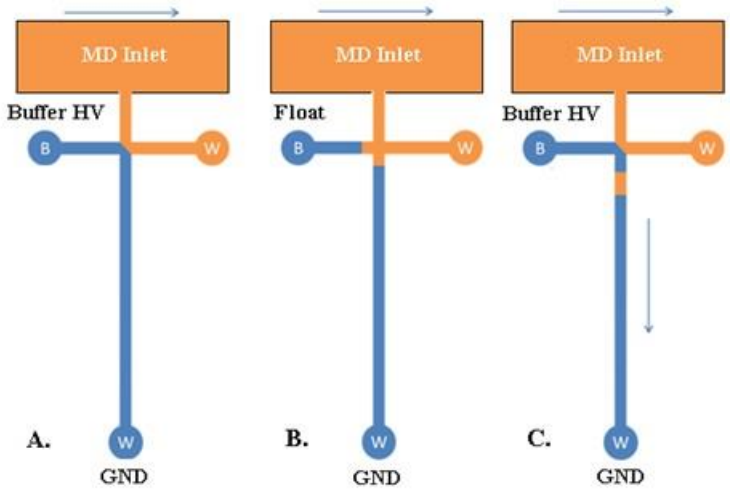

Figure 3.8: A) Similar to the T chip shown in Figure 3.7, the MD-ME interface shown here has sample applied to the top port via integration with an MD probe and run buffer added to the remaining 3 ports. A potential is applied to the run buffer reservoir (B), resulting in electroosmotic flow toward the waste ports (W), while pressure from the MD interface results in sample flow to sample waste. The MD flow must be grounded between the microdialysis probe and the ME device (not show in this diagram) to prevent electrocution. However, the distance to this ground must be longer than the distance to the ground potentials on the ME device itself to prevent a counter EOF flow. B) Buffer voltage is floated, allowing sample to be injected. C) Buffer voltage is reestablished, analyte separation proceeds.

3.11 Applications

The first report of the use of microchip electrophoresis with fluorescence detection to detect Glu in microdialysis samples came from the Robert Kennedy group, who published a study investigating amino acids with OPA derivatization [12]. These experiments had limits of detection near 200 nM and achieved a separation in 95 seconds using an all-glass microchip. By using a different chip design and high potential field, they also managed to achieve the separation in under 20 seconds. They continued this work using a segmented flow PDMS-glass microchip design and

the NDA/CN derivatization reaction [13]. This separation also occurred in under 20 seconds, and had improved limits of detection. This method was used to track the *in vivo* change of aspartate and Glu following the introduction of a glutamate transport inhibitor and microdialysis sampling. More recent work from this group has further improved separation speeds and detection limits using "water-in-oil" schemes that can provide excellent temporal resolution by derivatizing samples in discrete plugs of 8–10 nL prior to injection and separation [13].

The Susan Lunte group has also used microchip electrophoresis for Glu detection, furthering their earlier work using capillary electrophoresis to analyze amino acid neurotransmitters [14] and microchip electrophoresis to detect fluorescein in the brain [15]. This led to the development of a PDMS-glass hybrid microchip that allowed continuous, online, *in vivo* monitoring with microdialysis sampling, as shown in Figure 3.9 [16].

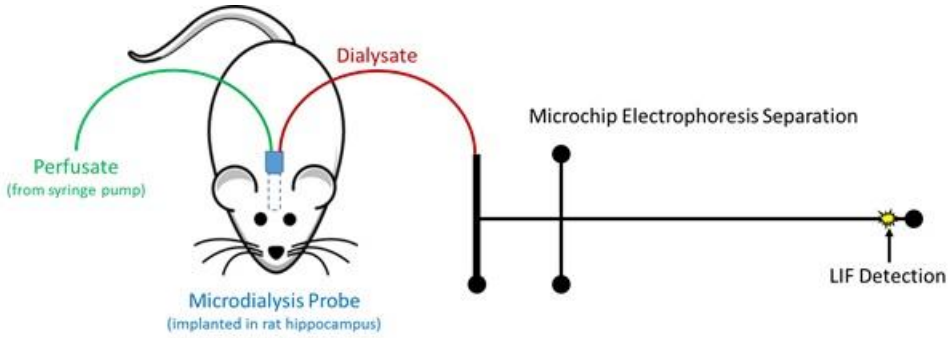

Figure 3.9: Schematic of a basic in vivo microdialysis-microchip electrophoresis system. In a brain experiment, the perfusate is normally artificial cerebrospinal fluid (aCSF) pumped at a flow rate of 1 µL/min. The derivatization reaction normally occurs between the collection of dialysate and its injection on the microchip system (not pictured).

This study used the NDA/CN reaction to detect amino acid neurotransmitters, using a 20-cm separation channel with on-chip mixing to facilitate derivatization. This method was used to study the change in concentration of fluorescein in rat brain dialysate over time, but was also capable of separating and detecting Glu. These results were expanded upon in an additional study, which improved the micromixer chip design and used a full-PDMS microchip [17]. This allowed near real-time *in vivo* monitoring of amino acid neurotransmitters, including Glu, with a 10-minute lag time. Further work has been done to design a robust and portable detection system with a light-emitting diode (LED) excitation source, shown in Figure 3.10. This will allow *in vivo* microdialysis experiments to be carried out in a medical setting, where the use of a laser excitation source is impractical. Using this system, Glu was separated from multiple other amines and detected in brain microdialysis samples derivatized using the NDA/CN reaction [6].

While the bulk of published studies involving Glu detection using microchip electrophoresis have used either NDA or OPA for derivatization, several other fluorophores have been explored. Among these, a ME-based chiral separation of D/L Glu as well as D/L Asp in rat and human cerebral spinal fluid samples was developed by Huang et al. [18]. The separation of each enantiomer was accomplished through the addition of 12 mM γ-cyclodextrin to a run buffer containing 30 mM sodium dodecylsulfate (SDS) and 25 mM sodium borate. Pre-column derivatization with fluorescein isothiocyanate (FITC) was used to label the amino acids prior to the separation on a 7.6 cm simple-T microchip, ultimately resulting in detection limits of 40 nM for D-Glu. FITC, like OPA and NDA, is selective for the amine moiety of amino acids. However, FITC is a fluorophore and is therefore fluorescent prior to derivatization, which can complicate

analysis. Additionally, the long reaction times of several hours necessary for derivatization limit its utility for rapid assays [19].

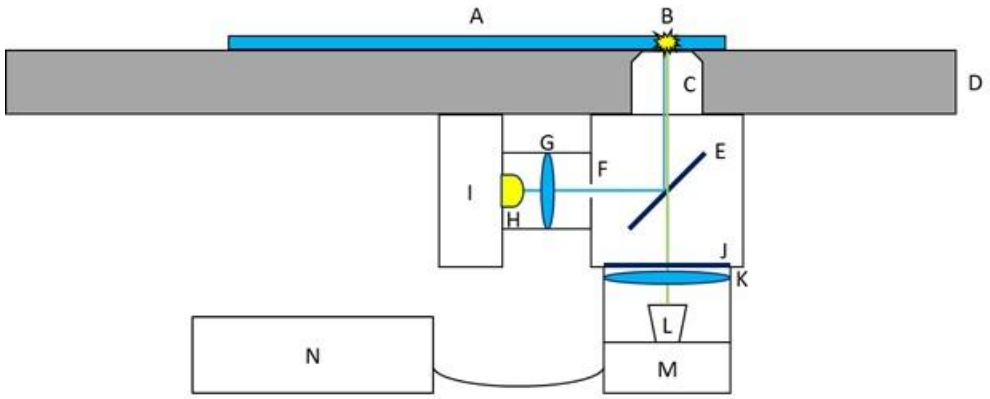

Figure 3.10: Schematic representation of portable LED excitation and fluorescence detection system. Given wavelengths are for a separation using the NDA/CN derivatization reaction. (A) Microchip. (B) In-channel detection point. (C) Focusing objective. (D) X-Y positioner. (E) Dichroic mirror. (F) Pinhole. (G) Collimating lens. (H) LED @ 445 nm. (Ii) Heat sink. (J) Long pass filter @ 470 nm. (K) Focusing lens. (L) Avalanche photodiode (APD). (M) APD power supply. (N) Lock-in amplifier and data acquisition software.

Another example of Glu detection via ME is the development of a system for *in situ* analysis of organic matter in Martian soil [20]. This method was first tested as a proof-of-concept study using soil samples from the Atacama Desert. Amino acids were first extracted and then derivatized using Pacific Blue succinimidyl ester, which is also selective for the primary amine of the amino acid. Following derivatization, an ME device with a 22.6-cm separation channel was used to separate the sample. With this system, a 200-fold increase in sensitivity was found compared to earlier techniques using fluorescamine [21]. The authors felt that the minimal increase in complexity from using a ME device was more than compensated by the smaller size, mass, and reagent use in this application.

3.12 Conclusions

Microchip electrophoresis provides an ideal platform for rapid separation of Glu as well as other neuroactive amines in neurological samples. Through either offline or online methods of sample acquisition and fluorescence derivatization, endogenous levels of Glu can be monitored in near real-time and for extended periods while simultaneously monitoring other analytes of interest, providing an important view of brain health.

Future research will focus on the development of techniques that will allow for better throughput, automation, and a wider analysis of neurobiological samples. The direct coupling of ME to continuous sampling methods still has room for improvement, as many current devices still suffer from irreproducibility and intensive fabrication procedures. This should also reduce the lag time between sampling and detection, allowing for near real-time analysis of neurobiological samples that can prove invaluable in a medical setting. There are already research efforts in this direction, such as the incorporation of microdialysis samples onto a microchip designed to be used on-animal [22]. Furthermore, expanding the scope of analytical analyses is important. Although the primary focus of this thesis is the detection of Glu, this is not the only biologically active neuromolecule that is of importance in assessing brain health. Since ME is primarily a separation technique, it has the potential to detect multiple analytes simultaneously with sufficient resolution for quantitation. Although there are other amines present in the brain that could be derivatized via the methods discussed in this chapter, a more universal method of measurement would allow for

a fuller picture of neurobiological methods. Studies coupling electrochemical sensors with ME will allow for this, but introduce their own complications regarding electrode sensitivity and robustness. Other detection schemes, such as bipolar electrochemical detection or the use of bioreactors, can also allow for a wider range of analytes to be measured in a single ME analysis.

3.13 References

1. Smithies, O., *Zone electrophoresis in starch gels: group variations in the serum proteins of normal human adults.* Biochemical Journal, 1955. **61**(4): p. 629.
2. Li, S.F.Y., *Capillary electrophoresis: principles, practice and applications*. Vol. 52. 1992: Elsevier.
3. Weinberger, R., *Practical capillary electrophoresis*. 2000: Academic Press.
4. Landers, J.P., *Handbook of capillary and microchip electrophoresis and associated microtechniques*. 2007: CRC press.
5. Ohlsson, P.D., et al., *Electrophoresis microchip with integrated waveguides for simultaneous native UV fluorescence and absorbance detection.* Electrophoresis, 2009. **30**(24): p. 4172-4178.
6. Oborny, N.J., et al., *Evaluation of a Portable Microchip Electrophoresis Fluorescence Detection System for the Analysis of Amino Acid Neurotransmitters in Brain Dialysis Samples.* Analytical Sciences, 2016. **32**(1): p. 35-40.
7. Molho, J.I., et al., *Optimization of turn geometries for microchip electrophoresis.* Analytical Chemistry, 2001. **73**(6): p. 1350-1360.
8. Paegel, B.M., et al., *Turn geometry for minimizing band broadening in microfabricated capillary electrophoresis channels.* Analytical Chemistry, 2000. **72**(14): p. 3030-3037.
9. Jacobson, S.C., A.W. Moore, and J.M. Ramsey, *Fused quartz substrates for microchip electrophoresis.* Analytical Chemistry, 1995. **67**(13): p. 2059-2063.
10. Duffy, D.C., et al., *Rapid prototyping of microfluidic systems in poly (dimethylsiloxane).* Analytical chemistry, 1998. **70**(23): p. 4974-4984.
11. Huynh, B.H., et al., *A microchip electrophoresis device with on-line microdialysis sampling and on-chip sample derivatization by naphthalene 2, 3-dicarboxaldehyde/2-mercaptoethanol for amino acid and peptide analysis.* Journal of pharmaceutical and biomedical analysis, 2006. **42**(5): p. 529-534.
12. Sandlin, Z.D., et al., *Microfluidic electrophoresis chip coupled to microdialysis for in vivo monitoring of amino acid neurotransmitters.* Analytical chemistry, 2005. **77**(23): p. 7702-7708.
13. Wang, M., et al., *Microfluidic chip for high efficiency electrophoretic analysis of segmented flow from a microdialysis probe and in vivo chemical monitoring.* Analytical chemistry, 2009. **81**(21): p. 9072-9078.
14. Zhou, S.Y., et al., *Continuous in vivo monitoring of amino acid neurotransmitters by microdialysis sampling with online derivatization and capillary electrophoresis separation.* Analytical chemistry, 1995. **67**(3): p. 594-599.
15. Huynh, B.H., et al., *On-line coupling of microdialysis sampling with microchip-based capillary electrophoresis.* Analytical chemistry, 2004. **76**(21): p. 6440-6447.
16. Nandi, P., D.P. Desai, and S.M. Lunte, *Development of a PDMS-based microchip electrophoresis device for continuous online in vivo monitoring of microdialysis samples.* Electrophoresis, 2010. **31**(8): p. 1414-1422.

17. Nandi, P., et al., *Development and optimization of an integrated PDMS based-microdialysis microchip electrophoresis device with on-chip derivatization for continuous monitoring of primary amines.* Electrophoresis, 2013. **34**(6): p. 895-902.
18. Huang, Y., M. Shi, and S. Zhao, *Quantification of D-Asp and D-Glu in rat brain and human cerebrospinal fluid by microchip electrophoresis.* Journal of separation science, 2009. **32**(17): p. 3001-3006.
19. Maeda, H., et al., *Reaction of fluorescein-isothiocyanate with proteins and amino acids.* The Journal of Biochemistry, 1969. **65**(5): p. 777-783.
20. Chiesl, T.N., et al., *Enhanced amine and amino acid analysis using Pacific Blue and the Mars Organic Analyzer microchip capillary electrophoresis system.* Analytical chemistry, 2009. **81**(7): p. 2537-2544.
21. Skelley, A.M., et al., *Organic amine biomarker detection in the Yungay region of the Atacama Desert with the Urey instrument.* Journal of Geophysical Research: Biogeosciences, 2007. **112**(G4).
22. Scott, D.E., et al., *Development of an on-animal separation-based sensor for monitoring drug metabolism in freely roaming sheep.* Analyst, 2015. **140**(11): p. 3820-3829.

4. Evaluation of a Portable Microchip Electrophoresis Fluorescence Detection System for the Analysis of Amino Acid Neurotransmitters in Brain Dialysis Samples

Nathan J. Oborny,[1,2] Elton E. Melo Costa,[2,3] Leena Suntornsuk,[2,4] Fabiane C. Abreu, [3] and Susan M. Lunte[1,2,5,†]

Republished with permission from "Evaluation of a Portable Microchip Electrophoresis Fluorescence Detection System for the Analysis of Amino Acid Neurotransmitters in Brain Dialysis Samples", Analytical Sciences, Vol 32 (2016) No. 1, p. 35-40[1]

[1]*Department of Bioengineering, University of Kansas, Lawrence, KS, 66045 USA*

[2]*Ralph N. Adams Institute for Bioanalytical Chemistry, University of Kansas, Lawrence, KS, 66047 USA*

[3]*Institute of Chemistry and Biotechnology, Federal University of Alagoas, Alagoas, Brazil*

[4]*Department of Pharmaceutical Chemistry, Faculty of Pharmacy, Mahidol University, Bangkok, Thailand*

[5]*Department of Chemistry, University of Kansas, Lawrence, KS, 66045 USA*

[†] To whom correspondence should be addressed.

E-mail: slunte@ku.edu

4.1 Introduction

Microdialysis (MD) is a popular *in vivo* sampling method that has been used to monitor neurotransmitters in both animal models and humans. In particular, microdialysis sampling has been employed to monitor chemicals in the brains of traumatic brain injury patients in intensive-care units (ICU). MD sampling can also be used to monitor the extent of tissue damage and the efficacy of treatment simultaneously through continuous and long-term sampling of multiple biomarkers [2-4].

The process of a MD sampling has been described elsewhere extensively [5-7], and in chapters 3 and 5 of this thesis. Of relevance here, however, is the fact that the recovery of any analyte of interest is governed by the flow rate of the perfusate liquid [8]. At a flow rate of 1 µL/min, typical analyte recoveries for small molecules are in the range of 10 – 40%. Lower flow rates result in higher analyte recoveries, approaching 100% at 100 nL/min, but with smaller volumes of dialysate collected per unit time [9, 10]. This tradeoff dictates which analytical technique can be used and how often analysis can be performed.

Typically, MD samples are collected until sufficient volumes are acquired to allow the use of the desired analytical method with requisite sensitivity and selectivity. The most common method employed for the analysis of microdialysis samples is liquid chromatography (LC) coupled to electrochemical, fluorescence, mass spectrometry (MS), or absorbance detection [11]. However, the time required to obtain a dialysate sample large enough for many LC-based assays can reduce the temporal resolution of the technique as well as add a significant delay between the sample

acquisition and clinical response. In order to address a clinical need for an analytical technique that can continuously analyze small volume samples, and selectively detect very low analyte concentrations with good temporal resolution, several groups have developed on-line MD methods using capillary (CE) and microchip electrophoresis (ME) [12, 13]. These systems, when combined with a sensitive detection method, such as laser- (or light emitting diode-) induced fluorescence (ME-LIF and ME-LEDIF), can rapidly analyze nanoliter-volume samples in a continuous manner, while providing clinicians with near real-time data.

There are many examples concerning the use of CE to monitor amino acid neurotransmitters in microdialysis samples,[14-19] and other examples have been reviewed by Poinsot *et al.* [20], as well as chapters 2 and 3 of this thesis However, these systems typically use off-line sample collection and precolumn derivatization, requiring samples large enough to be handled accurately off-line. Coupling CE or ME directly to MD makes it possible for much smaller samples volumes to be analyzed, leading to better temporal resolution as long as the method displays the requisite sensitivity [21] To this end, our group previously developed a polydimethylsiloxane (PDMS)-based microchip electrophoresis device that was coupled to microdialysis (MD-ME) for the continuous on-line monitoring of amino acid neurotransmitters [18, 19]. The microchip was completely integrated with the MD sampling system, which provided on-line derivatization of the amino acids with naphthalene-2,3-dicarboxyaldehyde/cyanide (NDA/CN^-), a flow-gate interface for injection, and electrophoresis separation using a serpentine channel with LIF detection. Although the chip itself was small, the associated instrumentation needed for fluorescence detection was quite large, and thus not amenable to a clinical setting.

The aim of the present work is to expand on the theme of miniaturization and integration of the on-line MD-ME-LIF device with the goal to obtain a system that can be used for the near real-time monitoring of amine-based neurotransmitters in the ICU or research laboratory. The particular focus of this report is miniaturization of the fluorescence detection system. To evaluate the system, figures of merit for the separation and detection of several NDA/CN-derivatized amines commonly found in rat brain dialysate were determined using a conventional benchtop ME-LIF system employing an epifluorescence microscope. These results were then compared to those obtained using the newly developed portable ME-LEDIF system. The portable system described here could potentially be placed near patients in an ICU (or next to animals for animal studies), permitting continuous near real-time monitoring of these neuroactive amines in injured brain tissue to assess damage and to monitor treatment.

4.2 Experimental

4.2.1 Reagents and Chemicals

Arginine (Arg), aspartate (Asp), citrulline (Cit), glutamate (Glu), histamine (Hist), and taurine (Tau) were obtained from Sigma Aldrich (St. Louis, MO). Standards of each amine were prepared at 2 mM concentrations in 18.2 MΩ /cm deionized water (Millipore, Billerica, MA). Subsequent dilutions of each stock solution were made prior to analysis. Naphthalene-2,3-dicarboxaldehyde (NDA) (Invitrogen, Carlsbad, CA) was prepared in acetonitrile (Fisher Scientific, Pittsburgh, PA) to a concentration of 5 mM. Sodium cyanide (NaCN) (Sigma Aldrich) was dissolved in water to a final concentration of 10 mM. Stock solutions of both NDA and NaCN were made weekly and stored at 4ºC, while being protected from light exposure. Stock solutions of sulfobutylether-β-

cyclodextrin (SBEC) (Life Technologies, Grand Island, NY) were made on a weekly basis to a concentration of 10 mM in deionized water, and stored at 4ºC. The background electrolyte (BGE) consisted of 1.4 mM SBEC, 10% by volume HPLC-grade dimethylsulfoxide (Fisher Scientific), and sodium tetraborate (Sigma Aldrich) at a final concentration of 15 mM. Finally, the pH of the BGE was measured using a pH meter and adjusted to 9.2 with 1 M sodium hydroxide (Fisher Scientific).

4.2.2 Animal Surgery and Microdialysis Sampling

Male Sprague-Dawley rats were housed in temperature-controlled rooms with free access to food and water prior to surgery. Rats were fully anesthetized prior to surgery through inhalation of isofluorane, followed by the injection of a mixture of ketamine (67.5 mg/kg), xylazine (3.4 mg/kg), and acepromazine (0.67 mg/kg). To maintain anesthesia throughout the surgery, doses of ketamine were administered by intramuscular injections. The body temperature was maintained using a Homeothermic Blanket Control unit (Harvard Apparatus, Holliston, MA) set at 37°C, and rats were given saline doses to keep them hydrated. All surgical instruments were sterilized before usage and after the surgical procedures. A guide cannula followed by a microdialysis probe with a 4 mm membrane was inserted in the striatum region at stereotaxic coordinates A/P +0.7, M/L -– 2.7, V/D –3.4 [18, 22]. Microdialysis samples were collected by perfusing the probe (CMA, North Chelmsford, MA) with an artificial spinal fluid (aCSF) at 1 µL/min. Animal experiments were performed in accordance with regulations of the Institutional Animal Care and Use Committee (IACUC) at the University of Kansas, which operates under accreditation from the Association for Assessment and Accreditation of Laboratory Animal Care (AAALAC).

4.2.3 Derivatization Reaction

Derivatization of the amino acid standards and MD sample was carried out using equal parts by volume of 5 mM NDA and 10 mM NaCN, 15 mM boric buffer (pH 9.2), and sample. NDA reacts with primary amines in the presence of cyanide to produce fluorescent 1-cyanobenz[f]isoindole (CBI) products.

4.2.4 Microchip Electrophoresis (ME)

The glass microfluidic devices used in these studies were fabricated using standard photolithographic techniques, as reported previously [23, 24]. To separate the six target analytes, a 15-cm serpentine separation channel with 3-cm side channels (Figure 4.1) was used. All channels were 15 μm deep and approximately 70 μm wide. Before each use, the chip was conditioned with 0.1 M HCl, water, 0.1 M NaOH, and then water again. Each solution was passed through the microchannels for 10 min via the application of negative pressure to one of the ports. Finally, the channels were filled with BGE using the same negative pressure procedure prior to use.

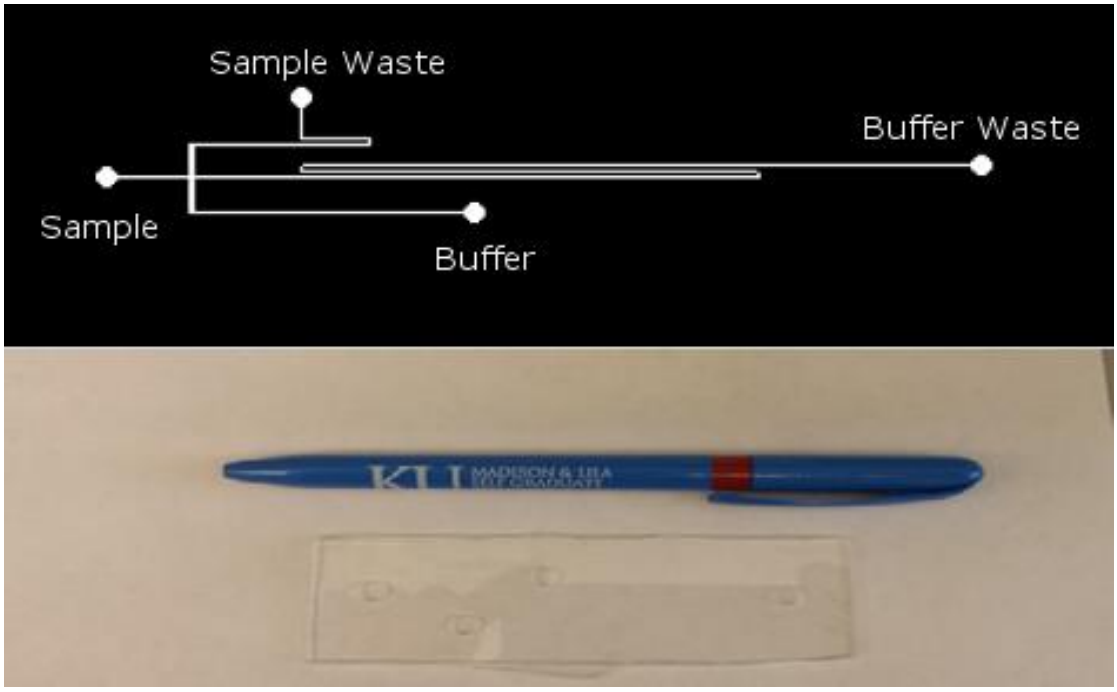

Figure 4.1:Top: 15 cm-length serpentine chip design with 2.7 cm-length side channels for sample waste and buffer, 0.5 cm length for sample inlet. All channels were 15 µm deep by 70 µm wide. Bottom: Actual glass chip used in these studies.

An UltraVolt HV Rack high-voltage power supply (Ronkonkoma, NY) was employed for the electrophoresis experiments and controlled by software written in Labview (National Instruments, Austin, TX). In these experiments, a voltage of 10 kV was applied at the buffer reservoir and 7 kV at the sample reservoir for an overall separation field strength of 420 V /cm. For sample electrokinetic injection, the injection time was 0.7 s and the analysis time lasted

420 s.

4.2.5 Benchtop ME-LIF System

Fluorescence was chosen as the detection method in these studies because it provides high sensitivity and, in the case of NDA/CN derivatization, selectivity for primary amines [25]. The cyanobenz(f)isoindole products of the NDA/CN reaction exhibit two excitation maxima in the visible range at approximately 420 nm and 442 nm [26, 27]. For the benchtop ME system used in these studies, excitation was accomplished using either a 445 nm PhoxX diode laser (Market Tech, Scotts Valley, CA) or a 442 nm CL-2000 diode laser (Crystal Laser, Reno, NV). The excitation light source was coupled to an epifluorescence microscope (Nikon, Melville, NY) via a fiber optic cable; it was optically filtered using a 445 nm band pass filter, and was focused on the separation channel approximately 0.2 cm from the waste reservoir via a long-pass dichroic mirror that directed the light to the chip and a 40× objective lens to focus onto the channel. The emission maxima for the products of the NDA/CN reaction occurs at 490 nm [26]. Once again, the epifluorescence microscope was used to focus the emission light through the long-pass dichroic mirror and long-pass edge filter (480 nm cutoff) before it was focused onto a photomultiplier tube (PMT). Signal acquisition from the PMT was performed using a National Instruments NI USB-6229 data acquisition card and Labview software, following amplification and low pass filtering with a 3 Hz filter cutoff using a model SR570 amplifier from Stanford Research Systems (Sunnyvale, CA). Origin software version 8.2 (Origin Lab Corporation, Northampton, MA) was used to analyze the subsequently collected data.

4.2.6 Portable ME-LEDIF System

The portable system has many commonalities with the benchtop ME system but also has several differences. As in the benchtop ME, fluorescence detection was accomplished by filtering and focusing excitation light onto the separation channel, followed by filtering and focusing subsequently emitted light onto a detector. However, in the case of the portable system, a 420 nm LED (LED Engin, San Jose, CA) was used instead of a laser. The LED was powered using a custom current driver circuit and constructed using a frequency-controlled variable current driver, a MAX16836 (Maxim Integrated, San Jose CA), driven by an LM555 timer IC (Texas Instruments). It was found that an input signal of 1.6 kHz resulted in a stable current output of 250 mA.

A microscope stage purchased from eBay is shown mounted in Figure 4.2. This stage, which was originally designed to be motor driven, was modified using 3D-printed motor brackets to couple two NEMA 17 stepper motors to the stage. This allowed controlled movement in the X and Y directions as the optics mount moved along threaded rods while fixing the Z direction, such that the channel was at the focal point of a 100x objective. These motors were subsequently driven by a stepper motor driver shield for the Arduino microcontroller or, alternatively, could be manually adjusted.

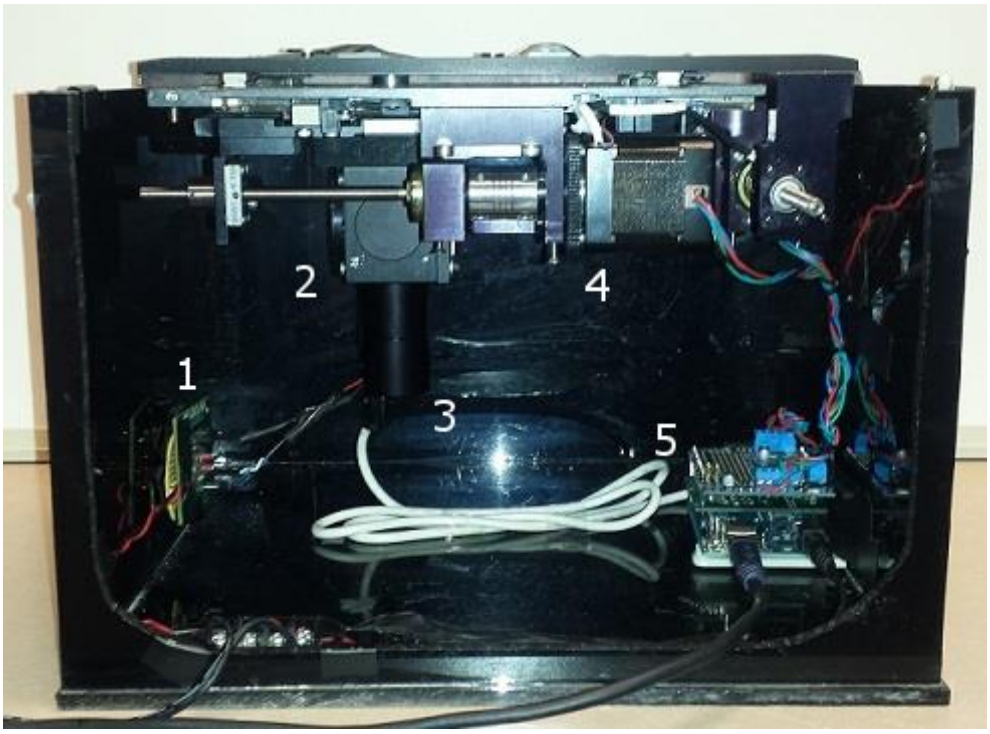

Figure 4.2A: Close-up view of the portable system. 1. LED current driver board. 2. Optical mounting containing dichroic mirror, LED, objective lens, and optical filter. 3. Photodiode and preamplifier board. 4. Positioning motors, seen here from the side. 5. Arduino microcontroller with stacked motor driver shield and amplifier and analog to digital converter shield connected to preamplifier via white USB cable. The system itself measures 12" wide x 11" deep x 8" tall and weighs approximately 10 lbs.

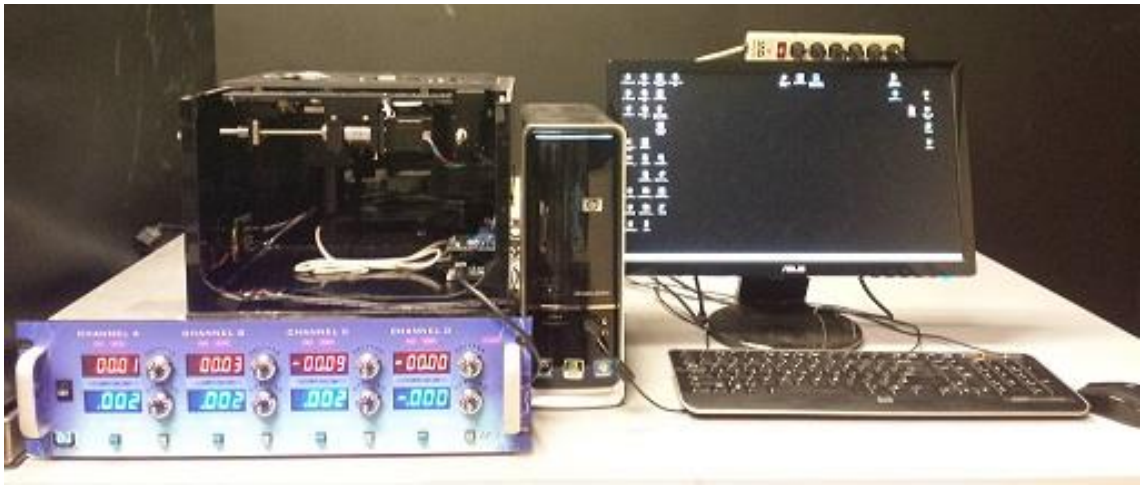

Figure 4.3B: Portable system shown with Ultravolt high voltage supply and PC for scale.

As mentioned previously, an LED was employed as the excitation light source in the portable system and was mounted parallel to the chip. This LED was collimated using a plano-convex lens, followed by spatial focusing via a 1 mm pinhole. The light from the LED was directed upward through an objective lens via a long-pass dichroic mirror with a 470 nm cutoff (Thorlabs, Newton, NJ) and mounted at a 90° angle. Emission light was focused via the same objective lens through the long-pass dichroic mirror followed by a long-pass emission filter and was finally focused onto a detection point using a second plano-convex lens, model LA1951-A-N-BK7 (Thorlabs). The final long-pass emission filter also had a cutoff of 470 nm (Thorlabs, Newton, NJ), allowing light of any longer wavelength to pass on to the detector.

The detector itself consisted of an OPT301 combination transimpedance amplifier/silicon photodiode (Texas Instruments, Dallas, TX) in a custom circuit, mounted on a 1"-dia printed circuit board (PCB). This PCB was subsequently mounted in the optics holder, such that the OPT301 was centered at the focal point of the plano-convex lens. This PCB was connected to the secondary amplifier via a 4-pin shielded USB cable, which also supplied the OPT301 with power. Finally, the output of the OPT301 was amplified by a custom second-stage amplifier circuit using an OPA726 IC (Texas Instruments) before passing the amplified signal to an analog-to-digital (ADC) converter, a Max11210 IC (Maxim Integrated). The secondary amplification and ADC circuit was designed in the format of an Arduino shield, which allowed it to be easily interfaced with the open source Arduino Uno Microcontroller used for signal processing as well as communication to a nearby PC via USB. While future versions of the portable system will have an integrated high-

voltage power supply for the separation as well as electrokinetic gates, the system used for this study relied on the UltraVolt HV Rack high-voltage power supply previously mentioned.

4.3 Results and Discussion

The on-line integration of MD to an analysis method, such as ME-LEDIF, has the potential to provide clinicians and animal researchers with minute-to-minute data regarding the tissue health of patients, or to track changes in neurotransmitters in animal models. While several groups have successfully coupled MD to both CE [24] and ME,[13, 18] in practice, the benefits of doing so have been limited by the size of the associated equipment needed for the separation and detection. In an already crowded intensive-care unit or neurobiology laboratory, this is a significant concern, because any increased distance from the patient or animal could result in a significant delay in response due to low sample flow rates from the MD probe to the microchip. The goal of miniaturizing and creating the self-contained ME-LIF system described here is to reduce the time-lag between sampling and analysis as well as the overall size of the external equipment necessary. The aim is to create a small, portable detection system that can be placed near the patient or animal for near real-time monitoring.

To miniaturize the system as much as possible, several design decisions were made. The first of these was the choice of an LED excitation light source rather than a laser. There are three reasons for this. First, lasers are considerably more expensive than LEDs. Second, the mechanical robustness of the overall design was a consideration for portability and, typically, lasers are more

fragile than LEDs. Finally, while we focused on NDA/CN derivatization in this study, the easy availability of a wide range of LED wavelengths for use in future studies with other fluorogenic compounds also influenced our decision to use an LED light source.

The requirements of portability and ruggedness also affected the physical/mechanical design of the system. Because microchip sizes and designs vary from application to application, and also because it is often necessary to move the chip for cleaning purposes, the alignment of the optics to the channel needs to be moveable in this portable system, unlike those of other miniaturized systems [22]. Because a high-voltage supply with wires leading to each port on the chip was necessary, moving the optics rather than the chip is the better option in order to avoid dislodging any of the high-voltage wires during alignment.

The use of the OPT301 photodiode for detection is another feature of this instrument. Other portable fluorescence detection systems [28, 29] have used a more sensitive, but ultimately more complex and costly PMT for detection. In this application, however, the use of a photodiode was adequate for the LODs required in these studies, and simplified the design by eliminating the need for a high-voltage supply for the PMT.

To evaluate the portable system for determining the amines in microdialysis samples, it was necessary to compare the function of a traditional benchtop ME-LIF system to the portable ME-LEDIF system for the same set of analytes. For this purpose, a mixture of six neuroactive amines (arginine (Arg), citrulline (Cit), taurine (Tau), histamine (Hist), glutamate (Glu) and aspartate

(Asp)) were derivatized using NDA/CN and electrophoretically separated using microchip electrophoresis. For each amine, the linearity over a range of physiologically relevant concentrations **(**Table 4.1**)** as well as the limits of detection (LOD) and the limits of quantification (LOQ) were determined using both systems. Following this, rat brain microdialysis samples were derivatized using NDA/CN, and analyzed on both systems. For the purposes of these proof-of-concept tests, all samples were derivatized off-line for 30 min prior to separation.

	Arg	Cit	Tau	Hist	Glu	Asp
Physiological Range [5, 30-32]	0.6-1.5µM	0.4-1µM	5-20µM	4.7-6.7nM	8-22 µM	0.8-1.6 µM
Benchtop system						
Calibration range/µM	0.1–10	0.1–10	0.1–10	0.1–10	0.1–10	0.1–10
Regression coefficient (R^2)	0.9956	0.9897	0.9940	0.9990	0.9792	0.9854
Limit of detection (S/N = 3) /µM	0.05	0.05	0.05	0.05	0.25	0.05
Limit of quantification (S/N = 10) /µM	0.15	0.15	0.15	0.15	1.0	0.15
Migration Time % RSD	1.81	1.46	1.26	1.34	1.85	2.61
Theoretical Plates /m	746485	693960	872808	473232	565178	600081
Peak Resolution	1.29	1.16	0.97	1.15	1.10	0.15
Portable system						
Calibration range/µM	2.0–50	2.0–50	2.0–25	2.0–15	2.0–50	2.0–50
Regression coefficient (R^2)	0.9956	0.9834	0.9870	0.9977	0.9931	0.9904
Limit of detection (S/N = 3) /µM	0.25	0.36	0.42	0.37	1.31	1.21
Limit of quantification (S/N = 10) /µM	0.84	1.2	1.4	1.24	4.35	4.04
Migration Time % RSD	1.71	1.8	2.52	3.22	4.75	5.23
Theoretical Plates /m	275165	270431	331367	406943	325993	277798
Peak Resolution	2.53	0.96	1.01	6.09	2.00	3.08

Table 4.1: Performance Parameters for the Benchtop and Portable LIF Systems

As can be seen in Table 4.1, both systems exhibited a linear response over the physiologically relevant concentration ranges. The LOD for each amine can be found in Table 4.1. The LODs were lower for the benchtop ME-LIF, mainly due to the use of a PMT instead of a photodiode. Five of the six amines (Arg, Cit, Tau, Glu and Asp) could be detected, and were present above the LODs determined with the portable system. The concentrations of aspartate and histamine were below

the calculated LOQs and, in the case of Hist, below the LOD. A peak that co-migrated with Hist was consistently visible in the electropherogram and identified via standard Hist spiking. The presence of this peak in the MD sample implies two possibilities. The first is that a substantial increase in extracellular Hist occurred due to tissue inflammation as a result of probe insertion [31]. The second is the co-migration of an as yet unknown analyte to be identified in future studies. However, even though the benchtop ME-LIF system exhibited lower LODs (and LOQs) for five of the six amines, the performance of the portable system was adequate for their detection at physiologically relevant concentrations. Figure 4.4 (Bottom) shows an electropherogram obtained with the portable system for a representative microdialysis sample and (Top) the same sample spiked with 5 μM (final concentration) of amine standards. In this study, identification of the peaks was based on migration time and spiking with standard solutions.

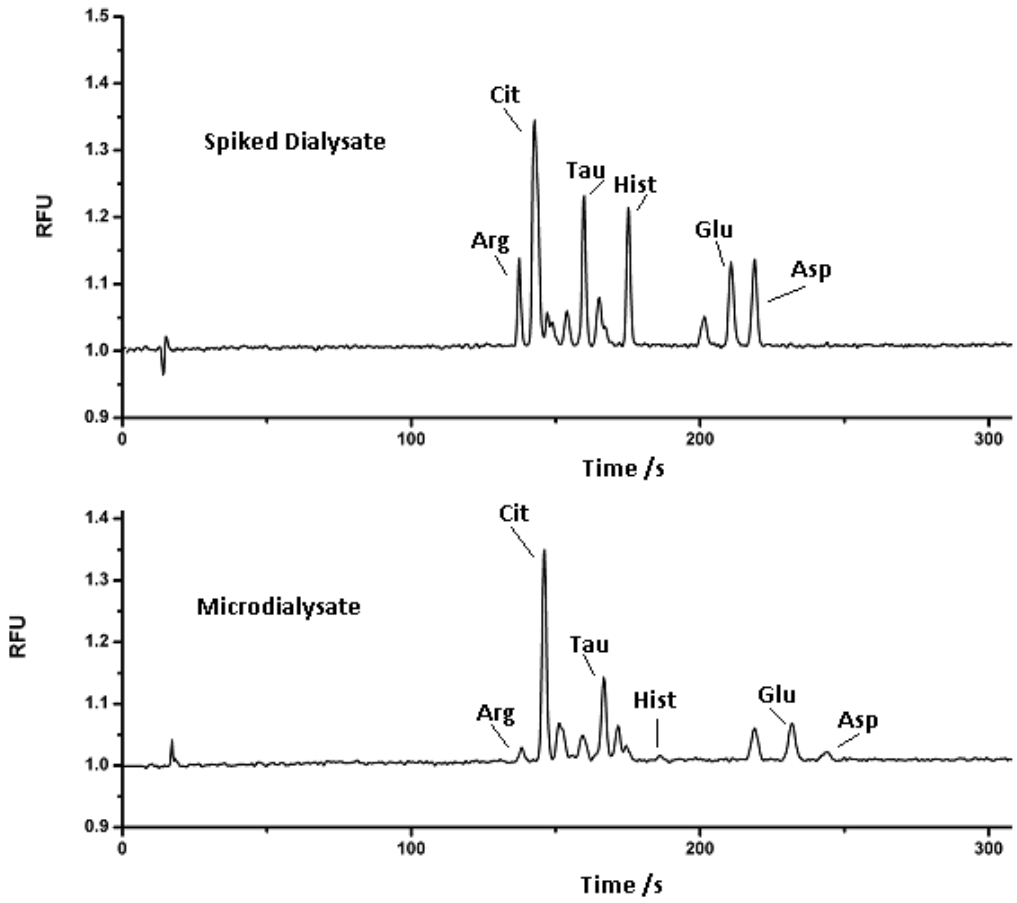

Figure 4.4: (Top) MD Sample spiked with an additional 5 µM Arg, Cit, Tau, Hist, Glu, and Asp. (Bottom) Electropherogram of a NDA/CN-derivatized microdialysate sample from striatum using the portable system.

4.4 Future Work

Future versions of the system will address the need for automated positioning and variable chip sizes as well as further decreases in the overall size of the system, which was larger than necessary in this design for convenience. As mentioned, the LOQs for two of the target analytes were too high for quantification in the microdialysis sample. In order to improve these LODs/LOQs, a programmable integrated circuit (PIC)-based (Microchip, Chandler, AZ) lockin-amplifier system is being developed for fluorescence detection and integrated into the system along

with a high-voltage module for sample separation. The use of lower microdialysis flow rates and on-line derivatization to enhance analyte recovery and fluorescence product formation, respectively, are also being investigated. Finally, future studies will be conducted using online MD-ME sampling to look at amine changes in a rat ischemia model.

4.5 References

1. Oborny, N.J., et al., *Evaluation of a Portable Microchip Electrophoresis Fluorescence Detection System for the Analysis of Amino Acid Neurotransmitters in Brain Dialysis Samples.* Analytical Sciences, 2016. **32**(1): p. 35-40.
2. Deibert, E. and M.N. Diringer, *THE INTENSIVE CARE MANAGEMENT OF ACUTE ISCHEMIC STROKE.* The Neurologist, 1999. **5**(6): p. 313-325.
3. Kirkman, M.A., G. Citerio, and M. Smith, *The intensive care management of acute ischemic stroke: an overview.* Intensive care medicine, 2014. **40**(5): p. 640-653.
4. Persson, L. and L. Hillered, *Chemical monitoring of neurosurgical intensive care patients using intracerebral microdialysis.* Journal of neurosurgery, 1992. **76**(1): p. 72-80.
5. Benveniste, H., *Brain microdialysis.* Journal of neurochemistry, 1989. **52**(6): p. 1667-1679.
6. Westerink, B.H. and T.I. Cremers, *Handbook of microdialysis: methods, applications and perspectives*. Vol. 16. 2007: Academic Press.
7. Robinson, T.E. and J.B. Justice, *Microdialysis in the neurosciences: techniques in the behavioral and neural sciences*. Vol. 7. 2013: Elsevier.
8. Stenken, J.A., et al., *Examination of microdialysis sampling in a well-characterized hydrodynamic system.* Analytical chemistry, 1993. **65**(17): p. 2324-2328.
9. Nandi, P. and S.M. Lunte, *Recent trends in microdialysis sampling integrated with conventional and microanalytical systems for monitoring biological events: a review.* Analytica chimica acta, 2009. **651**(1): p. 1-14.
10. Menacherry, S., W. Hubert, and J.B. Justice Jr, *In vivo calibration of microdialysis probes for exogenous compounds.* Analytical chemistry, 1992. **64**(6): p. 577-583.
11. Davies, M.I., et al., *Analytical considerations for microdialysis sampling.* Advanced drug delivery reviews, 2000. **45**(2): p. 169-188.
12. Zhou, S.Y., et al., *Continuous in vivo monitoring of amino acid neurotransmitters by microdialysis sampling with online derivatization and capillary electrophoresis separation.* Analytical chemistry, 1995. **67**(3): p. 594-599.
13. Sandlin, Z.D., et al., *Microfluidic electrophoresis chip coupled to microdialysis for in vivo monitoring of amino acid neurotransmitters.* Analytical chemistry, 2005. **77**(23): p. 7702-7708.
14. Tůma, P., et al., *Large-volume sample stacking for in vivo monitoring of trace levels of γ-aminobutyric acid, glycine and glutamate in microdialysates of periaqueductal gray matter by capillary electrophoresis with contactless conductivity detection.* Journal of Chromatography A, 2013. **1303**: p. 94-99.
15. Lorenzo, M., et al., *Optimization and validation of a CE-LIF method for amino acid determination in biological samples.* Journal of pharmaceutical and biomedical analysis, 2013. **73**: p. 116-124.
16. Male, K.B. and J.H. Luong, *Derivatization, stabilization and detection of biogenic amines by cyclodextrin-modified capillary electrophoresis–laser-induced fluorescence detection.* Journal of Chromatography A, 2001. **926**(2): p. 309-317.
17. Liu, X., L.-X. Yang, and Y.-T. Lu, *Determination of biogenic amines by 3-(2-furoyl) quinoline-2-carboxaldehyde and capillary electrophoresis with laser-induced fluorescence detection.* Journal of Chromatography A, 2003. **998**(1): p. 213-219.

18. Nandi, P., D.P. Desai, and S.M. Lunte, *Development of a PDMS-based microchip electrophoresis device for continuous online in vivo monitoring of microdialysis samples.* Electrophoresis, 2010. **31**(8): p. 1414-1422.
19. Nandi, P., et al., *Development and optimization of an integrated PDMS based-microdialysis microchip electrophoresis device with on-chip derivatization for continuous monitoring of primary amines.* Electrophoresis, 2013. **34**(6): p. 895-902.
20. Poinsot, V., C. Bayle, and F. Couderc, *Recent advances in amino acid analysis by capillary electrophoresis.* Electrophoresis, 2003. **24**(22-23): p. 4047-4062.
21. Saylor, R.A. and S.M. Lunte, *A review of microdialysis coupled to microchip electrophoresis for monitoring biological events.* Journal of Chromatography A, 2015. **1382**: p. 48-64.
22. Mayer, A.P., I. Osorio, and C.E. Lunte, *Microperfusion of 3-MPA into the brain augments GABA.* Epilepsy & Behavior, 2013. **29**(3): p. 478-484.
23. Coltro, W.K.T., S.M. Lunte, and E. Carrilho, *Comparison of the analytical performance of electrophoresis microchannels fabricated in PDMS, glass, and polyester-toner.* Electrophoresis, 2008. **29**(24): p. 4928-4937.
24. Linz, T.H., C.M. Snyder, and S.M. Lunte, *Optimization of the Separation of NDA-Derivatized Methylarginines by Capillary and Microchip Electrophoresis.* Journal of laboratory automation, 2012. **17**(1): p. 24-31.
25. Culbertson, C.T., et al., *Micro total analysis systems: Fundamental advances and biological applications.* Analytical chemistry, 2013. **86**(1): p. 95-118.
26. De Montigny, P., et al., *Naphthalene-2, 3-dicarboxyaldehyde/cyanide ion: a rationally designed fluorogenic reagent for primary amines.* Analytical Chemistry, 1987. **59**(8): p. 1096-1101.
27. Melanson, J.E. and C.A. Lucy, *Violet (405 nm) diode laser for laser induced fluorescence detection in capillary electrophoresis.* Analyst, 2000. **125**(6): p. 1049-1052.
28. Mora, M.F., A.M. Stockton, and P.A. Willis, *Microchip capillary electrophoresis instrumentation for in situ analysis in the search for extraterrestrial life.* Electrophoresis, 2012. **33**(17): p. 2624-2638.
29. Culbertson, C.T., et al., *Microchip separations in reduced-gravity and hypergravity environments.* Analytical chemistry, 2005. **77**(24): p. 7933-7940.
30. Alabadí, J.A., et al., *7-Nitroindazole, a selective inhibitor of nNOS, increases hippocampal extracellular glutamate concentration in status epilepticus induced by kainic acid in rats.* Brain research, 1999. **839**(2): p. 305-312.
31. Adachi, N., et al., *Direct evidence for increased continuous histamine release in the striatum of conscious freely moving rats produced by middle cerebral artery occlusion.* Journal of Cerebral Blood Flow & Metabolism, 1992. **12**(3): p. 477-483.
32. Böckelmann, R., et al., *Influence of nitric oxide synthase activity on amino acid concentration in the quinolinate lesioned rat striatum: A microdialysis and histochemical study.* Amino acids, 2000. **19**(2): p. 423-437.

5. **The design, modeling and construction of a microfluidic device coupled to microdialysis for integrated sample derivatization and electrophoretic separation**

5.1 Introduction

The relationship between patient outcomes and the initial severity of a traumatic brain injury (TBI) has long been established. An increase in injury severity directly leads to a decrease in likelihood of patient survival [1]. In recent years, it has become clear that TBI patients are at further risk of secondary tissue damage including inflammation, interruption of cellular metabolism, and hypoxia that lead to localized cell death [2]. Immediately following a TBI, these processes are initiated and behave in a self-reinforcing manner. As inflammation and intracranial pressure increase, oxygenated blood flow to tissue decreases, resulting in hypoxia and limiting glucose availability. The resulting deficit in ATP production leads to the destabilization of cellular membranes, the release of the excitatory amino acid neurotransmitters glutamate (Glu) and aspartate (Asp), and an influx of Ca^{2+} and Na^{+} ions. The influx of these ions ultimately results in apoptosis or necrosis of the neuron. As the neuron dies, the release Glu and Asp into the extracellular space causes the cycle to spread as nearby neurons are affected [3-6].

In an intensive care unit, a variety of methods are used to monitor patient health including sensors that measure partial oxygen pressure and pH to monitor tissue hypoxia [7]. Biomarkers of metabolism, such as glucose, lactate and pyruvate as well as neurotransmitters implicated in neuronal death such as Glu, have been monitored by biosensors [8] and by microdialysis coupled to liquid chromatography or enzymatic reactions [9]. These techniques allow a clinician to monitor tissue health in near real time. If microdialysis sampling is employed, it is possible to evaluate changes in several biomarkers simultaneously. Microdialysis also makes it possible to administer

a drug directly to the site of tissue damage, making it extremely attractive as a technique. Microdialysis sampling functions by passing a sterile fluid, isotonically matched to the environment being sampled and known as the perfusate, into a dialysis probe. As the fluid enters the probe, it can interact with the environment outside via a porous membrane. As analytes, smaller than the pore size of the membrane diffuse into the sterile diffusate, the fluid, now referred to as the perfusate, is withdrawn from the probe for analysis.

Microdialysis can sample virtually any set of analytes from a single location provided they are less than a given size dictated by the pores of the microdialysis probe. Microdialysis sampling, however, has the disadvantage of being a largely diffusion limited process with sample recovery highly dependent on flow rate. For example, at a fluid flow rate of 1 µL/min, analyte recovery is limited to approximately 40%, reaching 100% recovery at a flow rate of 0.1 µL/min [10]. In practice, this has the consequence that if a target analyte exists at a very low concentration, sampling must either be performed for extended period at a low flow rate to obtain enough of the analyte to be analyzed, or very sensitive assays must be employed. Small sample volumes can also be a limiting factor for timely measurements. Since flow rates from microdialysis are on the order of 0.1-1 µL/min, gathering 10 µL of sample can take between 10 and 100 minutes. Finally, such small volumes can be a challenge to manage. The most commonly used microdialysis system in hospital settings, the ISCUS Flex Microdialysis Analyzer for reference, is typically used at a flow rate of 0.3 µL/min and requires 8 µL of sample per single measurement of Glu concentration [11, 12] implying a minimum time lag of 26 minutes between measurements.

With this in mind, recent work has led to the development of capillary and microchip electrophoresis (CE and ME respectively) assays coupled to microdialysis (MD-CE and MD-ME). These techniques have the benefit of having extremely low sample dispersion and ability to handle samples on the order of tens of nanoliters (nL) in volume. Efforts to interface MD to ME and CE have demonstrated a decrease in overall time lag from sample acquisition to analysis to minutes [13].

As mentioned in chapter 1 increasing extracellular concentrations of Glu and Asp following TBI are not only biomarkers of spreading secondary damage but are also implicated as causative agents of that damage. This has, of course, made them attractive targets for monitoring as well as targets of pharmaceutical intervention. The fact that neither Glu nor Asp are electroactive or fluorescent complicates detection however, leading to the requirement of enzymatic biosensors [8], colorimetric assays [14], or fluorescence derivatization [13]. With regard to the latter technique, derivatization with a fluorogenic compound such as naphthalene-2,3-dicarboxaldehyde (NDA) is a common procedure for derivatizing primary amines, such as amino acids, rendering them fluorescently active.

The process of derivatization can be performed either offline, in which a sample is reacted with NDA and a nucleophile such as sodium cyanide (CN) or 2-mercaptoethanol (2ME) [13] prior to injection into a CE or ME system for analysis, or online where the derivatization occurs on chip after the sample is introduced. Online derivatization has the advantage that much smaller volumes of liquid can be handled as samples collected via microdialysis are derivatized and subsequently

analyzed all within a single device. This prevents sample loss during transfer due to evaporation. Online derivatization is typically performed with MD-ME, as opposed to MD-CE, due to the need for custom microfluidic architectures that allow several inlet fluid streams, including that of the MD sample, to be mixed prior to injection into the electrophoresis separation channel. However, the derivatization reaction can take several minutes and is complicated by inadequate mixing of laminar flows during this process. Should the mixing process be incomplete, or a lack of time result in an incomplete derivatization before the sample reaches the separation channel, the effective limit of detection for the assay will be negatively impacted.

Derivatization using NDA/2ME has been used in the past due to its faster reaction time [13], however, the noxious smell of 2ME makes it undesirable in a medical (or research) setting. Consequently, here we use NDA/CN for sample derivatization. To address the possibility of incomplete mixing in the device, this work investigates the use of an extended microfluidic mixing geometry to enhance sample derivatization in conjunction with MD-ME. This is first explored *in silico*, followed by construction and evaluation of the microfluidic device. By integrating sample mixing, derivatization, and analysis into a single, standardized format, the equipment footprint can be dramatically reduced while simultaneously improving the overall time lag between sample acquisition and actionable information. To optimize the derivatization reaction, ensure mixing, and establish an electrokinetic gate, a Comsol Multiphysics model of a MD-ME device was created.

5.2 Materials and Methods

5.2.1 Comsol Multiphysics Modeling

Comsol modeling of the MD-ME device was performed using version 5.3 of Comsol's Multiphysics software. Included were add-on packages for Laminar Flow in Microfluidic Devices, Electrostatic Potentials, and Transport of Dilute Species. Laminar flow and electric field studies were performed as a stationary study. Transport of dilute species studies were performed as a time-dependent study to evaluate the production of derivatized Glu as a function of time.

5.2.2 Microchip Fabrication

For this study, the following chemicals and materials were used. For microchip manufacture, glass was purchased from Telec Co. (Telic, Valencia, CA). This glass was pre-coated with a 500 nm layer of chrome beneath a 1.8 μm thick layer of AZ1518 positive photoresist (AZ Electronic Materials Corp, Somerville, NJ). Photolithography was used to pattern the AZ1518 photoresist. Designs of the microfluidic chips were first drawn using Autodesk AutoCAD (San Rafael, CA) before being evaluated using Comsol Multiphysics (Burlington, MA). Following this evaluation, negative transparencies were created using these designs at a resolution of 40,000 dpi by Infinite Graphics (Minneapolis, MN). Photolithography was performed using a UV a flood-source with output intensity of 21 mW/cm^2 and an exposure time of 4 seconds. Following exposure, the pattern

was developed using MIF300 AZ1518 developer (EMD Performance Materials, Somerville, NJ) for 30 seconds to remove exposed regions of AZ1518. The exposed regions of chrome mask were removed using Chrome etchant (Cyantek, Fremont, CA) before microfluidic channels were wet etched into the glass substrate using a 20% hydrofluoric acid solution to a depth of 25µm. Etched devices were stripped of remaining AZ1518 and chrome using acetone to remove all AZ1518 and chrome etchant to remove the chrome layer. Finally, poly-dimethylsiloxane (PDMS) (Dow Corning, Auburn MI) polymer was used to seal the microchip as well as to construct the microdialysis interface.

5.2.3 PDMS Bonding

Initial work with the online mixing design discussed here focused on the construction of a glass-glass microchip. As the name would suggest, these devices are constructed by thermally bonding a glass blank to the etched glass microchip to construct a sealed device entirely made from glass. This method however, relies on a complete bonding of the entire surface area of the device. Because of the relatively large surface area of these devices, and consequent difficulties found in their reproducible construction, we chose to use PDMS-glass hybrid chips for this proof of concept microchip.

PDMS was mixed to a ratio of 1 part in 10, polymerizing agent to monomer, and allowed to cure at 70º C for 3 hours prior to bonding. Additionally, the surface of the glass device was

thoroughly cleaned using Alconox glass cleaning solution (Fisher Scientific, Pittsburgh, PA) and water followed by drying using nitrogen gas.

Bonding was performed by exposing both the PDMS and the glass surface to an electrostatic field, generated using a BD-20AC Laboratory Corona Treater (Electro-Technic Products, Chicago, IL), for approximately 30 seconds before the PDMS was placed on the glass surface and smoothed to eliminate bubbles. Holes were cut into the PDMS to create inlet ports to the chip using a 5mm biopsy punch after allowing 2 hours for the bond to form.

5.2.4 Coupling to Tubing

Following bonding of the PDMS top layer to the etched glass microfluidic device, a second PDMS layer was added over the reservoir holes. The purpose of this layer was to provide structural support and seal around 24-gauge metal coupling pins at the interface of the mixer section and the microdialysis flow. Polyurethane tubing 0.5 mm in diameter was used to directly connect the syringes containing NDA, CN, and stock amino acid samples to these coupling pins during tests of online derivatization. The coupling pins had been embedded in a permanently sealed layer of PDMS at the inlet to the device. To prevent leakage, a small amount of PDMS was prepared (at a ratio of 1:10 once again) and used as a sealant at the interface of each pin and the PDMS layer. The seal was allowed to cure for 3 hours at 70º C prior to use. In this way, sample leakage due to backpressure was prevented.

5.2.5 Chemicals and Reagents

To calibrate the system, syringes each containing the same pre-derivatized amino acid standards were used. For both online and offline experiments, 3 syringes, each at a flow rate of 1 µL/min were used to maintain a constant combined flow rate of 3 µL/min throughout the evaluation of the microfluidic device.

Stock solutions of sodium cyanide (NaCN) (Sigma Aldrich) were prepared at a concentration of 10 mM in 15 mM sodium tetraborate and 50 mM EDTA (pH adjusted to 9.2 using NaOH and HCL). Stock solutions of naphthalene-2,3-dicarboxaldehyde (NDA) (Invitrogen, Carlsbad, CA) were prepared in acetonitrile (ACN) (Fisher Scientific, Pittsburgh, PA) at a concentration of 5 mM. Both NDA and NaCN were stored at 4º C, protected from light, and made fresh weekly. Glutamate (Glu) was obtained from Sigma Aldrich (St. Louis, MO) and prepared at a 20 mM concentration in artificial cerebral spinal fluid (aCSF) consisting of 145 mM NaCl, 2.7 mM KCl, 1.0 mM $MgCl_2$, 1.2 mM $CaCl_2$, and 0.45 mM NaH_2PO_4. The aCSF was pH adjusted to 7.4 using NaOH and HCl. All buffer components were obtained from Sigma Aldrich. Dilutions of each solution were made prior to analysis and stored at 4ºC. Finally, a stock solution of fluorescein (Fluor) at a concentration of 2.5 mM was prepared in aCSF and used as an internal standard. It was also stored in darkness at a temperature of 4º C.

A stock solution of 200 mM sodium tetraborate (Sigma Aldrich) was diluted to 20 mM as a component of the background electrolyte (BGE). This stock solution was adjusted to pH 9.2 using 1M NaOH and 1M HCL. Additionally, a 100 mM solution of sodium dodecyl sulfate (SDS) (Sigma Aldrich) was prepared in nanopure water. Each of these were subsequently filtered using a 0.22 µm filter. Prior to each use, 1.5mL of BGE was made consisting of 20 mM sodium tetraborate (150 µL of the 200 mM stock), 2 mM SDS (30 µL of the 100 mM stock) and 1320 µL of water. Finally, the BGE was sonicated for 20 minutes to eliminate dissolved gasses before use.

5.2.6 Derivatization Reactions

Initial tests of the derivatization microchip were performed using stock solutions derivatized offline to evaluate microchip function. These tests were followed by evaluating the same stock solutions derivatized online. The proportions of each component (sample, NDA, and CN etc.) were kept constant for both the online and offline tests. For each experiment, a total reaction volume of 1.5 mL was used. This total volume consisted of a mixture of three components divided into equal volumes of 0.5 mL to simulate the mixing of three flows at equal flow rates.

In these experiments, the first component consisted of the sample to be tested dissolved in aCSF. The second component was NDA at a concentration of 1mM dissolved in 50:50 ACN:water. The third component consisted of NaCN, EDTA, fluorescein as an internal standard dissolved in borate buffer. The final concentrations of each component in the total 1.5 mL volume were: 1 mM

NaCN with 5 mM EDTA (150 µL of stock), 25 µM fluorescein (15 µL of stock), and 20 mM borate (150 µL of stock).

For offline analysis and optimization, these three volumes were combined and allowed to react for 20 minutes before being divided into three equal volumes of 0.5 mL in three 1 mL Hamilton 1000 Series Gastight® syringes (Fisher Scientific, Pittsburgh, PA). The solutions were protected from light for the duration of the experiment. Each derivatized sample was then injected into the microchip at a flow rate of 1 µL/min for a combined flow rate of 3 µL/min.

Finally, during online tests of microdialysis sampling, the syringe containing the sample was replaced with one containing only aCSF. This syringe was connected to a microdialysis probe which was then used to sample from a stock solution of Glu with the output of the probe connected to the inlet of the microchip. This allowed Glu to be sampled in real time and derivatized in an online fashion.

5.2.7 Microdialysis Probe and Sampling

CMA12 Microdialysis probes were used to evaluate online derivatization with MD sampling. These probes used a 2mm Polyarylethersulfone (PAES) membrane with a 20 kDa cutoff. The probe was coupled to polyethylene tubing. Prior to use, the probe was flushed with water for 20 minutes at 5 µL/min to remove any air bubbles.

Sampling was performed by placing the probe in a sample containing 250 µM Glu in aCSF. Using a syringe pump, aCSF was then applied at a flow rate of 1 µL/min. The output of the probe was connected to the inlet coupling pin of the microchip using polyethylene tubing.

5.2.8 Microchip Operation

Prior to each use, the microchip was cleaned and conditioned by rinsing the channels with consecutive solutions of 0.1 M HCl, water, and 0.1 M NaOH, followed by water and then finally BGE using the application of negative pressure via a water aspirator. Each solution was passed through the device for 10 minutes. Finally, the channels were filled with BGE any bubbles present were eliminated. High voltage was generated using an UltraVolt HV rack high-voltage power supply (Ronkonkoma, NY). This supply was controlled by software written in Labview (National Instruments, Austin, TX).

During both the online and offline tests, an electrokinetic gate was established using 3 voltages. At the top of the sample inlet, 600V was applied while 2kV was applied to the buffer waste channel. Finally, at the end of the separation channel a -4.85kV potential was applied creating an electric field of 431 V/cm. These voltage ratios were found to establish the most consistent electrokinetic gate. During operation, the inlet to the mixer section of the microchip was held at ground, as was the sample waste reservoirs. Sample injection was performed for 1 second, with 300 seconds of separation time between injections.

5.2.9 Detection Instrumentation

Fluorescence excitation and emission of the 1-cyanobenz[f]isoindole (CBI) product formed via the reaction of NDA and CN with a primary amine occurs maximally at 420nm and 442nm (excitation) and 510nm (emission). Consequently, for this work a 445 nm PhoxX diode laser (Market Tech, Scotts Valley, CA) was used for excitation during separation. This wavelength was not ideal for fluorescein which is maximally excited at 488nm. However, for use as an internal standard, its excitation at 445nm is more than adequate.

Focusing the laser on the separation channel and subsequent capture of emitted light was accomplished using an epifluorescence microscope. Light from the laser was reflected through a 445nm bandpass filter, before being directed 90º upward by a long pass dichroic mirror with a 490nm cutoff wavelength. Finally, the excitation light was focused onto the channel using a 40x objective lens. Emission light was captured by this same objective lens and focused downward, passing through the dichroic mirror and through a long pass filter, cutoff 480nm, before being focused onto a photomultiplier tube (PMT). The output of the PMT was amplified using a SR570 amplifier from Stanford Research Systems (Sunnyvale, CA). Final data acquisition was performed using a National Instruments NI USB-6229 data acquisition card and custom Labview software. Finally, data analysis was performed using Origin software version 8.2 (Origin Lab Corporation, Northampton, MA).

5.3 Results and Discussion

A major limitation in the study of TBI's has been the ability to monitor the concentration of multiple analytes with high temporal resolution and low limits of detection over time. To address this, various efforts have made, by our group [15-17] and others [13, 18-22] to interface a MD flow directly to an ME system. Several of these interfaces have subsequently been used to fluorescently derivatize samples of neuroactive amines on-chip using OPA/2ME [13] and NDA/2ME [17]. More recently, NDA/CN has been the derivatization agent of choice for online MD-ME devices [15, 16, 21, 22].

As mentioned earlier in this thesis, this work focuses on the use of NDA/CN rather than NDA/2ME. The reaction products of NDA with either 2ME and CN are excited by visible light (excitation maxima at 442nm) and is less sensitive to changes in BGE chemistry. The CBI derivatives exhibit higher quantum efficiencies than products with OPA/ME [23] are more stable [24]. The downside to using NDA/CN is the added time necessary to complete the reaction, which can take up to 180 seconds [25]. Practically speaking, the requirement of 180 seconds for full derivatization places significant limitations on the geometry of the MD-ME device. For instance, at an MD sampling flow rate of 1 µL/min as mentioned previously, we can expect approximately 10-40% sample recovery. If that inlet flow is combined with flows for NDA and CN at the same 1 µL/min we have a resulting 3 µL/min total flow rate. As the flow enters the MD-ME device, the

internal volume of the microchip mixer must be at least 9 µL to accommodate a continuous 3 µL/min flow for 180 seconds and guarantee full derivatization.

The interface between the continuous MD flow and the electrokinetic sample injection into the separation channel of the MD-ME device also places limitations on device geometry. As derivatized dialysate sample arrives at the gate region, the hydrodynamic pressure of the flow must be balanced by the electroosmotic force generated at the gate. A theoretical model for this balance of forces was developed by Lin et al. [20], and was used to develop a sampling method that allowed for nL sized samples to be taken from a continuous MD flow. Building on, and expanding this method, we demonstrate a Comsol Multiphysics model of an MD-ME device including on-line derivatization and MD flow coupling to an electrokinetically gated ME device.

5.3.1 MD-ME Design Considerations

Several things must be considered when designing a complete MD-ME device. First among those is the substrate material used. In this case, we chose to use a glass substrate to limit fouling from species adsorption over time and maintain consistent device EOF and performance throughout usage, something that fully PDMS based devices typically lack. In our case, the glass devices were fabricated using photolithography and wet etching methods. Wet etching using HF is an isotropic process resulting in simultaneous widening and deepening of structures as etching occurs, a process that must be compensated for in the design and modeling. The etching process also creates structures of uniform depth across the entire device. Practically, this means that

structures cannot rise from the channel floors to aid in mixing and that all regions will have the same depth. Because the etching process occurs from all directions, structures of small dimensions such as posts tend to be etched away. To control the volume of regions and to ensure mixing for analyte derivatization, we were consequently limited in both the types of structures that could be implemented as well as the number of structures as a significant increase in the back pressure created by the device geometry could cause the MD-ME interface to leak.

A final consideration was the fact that it would ultimately be desirable to build the device entirely from glass. To create a glass-glass device, the glass substrates would require bonding at approximately 600ºC. This, and the fact that analyte separation and mixing needed to occur in a single device, prevented the addition of active mixing components.

In order to ensure mixing, under these design constraints we, therefore, chose to use a passive mixing geometry developed first by Wang et al. [26]. This geometry was well suited to our design constraints as it was adaptable to HF etching of glass while providing a good passive mixing process.

5.3.2 Mixing at the Microscale

Fluid mixing at micron scales can be a challenging task. For multiple reasons, including the need to handle the vanishingly small sample sizes produced by microdialysis sampling as well as

the use of electrophoresis as a separation technique (discussed in the following section), the channel dimensions of MD-ME devices are typically quite small. For instance, the dimensions of the channels in the larger regions of the device measure a maximum of 450 µm wide by 25 µm deep. For the separation channel, the width can shrink as small as 50 µm to 100 µm. At these scales and low flow rates, fluid motion can be characterized as *laminar* in nature.

Laminar fluid flow is defined as having a Reynolds number (a measure of the turbulence of a given flow) where: $\boldsymbol{R_e} < 200$, given by the equation:

$$\boldsymbol{R_e} = \frac{\boldsymbol{\rho \cdot U \cdot D_h}}{\mu}$$

Equation 5.1: Reynolds number

Where ρ is the fluid density ($\frac{m^3}{kg}$), U is the average fluid velocity ($\frac{m}{s}$), D_h is the hydraulic diameter (m), and µ is the viscosity (Pa · s). Because of the channel profile created by HF etching, the hydraulic radius in this case can best be approximated by a square channel given by the equation:

$$\boldsymbol{D_h} = \frac{4 \cdot A}{p}$$

Equation 5.2: The hydraulic radius of a channel

In which A is the cross-sectional area of the channel (m^2) and p the wetted perimeter of the channel (m). Under a laminar flow regime, the streamlines lines of the fluid can be thought of as travelling parallel to each other. These parallel streamlines can be seen in Figure 5.1 which depicts the intersection of two fluids, both of which are in the laminar domain. As can be seen from the image, because the fluid streams move in parallel, the only source of mixing (i.e. mass transport) between the flows is due to lateral diffusion.

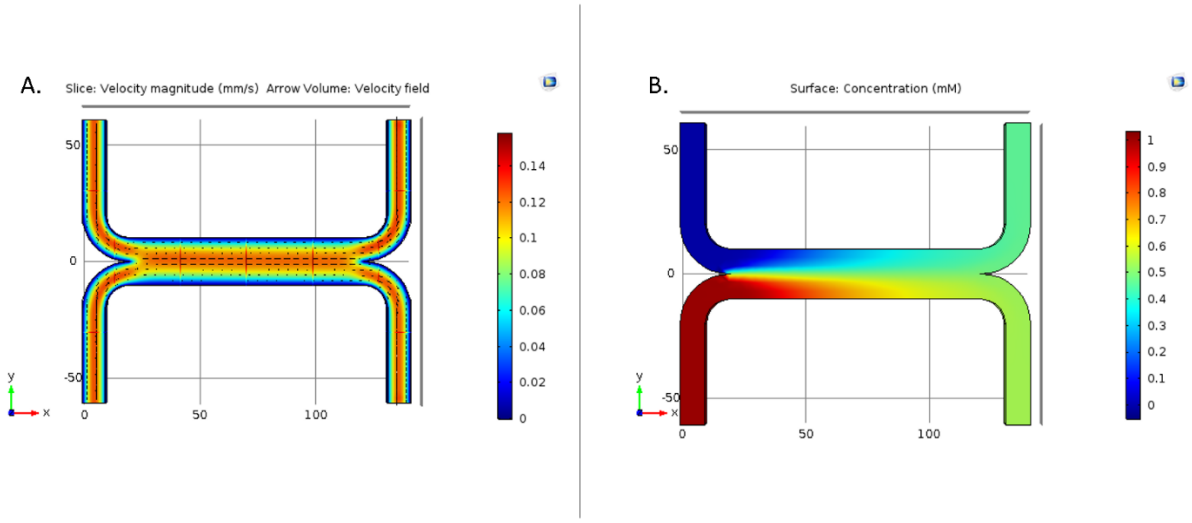

Figure 5.1: Modeling the intersection of two fluids, both flowing within the laminar domain. A. The streamlines of the fluid velocity can be seen to be parallel after the fluid meets indicating a lack of turbulent mixing. Consequently, the mixing process shown in B. proceeds only due to the passive diffusion of species from the inlet in the lower left of the figure to the outlets.

To maximize the degree of mixing in the shortest amount of time, it is necessary to effectively increase the Reynold's number associated with the fluid flow. As the Reynold's number increases, the degree of convective mixing increases. Once the value for Re > 2300, then the flow enters a region defined as "turbulent" flow. This type of flow is characterized by rapid, convective mixing. The ratio of convective to diffuse mixing is known as the Peclet number and is given by:

$$\boldsymbol{Pe = \frac{U \cdot D_h}{D}}$$

Equation 5.3: Peclet number

Where D is the diffusion coefficient ($m^2 \cdot s^{-1}$) of the analyte being mixed. When the value of Pe is high (>100), it is an indication that diffusion is the primary mode of mixing and that consequently, channels of longer length will be necessary to ensure proper mixing.

In microdevices, turbulent flow is essentially nonexistent. Mixing therefore depends on the diffusive flux of the dissolved solute(s) which is given by:

$$\boldsymbol{D_f = D \cdot A \cdot \nabla c}$$

Equation 5.4: The diffusive flux of a dissolved solute

Where D_f is the diffusive flux, D is the diffusion constant, A the interfacial area, and ∇c the concentration gradient. In microscale devices, locally increasing the diffusive flux can be accomplished in two general ways: active mixing and passive mixing.

5.3.2.1 Active Mixing

Active mixing strategies, as the name would suggest, involve the addition of external energy to the system to disrupt flow and cause additional mixing. The method by which active mixing is accomplished varies but can include ultrasound, magnetic stirring, pumping, injection of bubbles, heat and electrokinetic forces [27]. For the purposes of this device, however, each of these was problematic with regard to this device due to its integrated nature.

The integrated microchip presented here was designed with the goal of minimizing the lag time between sample acquisition and analyte detection. As a result, the derivatization step was necessarily located physically close to the separation channel, within a single monolithic substrate. A consequence of this decision was a concern that adding active mixers such as ultrasonic sound would disrupt the nearby electrophoretic separation. Additionally, the use of a glass substrate, while providing for repeated and consistent separations of our analytes of interest, limited the degree to which mechanisms such as pumps or magnetic beads could be integrated.

Two factors also prevented the use of electrokinetic mixing as an option. The first of these was the fact that to facilitate full sample derivatization, a process that will be discussed in the following section, it was necessary that a volume of 9 µL be accommodated by the mixer. To meet this requirement, it was necessary that the channels be wide (450 µm). At that width, electrokinetic flow cannot be generated with sufficient magnitude. In addition to this, the use of electrokinetic

mixing at the interface between a microdialysis probe and the microfluidic device could present safety concerns for online animal or human experiments. Finally, while the addition of heat to the system would seem an ideal solution to both the problem of increasing diffusive flux and accelerating the rate of the derivatization reaction, this too would negatively impact the subsequent analyte separation. With these factors in mind, a passive mixing design was chosen for this device.

5.2.3.2 Passive Mixing

Passive mixing, in contrast to active mixing, deflects the energy of the flow itself to enhance the either the interfacial area or concentration gradient terms of the diffusive flux equation. This can best be accomplished by engineering the environment of the flow to force the parallel flow lines to intersect. Several geometries are considered as passive mixing geometries. Among these, are the simple T mixer geometry [28] and the Staggered Herringbone mixer design [29]. Initial COMSOL models of the T mixer indicated that the pressure resulting from the directly opposing inflows could be problematic, resulting in high inlet pressures. (Figures 5.2 and 5.3).

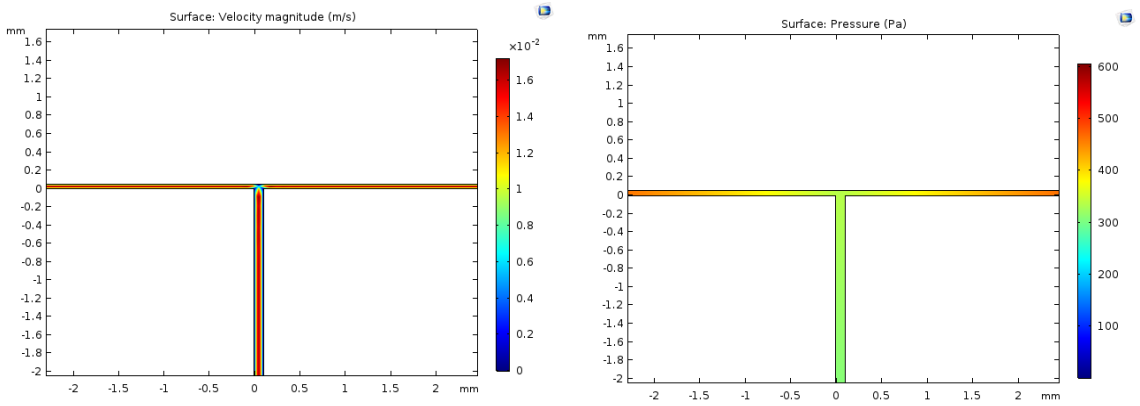

Figure 5.2: On the left, the fluid velocity (m/s) and on the right the pressure (Pa) for a 2-dimensional cross-section of a microfluidic device consisting of two opposing flows meeting in a T junction. In this example, the channel dimensions are 50 µm for the inlet channels and 100 µm for the combined outflow with the inlet flow rate of 1µL/min.

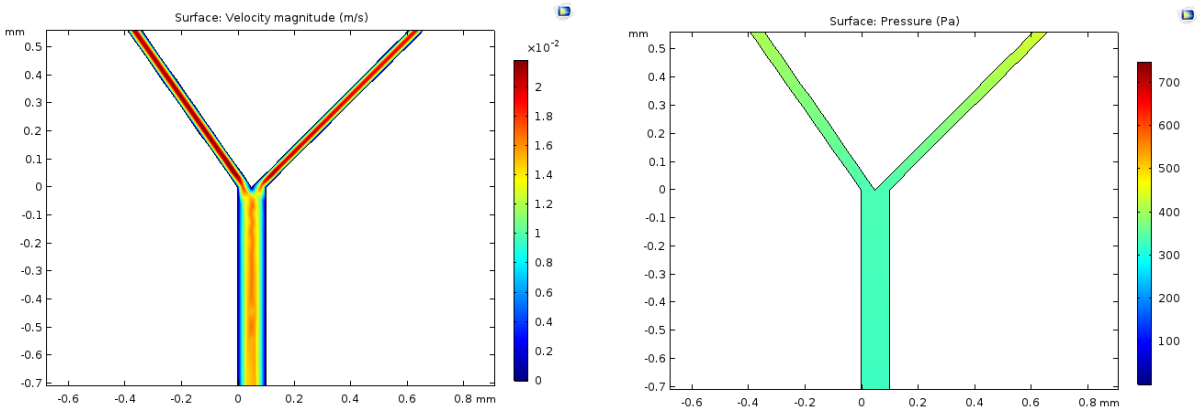

Figure 5.3: The velocity (m/s, on left) and pressure (Pa, right) for a simple T with inlets at 45° to the main channel. Again, the side inlet channels are 50 µm wide and main channel is 100 µm. Inlet flow rate is 1µL/min.

The Staggered Herringbone, while having been demonstrated elsewhere to be almost an ideal passive mixing geometry, could not be implemented here due to its need for variation in the depth

of the mixer device. For these reasons, a third option was explored and ultimately implemented: The Triangle Baffle mixing geometry.

5.3.3 Triangle Baffle Mixing Geometry

As mentioned, the choice of passive mixing geometry for the integrated derivatization and separation chip discussed here was made under a variety of constraints. Following an extensive literature review, a mixing geometry based on a repeating triangle baffle design was selected. This design, developed by Wang et al. [26], is shown in Figure 5.4. This geometry consisted of a series of triangle baffles spaced at regular intervals, every 100 µm, with right triangles measuring 25 µm on both the base and height side extending from the channel walls and equilateral triangles having a base of 50 µm and heights of 25 µm we spaced in the center of the channel.

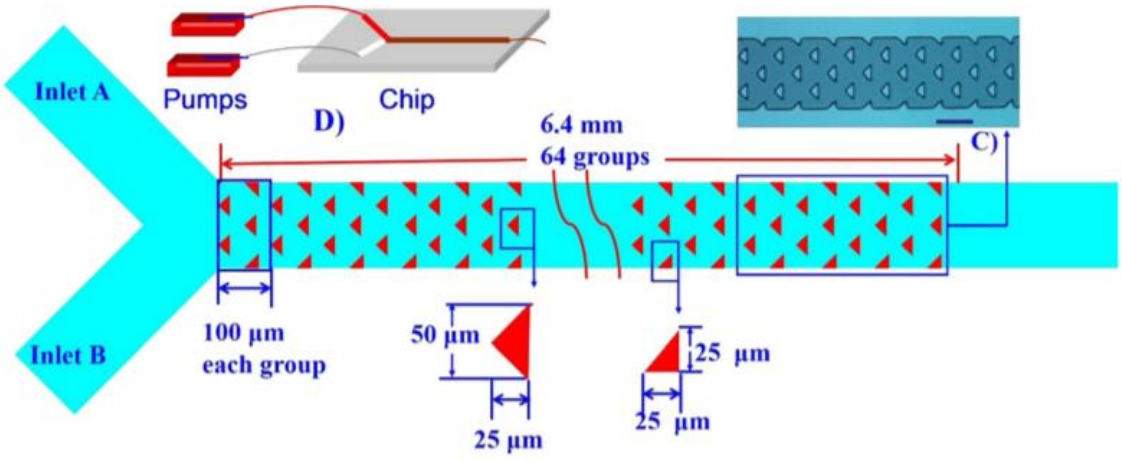

Figure 5.4: The initial geometry of the triangle baffle passive mixer from Wang et al. Republished with permission from [26].

Due to the symmetric nature of the etch profile (in the z/depth axis), it was possible to model the fluid flow profile as a 2D cross section, saving considerable computational time. The initial COMSOL simulations of the geometry specified by Wang et al. showed that with a combined flow rate of 3 µL/min the back pressure on the system was substantial with inlet pressures of nearly 2.5 x10^4 Pa. (Figure 5.5)

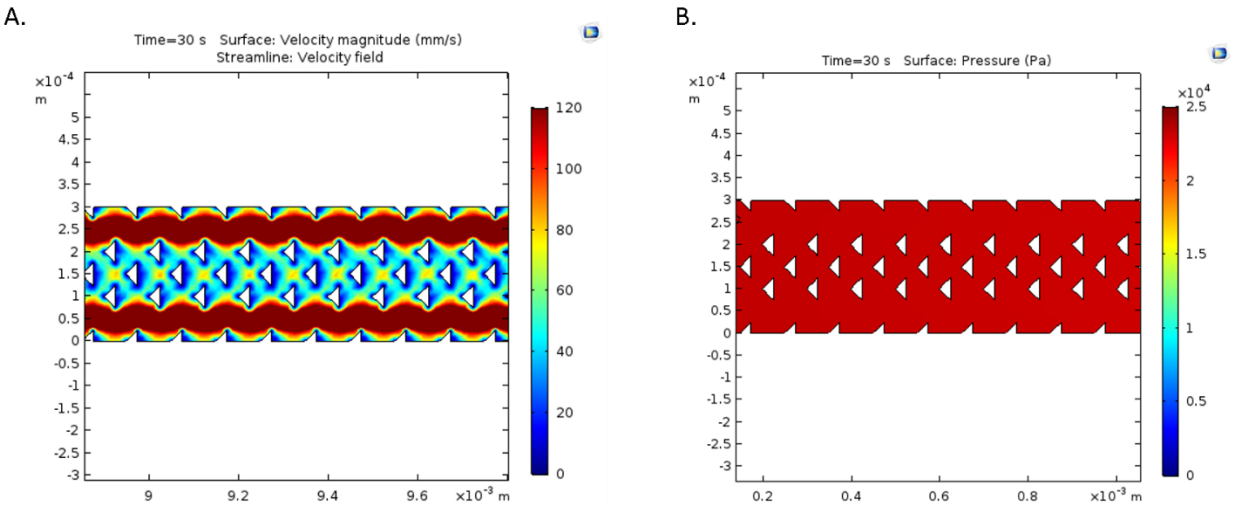

Figure 5.5: Initial test of microchip used by Wang et al. [26] Modeled using Comsol. A. Fluid velocity is shown, B. Press at the beginning of the mixer channel.

Out of a concern that this back pressure would lead to leakage at the interface with the MD flow, or through the probe itself, the center triangles were removed. At the same time, the side triangles, were increased in size to 100 µm on each side such that at the narrowest point in the channel design, only 100 µm separated the tips of the triangles. The effect on the fluid flow can be seen in Figure 5.6 which shows fluid velocity streamlines as they repeatedly part and come together, mixing the sample.

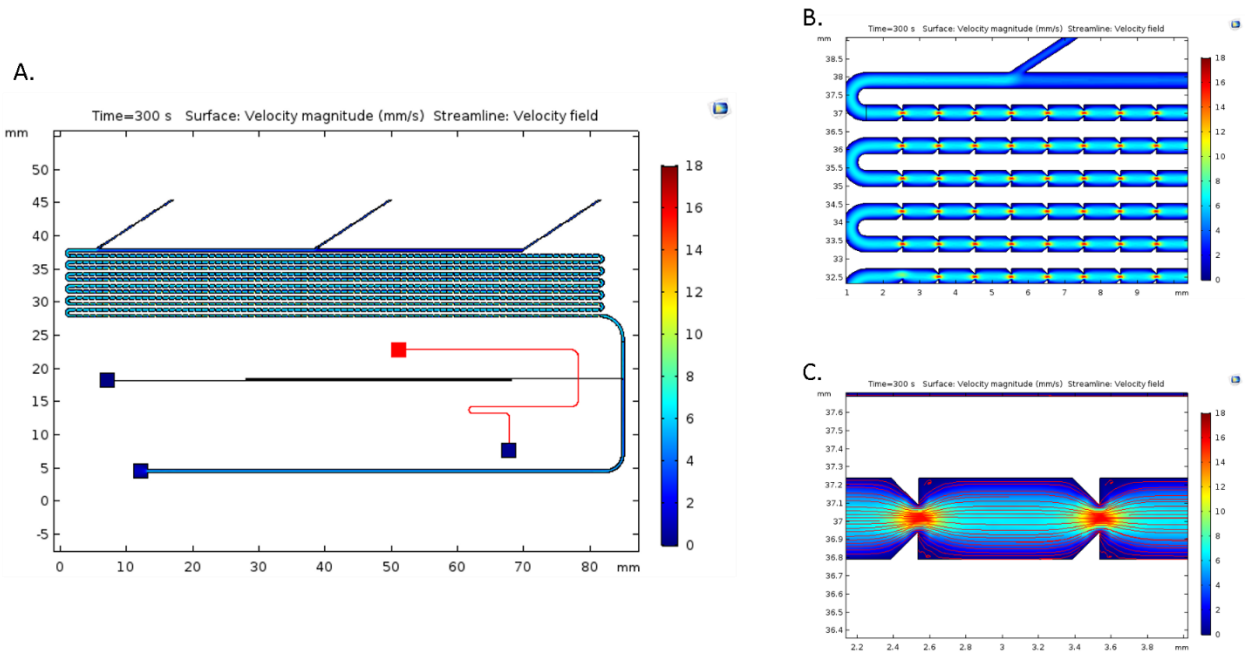

Figure 5.6 A-B: The modified design shown here removes the central triangles in the original design which significantly decreases the back pressure on the probe. The triangular baffles on the sides however do still enhance mixing by redirecting the fluid velocity streamlines as the simulation shows. A: A view of the fluid velocity across the entire microchip. B: A zoomed in view of the mixer showing the repeating pattern caused by the triangles.C: A zoomed in view of the mixer showing fluid velocity and streamlines.

The MD-ME device constructed based on these simulations consisted of 3 inlet ports, one each for the dialysate sample, NDA, and CN (as well as internal standard). These ports allowed inlet flows of 1 µL/min to combine and mix passively through the triangle baffle geometry in a channel 25 µm in depth, 450 µm in width, and 80 cm long, dimensions which result in 9 µL of internal volume, resulted in the flow requiring 180 seconds to traverse the mixer, after which full derivatization of the sample had occurred [25]. Following the passive mixer, the flow was directed past the sample inlet of the electrokinetic gate on its way to a large waste reservoir such that a continuous flow could be sampled discretely. The full microchip can be seen in Figure 5.7 including the electric field distribution across the device.

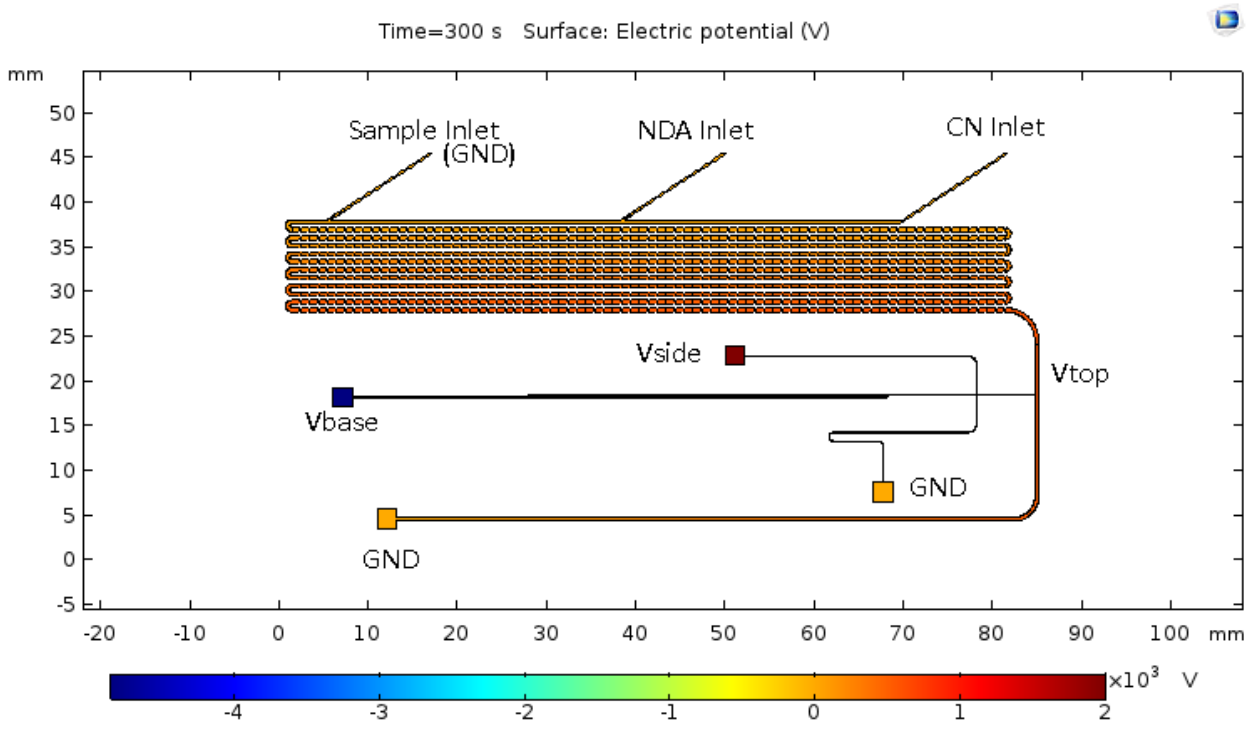

Figure 5.7: The full microchip design with electric field modeled. For this model, the 3 voltage gate is modeled (discussed in the next section) with Vtop = 600 V, Vside = 2000 V, and Vbase = -4850V.

As previously described, sample, NDA and CN (as well as the internal standard) enter this chip at the three inlets and proceed to mix passively. As they exit the mixer, the derivatized sample was electrokinetically injected when it flows by the separation channel. The separation channel itself consisted of a channel 15 cm in length, 25 µm in depth and 70 µm wide with channel turns tapered to 50 µm to prevent band broadening.

Modeling the combined mixer and separation channel was performed by defining two separate domains within Comsol. These domains differed primarily in the wall conditions applied to each

(no-slip for the mixer section, electroosmotic for the separation channel section). However, the device itself was simulated in its entirety to ensure that 1. The applied separation field would not adversely affect the mixer or the upstream dialysis pumps or 2. That the pressure from the mixer was accounted for in the modeling of the electrokinetic gate.

5.3.4 Electric Field Distribution and Electrokinetic Gate Modeling

The electric field applied to the MD-ME device was modeled using Comsol's Electrostatics module. Three methods of establishing an electrokinetic gate were tested. The first was to simply use a single high voltage source from one of the side channels to create a gate, while hydrodynamic pressure from the dialysate flow forced sample down the channel to the gate where it would be prevented from entering the separation. When the voltage was floated, sample would be forced into the separation channel hydrodynamically. In order to produce the target ~420V/cm separation potential previously established as necessary to separate the target analytes commonly found in brain dialysate [30], a potential of at least 7.7kV would be required. This scheme had the benefit of minimizing the number of high voltage supplies necessary. In practice, however, it was quickly apparent that too little of the dialysate sample was directed to the gate for this to be effective and in fact, the EOF created by the single voltage would expel sample from the separation channel back into the mixer. This of course could be prevented by decreasing the voltage, but at the cost of a lower separation potential, leading to a longer analysis time.

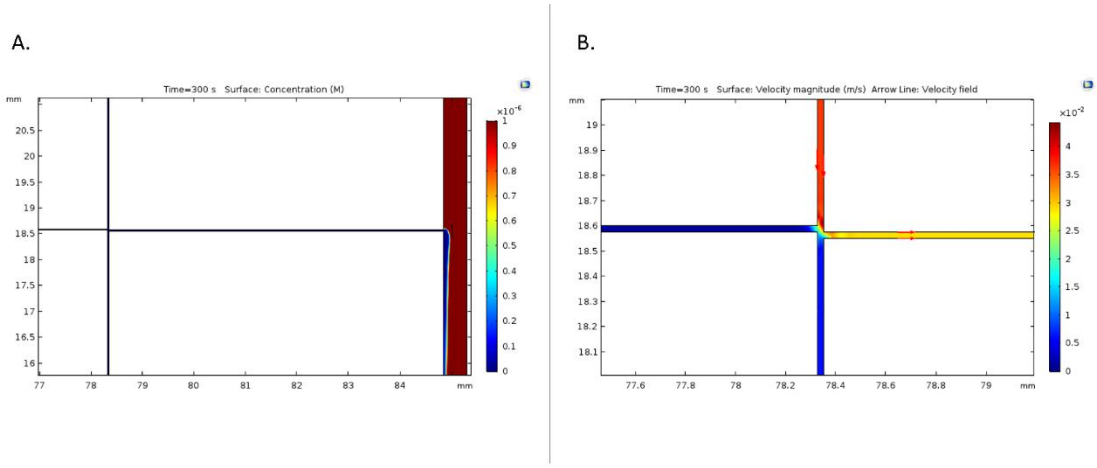

Figure 5.8: A single voltage supply at a high enough potential to maintain a separation potential of over 420 V/cm was found to expel sample from the gate region. A: The concentration of derivatized sample as it is expelled from the channel. B: The fluid velocity as a result of EOF is shown.

Therefore, rather than rely on a single voltage source, a second voltage source at was added at the top of the sampling channel at a potential of 5.062kV and the side channel voltage was lowered to 6.75kV (0.75:1 ratio). This source created an EOF from the dialysis flow to the electrokinetic gate and was effective in delivering the sample to the gate. However, it failed in practice because the high field strengths in the gate region resulted in joule heating and bubble formation. Additionally, as can be seen in Figure 5.9, the gate established in this fashion was unable to completely eliminate sample leakage into the separation channel, a fact later verified experimentally.

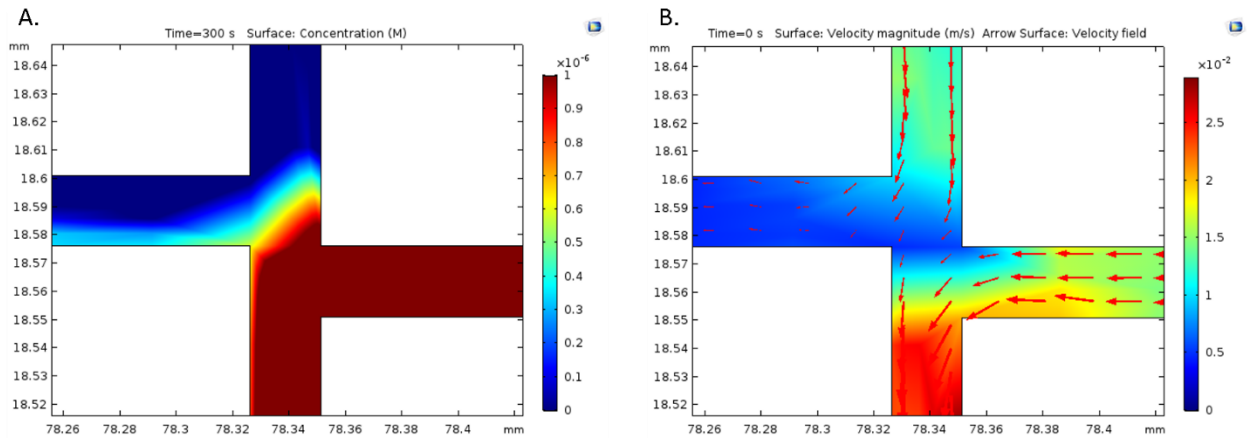

Figure 5.9: A: The gate established using the two voltage system was found to be unstable, resulting in sample leakage into the separation channel. B: The velocity profile of the two voltage gate.

Finally, this led to the addition of a third high voltage source with a negative potential at the end of the channel of -4.85kV. By using a negative voltage at the base of the separation channel, the gate voltages could be lowered to 600V at the sample inlet, and 2.0kV in the side channel. The net effect of this is to preserve the overall separation potential at roughly 431 V/cm while lowering the field strength at the gate, thereby preventing bubble formation while still creating a stable and closed electrokinetic gate to prevent sample leakage. A second consequence was to create a more substantial injection plug as the EOF generated in the sample channel from the 600V injection voltage to the -4.85kV end of channel voltage was significantly higher than that from 2kV to ground. (Figure 5.10)

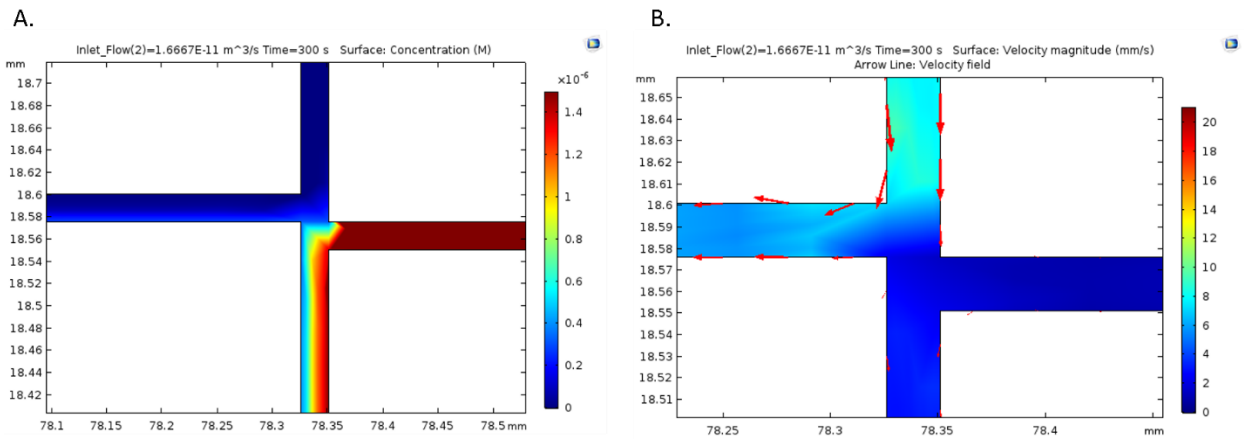

Figure 5.10: The gate established using the three voltage model was found to result in the most stable injection scheme. A: The concentration profile of derivatized sample at the gate. B:The fluid velocity due to EOF at the gate region.

5.3.5 Derivatization Reaction

To model the transport, mixing, and subsequent derivatization reaction of analytes within the MD-ME device, boundary concentrations of Glu (10uM), NDA (1mM), and CN (1mM) were defined at the entrance to each respective fluid inlet. Transport of these species was coupled to the fluid inflow, providing a constant source of each.

Using the experimental conditions described by Shou et al. [25] under which the derivatized mixture of amino acids was found to have a maximal fluorescence output after 180 seconds, as well as the observation by De Montigny et al. [31] that in conditions of excess NDA and NaCN, the derivatization of amino acids by NDA can be modeled as a pseudo-first order equation, we calculated the rate constant for Glu derivatization as k= 25E-3 s^{-1}. Under these conditions the rate of CBI-Glu (the derivatized form) production depends only on the concentration of Glu. The rate

of CBI-Glu formation, referred to in the following sections as GNDA, and concentration at a given time can be modeled using the following equations:

$$Rate_{GNDA} = \frac{d[Glu]}{dt} = -k[Glu]$$

Equation 5.5: First order rate question

And

$$[GNDA] = [Glu]_0 e^{-kt}$$

Equation 5.6: Integrated form of the first order rate equation

Where [Glu] is the concentration of Glu at a given time (t), k is the rate constant, and [GNDA] is the concentration of the derivatized product [GDNA].

The simulated reaction of Glu, NDA, and CN was accomplished using the reaction modeling capacity of the Transport of Dilute Species module within COMSOL and defining stoichiometric reaction equations as a pseudo first order reaction. To verify the reaction was being modeled correctly, the flow into the device was disabled while the initial concentrations of the three reactants were set to 10μM Glu, 1mM NDA, and 1mM CN respectively. The reaction was subsequently modeled for 200 seconds with the concentrations of Glu and GNDA (the derivatized product) shown in Figure 5.8 as measured at the exit of the mixer section of the microchip.

The primary reason for modeling the reaction was to demonstrate that the derivatization proceeded to completion at the target flow rate of 1 µL/min before the analyte was injected into the separation channel. In fact, in an earlier version of the MD-ME device, it had been demonstrated that the derivatized product flowed from the chip well before the reaction could proceed to completion. As a result, the limits of detection for the MD-ME device were much higher than they otherwise would be. As mentioned, the design of this device anticipated that at a combined flow rate of 3 µL/min, the collected sample would have sufficient time to fully react. Above this rate however, the amount of derivatized sample would be limited by the flow from the device. This pattern can be seen in Figure 5.11 which shows the estimated concentration of GNDA at the inlet of the separation channel for a variety of flow rates.

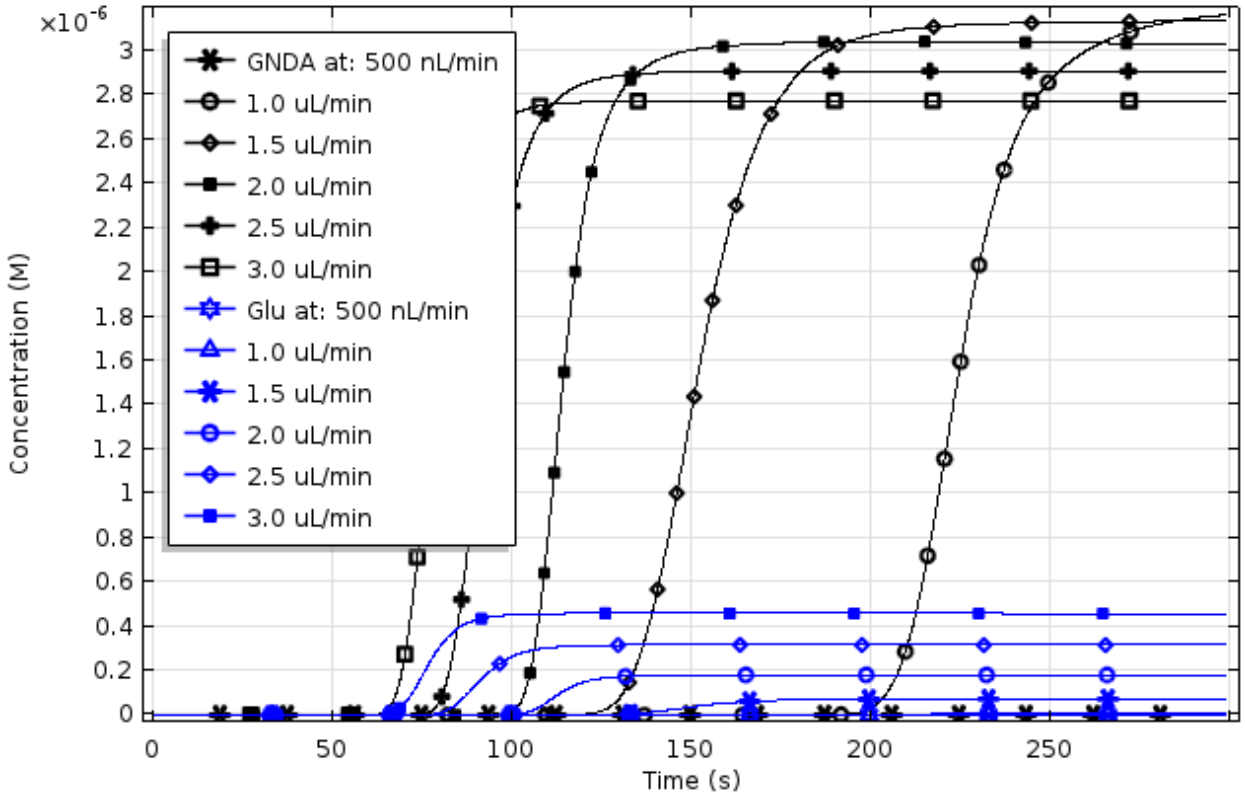

Figure 5.11: A comparison of GNDA production vs Glu for flow rates from 500 nL/min to 3 µL/min (for each inlet channel) over a 300 second time period. Of note, at flow rates higher than 1.0 µL/min, a substantial quantify of Glu exits the microchip prior to being derivatized. Full sample derivatization in this example is 3.3µM GNDA.

5.3.6 Construction and Evaluation of Online System

To evaluate the model used in this paper, a glass-glass device was initially constructed. However, due to the difficulties in uniformly bonding such a large surface area, a glass-PDMS hybrid device was ultimately used. This device was etched to a depth of 25µm into the glass substrate providing three walls of a glass channel within which to generate an EOF with the PDMS

layer being used to seal the device. Access ports were cut in the PDMS layer for buffer and waste. Three coupling pins for the microdialysis inlets were mounted through the PDMS layer and sealed via the application of liquid PDMS, left to cure for 3 hours before use. These coupling pins were used for convenience during this prototyping process. It should be noted however that because they were 20 mm long and 0.5 mm in diameter, their use added an additional 3.9 µL of dead space for the fluid to fill before reaching the chip. Additionally, the wells created to in the 2.5 mm thick PDMS layer using a 5.0 mm biopsy punch resulted in another 49.2 µL which will be discussed further in the future directions section of this chapter.

To evaluate the performance of the microchip, NDA, NaCN, and a series of Glu concentrations ranging from 5 – 50 µM Glu were used to create two calibration curves. The first of these used offline derivatizations followed by the application of sample directly to a sample well at the top of the injection channel. Following this, a second calibration curve was generated using online derivatization at a flow rate of 1 µL/min. These calibration curves can be seen in Figure 5.9. Sample injection into the separation channel began immediately to register the earliest change in concentration at the electrokinetic gate.

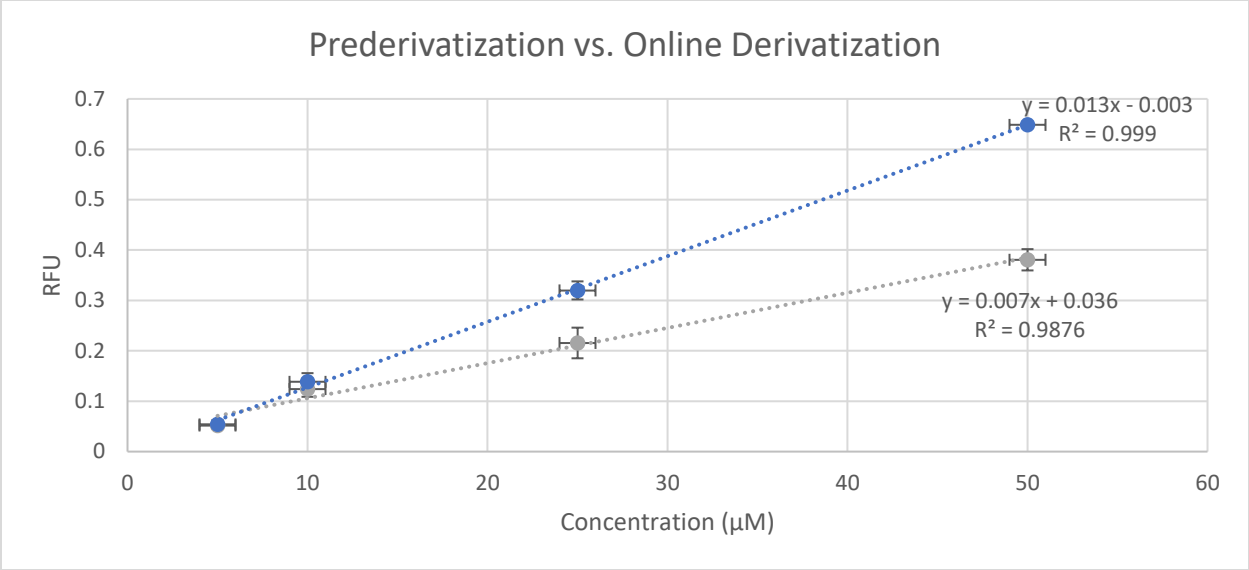

Figure 5.12: A comparison of two calibration curves using the microchip. The first using a prederivatized sample, and the second via online derivatization. Of note is the departure of the two curves as concentration increases, indicating potential a departure from a pseudo-first order reaction rate.

As Figure 5.12 shows, both pre and online derivatization schemes resulted in a linear response with signal intensities for both corresponding closely at lower concentrations. However, as concentrations increase, a clear departure was noted between the measured signal strengths. This difference between prederivatized sample and sample derivatized online is indicative of an incomplete derivatization process. Further evaluation using NDA and CN stock of double the concentration (2mM rather than 1mM) resolved this.

5.3.7 Online Sampling via MD-ME

The calibration curves shown in Figure 5.12 demonstrate linearity over a physiologically relevant range of concentrations for glutamate [30]. In order to demonstrate the ability of such a device to function in a medical setting however, it was necessary to evaluate the device using a microdialysis probe identical to the probes typically used for *in vivo* studies as well as in an ICU setting. For this reason, a CMA brain cannula microdialysis probe, model CMA 12, was used. As mentioned, the membrane of the CMA 12 probe has a 20 kDa cutoff, which excludes large proteins and cellular components, while allowing the target amino acids to be sampled.

The 2mm PAES membrane is a common membrane used in CNS microdialysis sampling and was used in these studies. Prior to use, the probe was flushed for 20 minutes at 5 µL/min using water according to the manufacturers specifications in order to remove any bubbles. Following this, the probe was placed in a sample of 250 µM Glu in aCSF. At this point, a syringe containing aCSF was connected to the inlet of the probe using polyethylene tubing while the outlet of the probe was connected to the microchip inlet coupling pin using additional tubing. For ease of use during the evaluation of the prototype microchip design, this tubing was approximately 4 cm long with an internal diameter of1.0 mm. This represented an additional 31.46 µL of dead volume which, at 1 µL/min was approximately 30 minutes of lag time.

A syringe containing NDA in acetonitrile (ACN) and another containing NaCN in 20mM borate buffer with 25 µM fluorescein were connected to the remaining two inlet pins of the microchip. By placing the fluorescein internal standard with the derivatization agents rather than in the sample *or* in the aCSF perfusate, potential loss due through the microdialysis probe could be prevented. It also obviated concerns regarding the presence of the internal standard in a perfusate entering a living subject. Once fully assembled and prepared, the sample and derivatization agents were delivered to the microchip at a steady rate of 1 µL/min.

As mentioned, the three different potentials were applied to the device, 600 V at the sample inlet, 2000V to create the electrokinetic gate, and a negative voltage applied to the end of the separation channel of -4850 V. This generated a separation field of approximately 431 V/cm. Sample was injected electrokinetically every 150 seconds for 1 second and was performed continuously for approximately 3 hours. A characteristic section of the resulting data, obtained 103 minutes after the initiation of sampling, is shown in Figure 5.13.

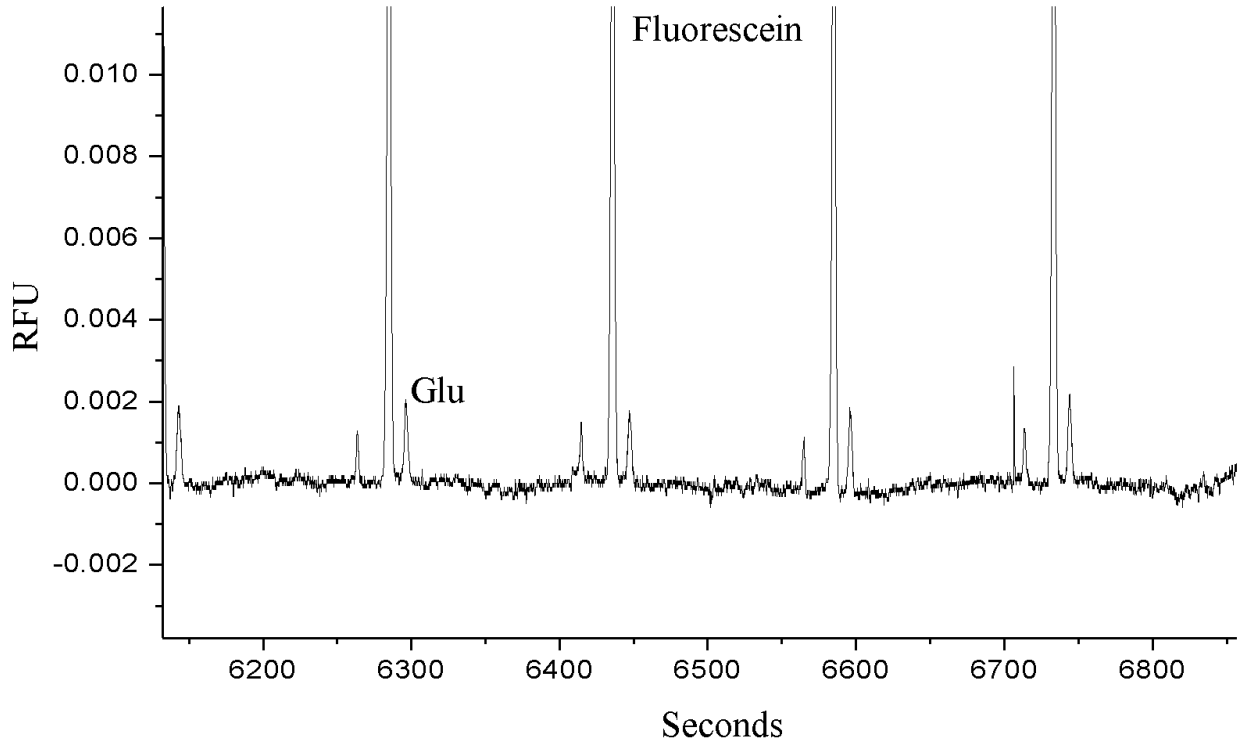

Figure 5.13: A representative section of the datafile with the peaks for the fluorescein internal standard (which extend out of frame) as well as the sampled Glu labeled. This particular range of data represents a 10 minute period, 1.71 hrs. into the sampling process.

Sampling was performed for 3 hours. During that time, it was evident that while the sampling peaks had substantial variability on an injection to injection basis, the use of the internal standard to correct for the Glu peak height worked well. The injection variability is a concern however and will be addressed in the future directions.

Data collection began immediately after starting the syringe pump. However, as mentioned, a time lag existed in the prototype system resulting in a delay of approximately 27 minutes before derivatized Glu was detected as shown in Figure 5.14.

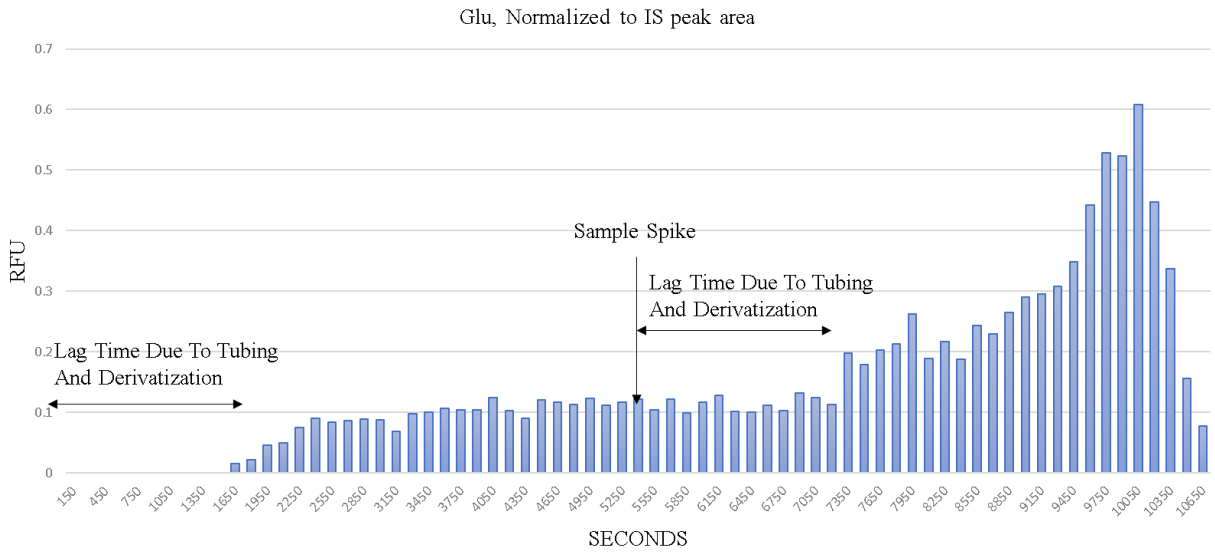

Figure 5.14: Online sampling and derivatization performed using microdialysis. The appearance of derivatized Glu appears after a 27 minute delay due to tubing lengths . Following an extended period of sampling, the concentration of Glu was doubled (by adding an additional 250 µM of Glu to the sample). An additional 27 minutes of delay pass followed by a doubling in signal. Finally, approximately 2.7 hours into the experiment, the microchip begins to fail.

As can be seen in the figure, the added tubing significantly increased the lag time between increases in Glu concentration in the sample and measured changes. At a time point of 1.5 hours, the concentration of the Glu sample was doubled to 500 µM through the addition of 12.5 µL of 20 mM Glu. Again, approximately 27 minutes passed before a change. As expected however, the signal output doubled. This doubling remained until at roughly the 2 hour time point, the normalized signal intensity climbed dramatically. This increase in signal was not due to a change in concentration however but reflected the current lifetime of the microchip. These shortcomings will be addressed in future iterations of this device.

Based on the normalized signal from the device, the recovered percentage of Glu using this probe was found to be fairly low. Given the initial concentration in the sample of 250 µM, and a signal of approximately 0.1 RFU, the corresponding concentration from the online derivatization calibration curve would indicate a measured concentration of Glu of approximately 10 µM. This represents a recovery of 4% which is well below the expected value of 13% estimated by CMA for Glu at this flow rate, for this probe size.

5.4 Conclusions

The nature of neurological conditions such as TBI and stroke pose significant challenges in an ICU environment. Conditions such as these, which simultaneously require constant and timely monitoring for changes in multiple biomarkers. While several methods exist to monitor relevant biomarkers such as ATP, glucose, lactate, pyruvate and Glu, most methods either rely on biosensors which are limited to single analytes or MD sampling with time consuming offline analysis. The online derivatization method developed here demonstrates the feasibility of using MD coupled directly to a microchip electrophoresis assay via an online derivatization process. Furthermore, the data presented here validates the Comsol model used to develop the microchip. By demonstrating the such a method can fully recapitulate the entire microfluidic device,

5.5 Future Directions

The device demonstrated here has successfully been used to detect Glu sampled via microdialysis for an extended period of time via online derivatization with NDA/CN. Two things must be addressed before the utility of the microdevice can be realized. First, as mentioned in the opening of this chapter, the initial intention for the design of this device was to use an all glass substrate. The rationale for this was that glass simply cannot be matched as a substrate in terms of ruggedness and reproducibility of the EOF. However, attempts at consistently manufacturing such a device were shown to be virtually impossible. Future work should therefore focus on either improving the manufacturing process or decreasing the size of the device to allow for easier bonding.

Secondly, the limits of detection for this device require improvement. This could largely be achieved by using an all glass device which would improve peak resolution, shape, and reduce background fluorescence. As mentioned, the calibration of the device was performed at physiologically relevant concentrations of Glu. However, the recovery of Glu via microdialysis can be very low as was demonstrated by this work and consequently, future efforts should continue to focus on improving recovery through the probe and the limits of detection, as well as limits of quantification for the device.

5.6 References

1. Timofeev, I., et al., *Cerebral extracellular chemistry and outcome following traumatic brain injury: a microdialysis study of 223 patients.* Brain, 2011: p. awq353.
2. Werner, C. and K. Engelhard, *Pathophysiology of traumatic brain injury.* British journal of anaesthesia, 2007. **99**(1): p. 4-9.
3. Benveniste, H., *Brain microdialysis.* Journal of neurochemistry, 1989. **52**(6): p. 1667-1679.
4. Sattler, R. and M. Tymianski, *Molecular mechanisms of calcium-dependent excitotoxicity.* Journal of molecular medicine, 2000. **78**(1): p. 3-13.
5. Kristián, T. and B.K. Siesjö, *Calcium in ischemic cell death.* Stroke, 1998. **29**(3): p. 705-718.
6. Chamoun, R., et al., *Role of extracellular glutamate measured by cerebral microdialysis in severe traumatic brain injury.* Journal of neurosurgery, 2010. **113**(3): p. 564.
7. Gupta, A.K., et al., *Measuring brain tissue oxygenation compared with jugular venous oxygen saturation for monitoring cerebral oxygenation after traumatic brain injury.* Anesthesia & Analgesia, 1999. **88**(3): p. 549-553.
8. Dale, N., et al., *Listening to the brain: microelectrode biosensors for neurochemicals.* Trends in biotechnology, 2005. **23**(8): p. 420-428.
9. Carpenter, K.L., A.M. Young, and P.J. Hutchinson, *Advanced monitoring in traumatic brain injury: microdialysis.* Current Opinion in Critical Care, 2017.
10. Stenken, J.A., et al., *Examination of microdialysis sampling in a well-characterized hydrodynamic system.* Analytical chemistry, 1993. **65**(17): p. 2324-2328.
11. Tholance, Y., et al., *Analytical validation of microdialysis analyzer for monitoring glucose, lactate and pyruvate in cerebral microdialysates.* Clinica Chimica Acta, 2011. **412**(7): p. 647-654.
12. Martínez-Valverde, T., et al., *Characterization of the ionic profile of the extracellular space of the injured and ischemic brain: a microdialysis study.* Journal of neurotrauma, 2017. **34**(1): p. 74-85.
13. Sandlin, Z.D., et al., *Microfluidic electrophoresis chip coupled to microdialysis for in vivo monitoring of amino acid neurotransmitters.* Analytical chemistry, 2005. **77**(23): p. 7702-7708.
14. Goodman, J.C. and C.S. Robertson, *Microdialysis: is it ready for prime time?* Current opinion in critical care, 2009. **15**(2): p. 110.
15. Nandi, P., D.P. Desai, and S.M. Lunte, *Development of a PDMS-based microchip electrophoresis device for continuous online in vivo monitoring of microdialysis samples.* Electrophoresis, 2010. **31**(8): p. 1414-1422.
16. Nandi, P., et al., *Development and optimization of an integrated PDMS based-microdialysis microchip electrophoresis device with on-chip derivatization for continuous monitoring of primary amines.* Electrophoresis, 2013. **34**(6): p. 895-902.
17. Huynh, B.H., et al., *On-line coupling of microdialysis sampling with microchip-based capillary electrophoresis.* Analytical chemistry, 2004. **76**(21): p. 6440-6447.
18. Fang, Q., et al., *Sequential injection sample introduction microfluidic-chip based capillary electrophoresis system.* Analytica chimica acta, 1999. **390**(1): p. 27-37.
19. Attiya, S., et al., *Design of an interface to allow microfluidic electrophoresis chips to drink from the fire hose of the external environment.* Electrophoresis, 2001. **22**(2): p. 318-327.

20. Lin, Y.-H., et al., *Flow-through sampling for electrophoresis-based microfluidic chips using hydrodynamic pumping.* Journal of Chromatography A, 2001. **937**(1): p. 115-125.
21. Wang, M., et al., *Microfluidic chip for high efficiency electrophoretic analysis of segmented flow from a microdialysis probe and in vivo chemical monitoring.* Analytical chemistry, 2009. **81**(21): p. 9072-9078.
22. Yassine, O., et al., *Electrophoresis PDMS/glass chips with continuous on-chip derivatization and analysis of amino acids using naphthalene-2, 3-dicarboxaldehyde as fluorogenic agent.* Analytica chimica acta, 2008. **609**(2): p. 215-222.
23. Manica, D.P., et al., *Analysis of the stability of amino acids derivatized with naphthalene-2, 3-dicarboxaldehyde using high-performance liquid chromatography and mass spectrometry.* Analytical biochemistry, 2003. **322**(1): p. 68-78.
24. Gyimesi-Forrás, K., et al., *Comparative study on the use of ortho-phthalaldehyde, naphthalene-2, 3-dicarboxaldehyde and anthracene-2, 3-dicarboxaldehyde reagents for α-amino acids followed by the enantiomer separation of the formed isoindolin-1-one derivatives using quinine-type chiral stationary phases.* Journal of Chromatography A, 2005. **1083**(1): p. 80-88.
25. Shou, M., et al., *In vivo monitoring of amino acids by microdialysis sampling with on-line derivatization by naphthalene-2, 3-dicarboxyaldehyde and rapid micellar electrokinetic capillary chromatography.* Journal of neuroscience methods, 2004. **138**(1): p. 189-197.
26. Wang, L., et al., *Mixing enhancement of a passive microfluidic mixer containing triangle baffles.* Asia-Pacific Journal of Chemical Engineering, 2014. **9**(6): p. 877-885.
27. Hessel, V., H. Löwe, and F. Schönfeld, *Micromixers—a review on passive and active mixing principles.* Chemical Engineering Science, 2005. **60**(8): p. 2479-2501.
28. Adeosun, J.T. and A. Lawal, *Numerical and experimental studies of mixing characteristics in a T-junction microchannel using residence-time distribution.* Chemical Engineering Science, 2009. **64**(10): p. 2422-2432.
29. Stroock, A.D., et al., *Chaotic mixer for microchannels.* Science, 2002. **295**(5555): p. 647-651.
30. Oborny, N.J., et al., *Evaluation of a Portable Microchip Electrophoresis Fluorescence Detection System for the Analysis of Amino Acid Neurotransmitters in Brain Dialysis Samples.* Analytical Sciences, 2016. **32**(1): p. 35-40.
31. De Montigny, P., et al., *Naphthalene-2, 3-dicarboxyaldehyde/cyanide ion: a rationally designed fluorogenic reagent for primary amines.* Analytical Chemistry, 1987. **59**(8): p. 1096-1101.

6. Future Directions

6.1 Near Term Future Directions

All discussions of the future of this project will center on what has been my primary focus for the last 5 years: improving the overall limits of detection for the system while maintaining or improving temporal resolution. By referring to the *system* here, I include the entire process from the sampling of the biomarker in tissue to the display of clinically actionable data. To fully understand how the system can be improved it is useful to understand its limitations.

As mentioned in previous chapters, the recovered concentration of any biomarker sampled via microdialysis is primarily a function of the flow rate of the dialysate since the sampling process itself relies on diffusion. This fact has several implications. First, a tradeoff is immediately apparent. Either the sampling rate must be optimized for sample recovery or for the volume of sample generated per unit time. In the case of the latter condition, any assay subsequently used for analysis must have sufficiently low limits of detection to compensate for the lowered sample concentration. The use of microfluidic devices can allow lower flow rates to be used without negatively impacting overall time lag due to their small volume requirements.

For the specific application described here, another constraint was placed on the time lag of the system by the rate at which the Glu in the dialysate sample could be derivatized. For instance, regardless of how high the concentration of Glu in the dialysate sample ultimately is, if the flow rate into the online microchip (described in chapter five) is too high to allow for the sample to be derivatized, it cannot be detected.

An example of this can be seen in Figure 6.1 below which compares flow rates vs derivatized Glu at the entrance to the separation channel. This image shows the effect of flow rate on the absolute amount of derivatized product produced. At the lowest flow rate modeled, 1.667E-11 m^3/s, the sample reaches full derivatization prior to reaching the separation channel. However, at a higher flow rate, 3.7495E-11 m^3/s, sample is pushed from the device before full derivatization can occur.

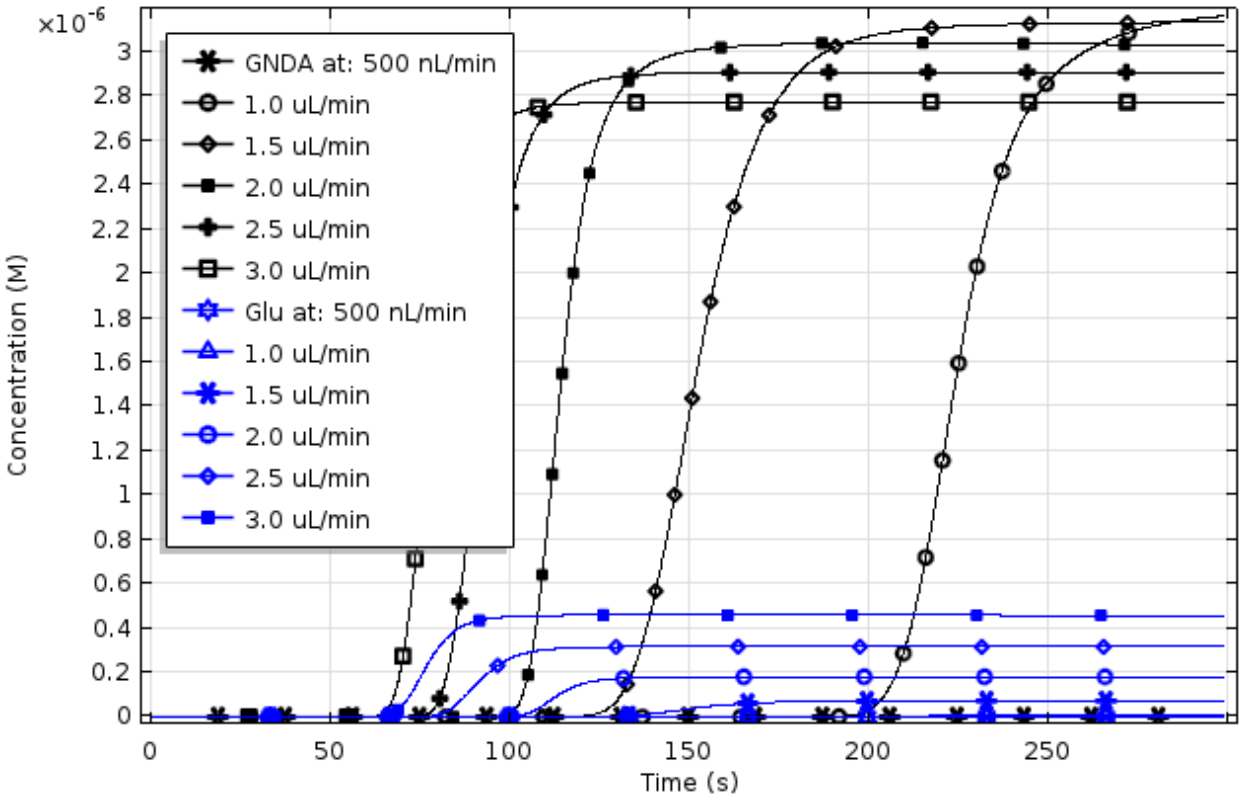

Figure 6.1:Shown on the upper portion of the figure is the output of derivatized Glu (GNDA) at the entrance to the separation channel and on the lower portion, the remaining underivatized Glu. Of note is the fact that over 1µL/min (1.6665E-11 m3/s), sample exits the microchip without being derivatized.

Looking at this from another perspective however, the flow rate problem becomes a limit of quantification (LOQ) problem. If we assume for instance that the recoverable, basal concentration of Glu in the extracellular space near at risk tissue is 1µM and that full derivatization using NDA/CN (described in chapter three) within the online microchip requires 180 seconds [1], then a detection system with an LOQ of 1µM would have a minimum response time of 180 seconds. If, however, the LOQ of the system were improved to 500 nM, the derivatization time could be decreased by ~50% without negatively impacting the overall system. In summary then, one way to decrease the time lag is to improve the LOQ of the system.

The rate of the derivatization reaction is another possible point of improvement. At present, NDA/CN is used primarily due to its selectivity for primary amines, fairly fast reaction rate, and reasonably high quantum efficiency of 0.4 [2], making it a good solution to this specific derivatization problem. However, to decrease the overall time lag of the system, we would ideally have either a derivatization reagent that was either faster or brighter (higher quantum efficiency), while maintaining the selectivity for primary amines.

6.1.1 Enhancing the Derivatization Reaction Rate

The choice of NDA as derivatization agent was based on it being a good combination of several desirable properties. However, other, faster methods of derivatization exist that could be explored. Among those options is the possibility of using a thiol rather than cyanide during the derivatization reaction. This method has been used in the past with NDA as well as a fluorogenic compound related to NDA known as *o*-phthalaldehyde (OPA).

NDA was designed as a replacement for OPA, an earlier fluorogenic compound that was specific for primary amines as well but had the downsides of being less stable over time and has an excitation wavelength at 350 nm. Like NDA, OPA requires a nucleophile such as cyanide or a thiol compound to react with a primary amine. Typically, OPA is used in the presence of a thiol compound such as 2-mercaptoethanol (2ME) for the derivatization reaction to take place [2]. However, the use of a thiol results in the formation of a much less stable fluorescent compound (an isoindole derivative). Despite this, it is an attractive option since the reaction of OPA/2ME is much faster than NDA/CN and is stable enough that, for an online system such as this, it could be adequate.

NDA/2ME has been evaluated by Manica et al. [3] among others and was observed to have an extremely rapid reaction rate (less than one minute) as compared to the 180 second minimum reaction time for NDA/CN. This rate however came at the cost of having a half-life of approximately two minutes. Such a short half-life would not be a problem for rapid online measurements of course but it would complicate method development.

The real impediment to the use of 2ME with NDA is in its noisome qualities. 2ME is used to give natural gas a detectable smell and its presence in any system designed for use in a hospital setting would be an impediment to adoption to say the least. Unfortunately, that smell is a property common to many thiol compounds that might conceivably be used with NDA.

6.1.2 Derivatization using OPA-SAMSA-F

A potential solution to the need for noisome thiol compounds for use with either NDA or OPA has been explored by Hapuarachchi et al. As they explain, by using a thiol functionalized fluorescein compound (5-2,3-S-acetylmercapto succinoyl amino fluorescein) (SAMSA-F) rather than a nucleophile such as 2ME or CN, a fluorophore with higher quantum efficiency (fluorescein) can be incorporated into the final product [4]. This can be seen in Figure 6.2 below.

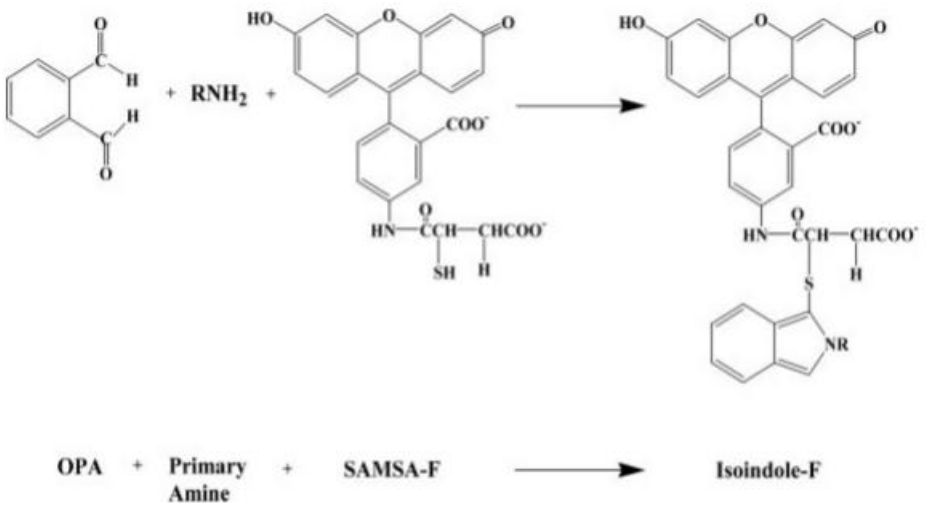

Figure 6.2: The derivatization of a primary amine using OPA/SAMSA-F.

The use of SAMSA-F would provide an almost ‘best of all worlds’ option with reaction times of 10-40 seconds and selectivity to primary amines, similar to OPA, but with an excitation wavelength of ~490 nM. SAMSA-F also has the added benefit of a much higher quantum efficiency approaching 0.9 as opposed to that of OPA or NDA at ~0.4 [2, 4]. There are two potential caveats to the use of OPA-SAMSA-F. First, the stability of the isoindole product is not

well characterized and method development may prove difficult as a result. Second, unlike NDA or OPA, SAMSA-F is not a fluorogenic compound but a fluorophore. This means that it is inherently fluorescent without reacting which complicates the electropherogram and could affect analyte resolution.

Initial work evaluating the possibility of using NDA/SAMSA-F appears to indicate quenching of the fluorophore likely occurs due to overlapping excitation and emission spectra of the two compounds [2, 4]. Future work should therefore focus on the use of OPA/SAMSA-F.

6.1.3 Improved Substrate Bonding and Separation Potentials

Chapter three discussed the development and testing of a microchip electrophoresis device with integrated sample derivatization for online monitoring of dialysate samples. Part of that discussion referred to the complications inherent in guaranteeing that a reaction has reached completion as it flows through a microchannel. The resulting design required 80 cm of a serpentine channel, 450 µm wide by 25 µm deep before reaching the entrance to a separation channel. That channel itself was 15 cm long, 70 µm wide, and 25 µm deep. Altogether, once additional channels for coupling the microdialysis flow to the device were factored in, the microchip had a bonding surface area of approximately 97 cm^2. To bond these devices, both the etched glass substrate and the blank had to be flat to an extremely small tolerance across that entire surface area with no contamination or air pockets. Ultimately, as devices failed due to clogs or breakage, or simply didn't bond properly, it became clear that glass-glass devices were proving too difficult to make

and poly-dimethyl siloxane (PDMS)-glass hybrid devices were used. These devices had three walls of glass and one of PDMS and could very closely approximate the glass-glass devices.

6.1.4 Separation Potential

An unfortunate effect of the hybrid PDMS/Glass device is a greater susceptibility of the PDMS channel wall to damage either chemically or due to heat in the channel caused by joule heating as the electric field increases. This is particularly unfortunate as early tests on smaller all glass devices using separation potentials approaching 700 V/cm have shown dramatically improved limits of detection for the target analytes mentioned in this thesis. These improvements are due to improved resolution and peak shape with increasing separation potentials. The application of potentials over ~500 V/cm to a PDMS/glass chip however will destroy the PDMS channel wall and consequently the separation making improvements using this method impossible.

6.2 Long Term Future Directions

One of the primary motivating factors for this work has been the lack of knowledge surrounding the long-term pathogenesis of TBI. This lack of knowledge would at first seem to be an odd thing given the long history of work in this area, going back several decades at least. After initial successes improving patient outcomes via interventions such as preventing hypotension (low blood pressure) and hypoxia (low oxygen), additional progress toward arresting the secondary effects of TBI has been disappointing. Part of this has been, as Park et al. [5] put it in their

discussion of current treatment, the “greater than anticipated complexity” of the underlying processes involved in secondary damage. The mechanisms involved in the excitatory amino acid cascade, inflammatory responses, and axonal disconnection have proven difficult to study. The difficulty in understanding these processes has been compounded by the high variability in clinical TBI cases as differing injuries can cause greatly varying types of secondary damage.

The combination of a complex mechanism with a highly variable clinical presentation limits available approaches such as high throughput screening to develop drug targets. To address this, multiple animal models have been developed. These models have primarily been rats but also include mice, cats, rabbits, swine, and of course primates [6]. These models, which become more directly applicable to humans as they move from mice to primates, also become more time consuming, expensive, and ethically dubious. One model currently under investigation, is the use of zebrafish to approximate many of the same pathologies while allowing rapid and inexpensive studies to be conducted. Zebrafish are small, 4 cm long vertebrate fish with a rapid generation time of approximately 3 months. They possess significant homology with mammalian anatomy including analogous receptors such as 2-amino-3-(3-hydroxy-5-methyl-isoxazol-4-yl) propanoic acid (AMPA) and N-methyl-D-aspartic acid (NMDA), two receptors implicated in the excitotoxic glutamate cascade, as well as homologous neuron cytoskeletal proteins [7]. Compared to other model organisms, these fish are small, with brain volumes of roughly 2mm x 2.5mm x 3mm making them difficult targets for many techniques including microdialysis. However, the ability to perform rapid studies might make up for this difficulty. Finally, embryonic fish can directly be used in a high throughput (96 well plate) format when screening for drug candidates before proceeding to a more specific TBI model such as a concussive force model [6-8].

An interesting possibility for the future of this work could lie in the integration of the online microchip system into a higher throughput system. This method could use either immobilized zebra fish exposed to a TBI event and monitored directly using microdialysis, or a continuous sampling of cell based cultures.

6.3 References

1. Shou, M., et al., *In vivo monitoring of amino acids by microdialysis sampling with on-line derivatization by naphthalene-2, 3-dicarboxyaldehyde and rapid micellar electrokinetic capillary chromatography.* Journal of neuroscience methods, 2004. **138**(1): p. 189-197.
2. De Montigny, P., et al., *Naphthalene-2, 3-dicarboxyaldehyde/cyanide ion: a rationally designed fluorogenic reagent for primary amines.* Analytical Chemistry, 1987. **59**(8): p. 1096-1101.
3. Manica, D.P., et al., *Analysis of the stability of amino acids derivatized with naphthalene-2, 3-dicarboxaldehyde using high-performance liquid chromatography and mass spectrometry.* Analytical biochemistry, 2003. **322**(1): p. 68-78.
4. Hapuarachchi, S. and C.A. Aspinwall, *Design, characterization, and utilization of a fast fluorescence derivatization reaction utilizing o-phthaldialdehyde coupled with fluorescent thiols.* Electrophoresis, 2007. **28**(7): p. 1100-1106.
5. Park, E., J.D. Bell, and A.J. Baker, *Traumatic brain injury: can the consequences be stopped?* Canadian Medical Association Journal, 2008. **178**(9): p. 1163-1170.
6. Xiong, Y., A. Mahmood, and M. Chopp, *Animal models of traumatic brain injury.* Nature Reviews Neuroscience, 2013. **14**(2): p. 128-142.
7. McCutcheon, V., et al., *A Novel Model of Traumatic Brain Injury in Adult Zebrafish Demonstrates Response to Injury and Treatment Comparable with Mammalian Models.* Journal of neurotrauma, 2017. **34**(7): p. 1382-1393.
8. McCutcheon, V., et al., *A Model of Excitotoxic Brain Injury in Larval Zebrafish: Potential Application for High-Throughput Drug Evaluation to Treat Traumatic Brain Injury.* Zebrafish, 2016. **13**(3): p. 161-169.

A. Quick Reference to Glass-Glass ME Device Construction

Glass-Glass ME Device Construction

The following quick reference guide is a step-by-step explanation of the steps necessary to construct a glass-glass ME device. This process is also shown graphically in Figure A.1 of Appendix A.

1. Required Cleanroom Facilities and Instrumentation

ABM UV Flood Source and Mask Alignment System (ABM, Scotts Valley, CA)

Brewer Science Cee 200CBX Spin Coater (Brewer Science, Rolla, MO)

Harrick PDC-32G Plasma Cleaner (Harrick Plasma, Ithaca, NY)

BD-20AC Laboratory Corona Treater (Electro-Technic Products, Chicago, IL)

Tencor Alpha-Step 200 Profilometer (KLA Tencor, Milpitas, CA)

Fisher Scientific Muffle Furnace **(**Fisher, Waltham, MA)

2. Required Glass-Glass Microchip Fabrication Materials

AZ1518 precoated glass substrates such as borosilicate (borofloat) or soda lime glass (Telic, Valencia, CA)

AZ1518 (AZ Electronic Materials Corp, Somerville, NJ)

MIF 300 AZ1518 developer (Emd Performance Materials, Somerville, NJ)

Acetone (Fisher, Waltham, MA)

Water

Chrome Etchant, CR-75 (Cyantek, Fremont, CA)

HF Etchant solution consisting of: 20% HF, Nitric Acid, Water

Ultra Pure Calcium Acetate (MP Biomolecules, Solon, OH)

Alconox™ Powdered Detergent (Fisher, Waltham, MA)

Diamond Drill Bits (Ukam Industrial Superhard Tools, Valencia, CA)

Programmable High Temperature Oven (Fisher, Waltham, MA)

3. Photolithography (Figure A.1-a,b)

1. Pre-bake glass substrate, photoresist side up, on a hotplate at 100 ºC for 2 minutes.

Note: The prebake time will vary according to the photoresist type and thickness. Consult the photoresist documentation for more information.

2. Allow glass to cool to room temperature before proceeding.

3. Place photomask on glass substrate such that the printed side of the photomask is in contact with the photoresist. Apply a vacuum to ensure minimal distance between mask and photoresist.

4. While maintaining a vacuum, expose the photoresist to UV through the photomask. Duration of exposure will depend on resist type, thickness, and UV intensity.

5. Place exposed glass substrate in developer to remove exposed area.

6. Wash with water and dry gently with compressed nitrogen or air.

7. Place on hotplate at 100 ºC for 10 minutes to fully evaporate developer.

4. Chrome Removal (Figure A.1-c)

8. Place wafer in a Pyrex™ dish of chrome etchant.

9. Agitate gently until chrome regions are clear + 45 seconds.

10. Rinse with water and dry using compressed nitrogen or air.

Note: Chrome and photoresist must be removed from glass before a glass cutter will be effective. If making multiple devices simultaneously, it is important to include these cut lines in the photomask design. Additionally, chrome-coated glass will appear transparent before all chrome has been removed. However, a thin layer of chrome that remains will prevent glass-glass bonding. For this reason, allow the glass substrate to remain in the chrome etchant for 45 seconds *after* it appears that the chrome has been removed. Additional etching beyond this period will begin to undercut features.

5. Glass Cutting and Drilling

11. Using a glass cutter, cut glass along exposed paths between individual devices.

Note: Extreme care should be taken not to scratch the surface of the photoresist. If this is a problem, the glass cutting and drilling steps can be performed after the HF wet etching.

12. Once separated, place individual ME devices in approximately 1 cm of water with a sacrificial layer under the chip to allow the drill to pass through without being damaged.

13. Slowly drill glass, applying constant pressure. It may be necessary to use gradually increasing drill bit sizes.

Note: More ME devices are destroyed in this step than any other. Using new diamond-coated bits can help prevent glass breakage. When choosing drill bit sizes, two things to consider are whether or not MD access ports will be glued into place over the holes and evaporation during operation. If the holes drilled in the glass to create sample and buffer wells are too small, these solutions will evaporate rapidly during operation. As this evaporation proceeds, ionic strength will change. This in turn will cause additional current draw and, consequently, alter migration times. If MD access ports are to be placed over the holes, the holes must of course be smaller than the ports themselves.

6. HF Wet Etching (Figure A.1-d)

14. Place glass with photoresist/chrome side up in HF etchant and agitate for duration of etching process. Etching time will depend on desired depth as well as glass type.

15. Remove from HF etchant, rinse with a solution of calcium acetate to deactivate the HF etchant. Following this, rinse with water and dry using compressed nitrogen or air.

16. Measure channel depth using a profilometer. If the desired depth has not been achieved, calculate the etch rate and place the device back in the HF for the necessary amount of time.

Note: Due to the extreme toxicity of HF, the best practice is to minimize the number of times the device is taken in and out of the HF etchant if at all possible. When handling the substrate, the HF remaining on the device should first be deactivated by rinsing with a slurry of calcium acetate in water, followed by rinsing with water.

7. Removal of Remaining Photoresist and Chrome (Figure A.1-e,f)

17. Remove all remaining photoresist by rinsing with acetone.

18. Rinse with water and dry with compressed nitrogen or air.

19. Place the glass substrate in chrome etchant, agitating gently, until all remaining chrome has been removed + 1 minute.

Note: The removal of all photoresist and chrome is necessary to facilitate a glass-glass bond.

8. Bonding Glass-Glass ME Devices (Figure A.1-g)

20. Cut blank glass to the necessary size.

Note: To avoid breakage due to differences in thermal expansion, blanks should be of the same glass type as the etched device.

21. Clean both glass pieces using Alconox™ mixed to the manufacturer's specifications.

22. Rinse both sides well with deionized water (DI) water

23. Incubate the glass surfaces to be bonded using a solution of 0.5% (w/v) calcium acetate, approximately 30 mM, and 0.5% (w/v) Alconox™ in DI water for no less than 30 seconds.

24. Rinse thoroughly with DI water.

25. Under running DI water, bring glass pieces together from bottom to top.

Note: Force out any remaining bubbles but allow a layer of water to remain.

26. Place the device in an oven for 1 hour at 60 ºC.

Note: Do NOT force all water from between the layers. The evaporation from the oven will force the glass together.

27. At the 1-hour mark, inspect the device for Newton rings indicating incomplete bonding of the surfaces. If found, separate using a razor blade and repeat steps 21–26.

28. Place binding clips around the device to apply additional pressure. Increase the temperature to 105 ºC for 2 hours.

29. Inspect device. If Newton rings have formed, separate using a razor blade and repeat steps 21–28.

30. If no Newton rings are found, execute the following program, slowly increasing the oven temperature to 630 ºC and holding before cooling gradually to room temperature. Steps shown in Table A.1.

31. If the ME device is meant to be used online (MD-ME), access ports must be glued to the chip to allow the flow from the syringe pump to enter the device. Polyethylene tubing connecting the syringe pump can be connected directly to ports glued to the surface of the device. To glue ports in place, a strong UV source such as the ELC-450 (Electrolite Corp, Bethel, CT) should be used. UV glue (Fisher Scientific, Waltham MA) should be applied carefully to the ports while holding them in place.

Note: Should glue enter the channels, flush with water and methanol until the glue has been cleared. Avoid UV exposure during this period if possible.

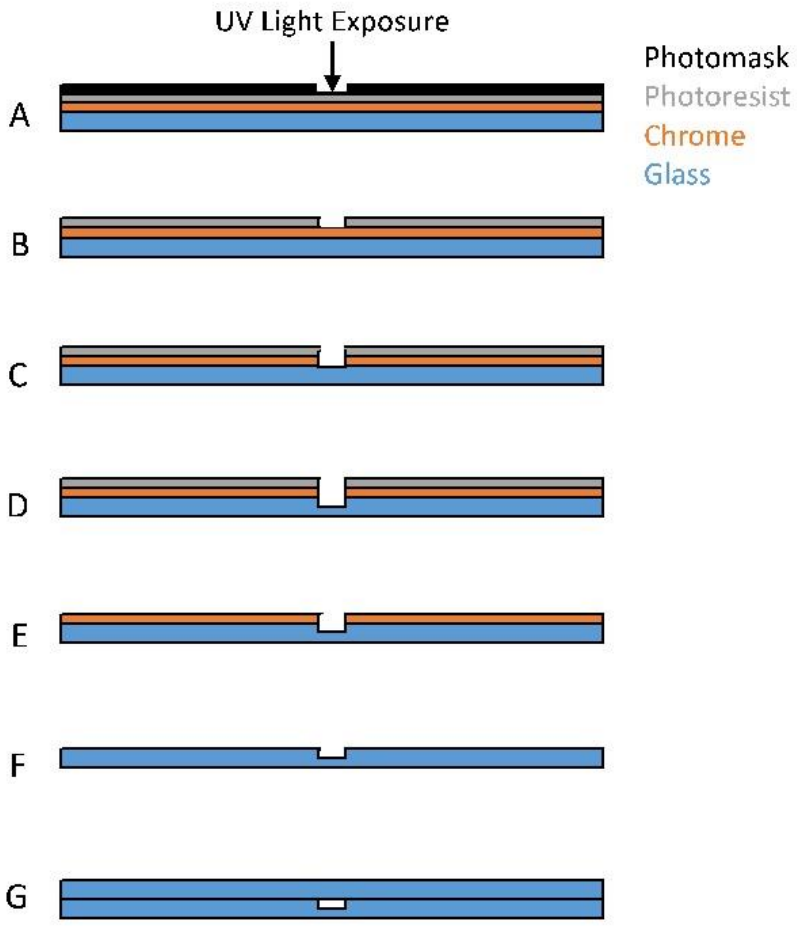

Figure A.1: Photolithography Steps for Glass-Glass Microdevice Construction

Elapsed Time, Hours	Time for Step, Hours	Oven Temp, C	Rate, C/Min
0.00	0.00	25	0.0
2.97	2.97	560	3.0
3.30	0.33	630	3.5
5.80	2.50	630	0.0
6.16	0.36	565	-3.0
6.77	0.61	510	-1.5
7.27	0.50	510	0.0
8.77	1.50	465	-0.5
10.24	1.47	25	-5.0

Table A.1: Oven Program for Thermal Bonding of Glass-Glass Microdevices

B. Quick Reference to PDMS-PDMS ME Device Construction

PDMS-PDMS Device Construction

The following quick reference guide is a step-by-step explanation of the steps necessary to construct a PDMS-PDMS ME device. This process is also shown graphically in Figure B.1 of Appendix B.

1. Required Cleanroom Facilities and Instrumentation

ABM UV Flood Source and Mask Alignment System (ABM, Scotts Valley, CA)

Brewer Science Cee 200CBX Spin Coater (Brewer Science, Rolla, MO)

Harrick PDC-32G Plasma Cleaner (Harrick Plasma, Ithaca, NY)

BD-20AC Laboratory Corona Treater (Electro-Technic Products, Chicago, IL)

Tencor Alpha-Step 200 Profilometer (KLA Tencor, Milpitas, CA)

Fisher Scientific Muffle Furnace **(**Fisher, Waltham, MA)

2. Required PDMS Microchip Fabrication Materials

Silicon wafer (100-mm thickness) (University Wafer, Boston MA)

SU-8 10 photoresist (Microchem Corp, Flanders, MA)

SU-8 developer (Microchem Corp, Flanders, MA)

Isopropyl alcohol (Fisher, Waltham, MA)

Sylgard™ 184 Silicone Elastomer Base (Dow Corning, Auburn, MI)

Sylgard™ 184 Silicone Elastomer Curing Agent (Dow Corning, Auburn, MI)

Parafilm™ (Fisher, Waltham, MA)

3. Silicon Master Spin-Coating (Figure B.1-a)

1. Use nitrogen flow to clean surface of silicon wafer.
2. Center silicon wafer on spin coater platform.
3. Pipette 4 mL of SU-8 10 photoresist onto the exact center of wafer and spin coat at 2000 rpm until fully coated.

Note: The amount of SU-8 10 photoresist used directly influences its thickness and, subsequently, the final depth of the microfeatures. The values stated in these steps are for a final thickness of 15 µm with SU-8 10. Values associated with other thicknesses and photoresists should be calculated based on manufacturers' specifications.

4. Prebake silicon wafer at 65 ºC for 2 minutes on hotplate, then increase temperature to 95 ºC for 5 minutes.

Note: To avoid breaking the silicon wafer, it is better to start the hotplate at room temperature and gradually ramp up to each specified temperature before heating it for the desired length of time. This should be done in any step requiring heating the silicon wafer.

4. Silicon Master Photomask Alignment and UV Exposure (Figure B.1-b)

5. Align negative photomask on top of wafer on photolithography platform; use vacuum to hold substrate and mask in place.

   Note: When using a printed photomask, make sure that the printed side is facing down (flush with the substrate). This will prevent any diffusion of light across the width of the transparency and avoid unwanted enlargement of the features. Make sure the silicon wafer has cooled to room temperature before aligning the photomask.

6. Expose to UV light for 16 seconds.

   Note: Full UV exposure of SU-8 is dependent on the substrate thickness and light source intensity. In this case, a flood-source with output intensity of 21 mW/cm^2 is used.

5. Silicon Master Post-Exposure Processing and Profiling (Figure B.1-c)

7. Post bake silicon wafer at 65 ºC for 1 minute on hotplate, then increase temperature to 95 ºC for 2 minutes.
8. Place developed wafer in SU-8 developer; gently swirl for 2 minutes to remove un-developed photoresist.
9. Remove master from developer; wash with isopropyl alcohol and dry with nitrogen flow.

   Note: Acetone will cause developed SU-8 to dissolve. Only isopropyl alcohol should be used for cleaning silicon masters using this photoresist.

10. Hardback at 200 ºC for 2 hours.
11. Use a profilometer to confirm the dimensions of the microfeatures on the master.

6. PDMS Curing (Figure B.1-d,e)

12. Measure 12 grams total of a 9:1 ratio of Sylgard™ 184 elastomer (10.4 g) and curing agent (1.6 g) into a small cup; mix thoroughly.

    Note: This amount of polymer was chosen because the surface tension will be sufficient to hold the mixture on the master's surface. Greater amounts can be used, but a mold will be necessary to hold the polymer on the wafer's surface. Using 12 g will result in a final thickness of approximately 1.2 mm.

    Note: Different ratios of elastomer to curing agent can be used in order to modify the elasticity of the PDMS. In general, the more curing agent used, the less elastic is the final polymeric substrate.

13. Place cup inside vacuum desiccator and remove all gas bubbles via repeated application of vacuum, being careful not to spill polymer over the edges of the container.
14. Pour mixture onto master and allow it to settle to a uniform thickness; place in oven and heat at 70 ºC for at least two hours.

    Note: Make sure that the master is level once it is placed in the oven. If it is placed at an angle, the PDMS will cure unevenly and potentially be unusable.

15. Use a razor blade to scrape the PDMS off of the edges of the master, then slowly peel off the polymer layer, being careful not to stretch or rip the substrate.
16. Either bond immediately (see next section) or place the PDMS on a piece of Parafilm™, channel-side down; fold Parafilm™ over the top of PDMS to fully seal it.

Note: If protected from air exposure, PDMS can safely be sealed within Parafilm™ for up to one week. If cracks are visible in the microchannels when examined using a microscope, the polymer has dried out and should not be used.

7. PDMS Hole Punching and Bonding (Figure B.1-f)

17. Use a PDMS hole puncher to remove PDMS at reservoirs and create wells, using a Kimwipe to clean the puncher surface between each use.
18. Peel Parafilm™ off PDMS.
19. Place the PDMS with the channels facing up next to another piece of PDMS.

    Note: Although the parafilm should keep any dust or other detritus from reaching the PDMS surface, it can still happen. This is most easily avoided by bonding the PDMS in a cleanroom environment, but a piece of clear tape can be used to remove any dust from the surface immediately before step 4.
20. Run a handheld plasma oxidizer over the surface with the electrode a centimeter above the polymer surface, spending around 30 seconds on each piece of PDMS [1].

    Note: A conventional plasma oxidizer can also be used.
21. Firmly press the substrates together, taking care to avoid touching the oxidized surface; run fingers over the PDMS to force out any air bubbles that form between the layers
22. Apply pressure with fingertips around the edges of the microchip until sealed, usually within one or two minutes.

    Note: Applying pressure directly over the channels can result in forcing them closed and ruining the device.

23. Examine device using a microscope to guarantee that the microfeatures are preserved and that no clogs are present.

Bonding of the PDMS layer to either glass or another PDMS piece can now be performed using either a reversible method, which allows for later separation of the device layers, or permanent bonding. If the device is to be used with either high voltages or high pressures, permanent bonding is recommended.

8. Reversible Bonding

24. Wipe down the glass substrate with a Kimwipe soaked in 50% isopropyl alcohol (IPA), then dry with lint-free paper and nitrogen flow.
25. If necessary, use a PDMS puncher to remove PDMS at reservoirs and create wells, using a Kimwipe to clean the puncher surface between each use.

    Note: This step is not needed if wells have been drilled in the glass substrate.
26. Peel Parafilm™ off PDMS

    Note: If bonding in a cleanroom facility, there should be no dust or other detritus on the substrate surface. A piece of clear tape can be used to remove any particulates on both glass and PDMS if necessary.
27. Slowly place PDMS on glass substrate, channels facing inwards; run fingers over the PDMS to force out any air bubbles that form between the layers.

28. Examine device using a microscope to guarantee the microfeatures are preserved and no clogs are present.

    Note: If there is particulate in the channels or improper sealing, the PDMS can be peeled off the glass and re-applied after using tape to clean both substrate surfaces.

9. Irreversible Bonding

29. Wipe down the glass substrate with a Kimwipe soaked in 50% IPA, then dry with lint-free paper and nitrogen flow.
30. If necessary, use a PDMS puncher to remove PDMS at reservoirs and create wells, using a Kimwipe to clean the puncher surface between each use.

    Note: This step is not needed if wells have been drilled in the glass substrate.
31. Peel Parafilm™ off PDMS.

    Note*:* If bonding in a cleanroom facility, there should be no dust or other detritus on the substrate surface. A piece of clear tape can be used to remove any particulates on both glass and PDMS if necessary.
32. Run a handheld plasma oxidizer (BD-20AC, Electro-Technic Products, Chicago IL) over the surface with the electrode a centimeter above the polymer surface, spending around 30 seconds on each piece of PDMS

    Note: A conventional plasma oxidizer (Harrick Scientific, Ithaca NY) can also be used. It is not recommended to oxidize PDMS for more than 2 minutes, as this can result in degradation of the surface and potential damage to any microfeatures or improper bonding.

33. Firmly press the substrates together, taking care to avoid touching the oxidized surface; run fingers over the PDMS to force out any air bubbles that form between the layers
34. Apply pressure with fingertips around the edges of the microchip until sealed, usually within one or two minutes.

    Note: Applying pressure directly over the channels can result in forcing them closed and ruining the device.
35. Examine device using a microscope to guarantee that the microfeatures are preserved and no clogs are present.

    Note: If there is particulate in the channels or improper sealing, the PDMS must be removed by scraping it off with a razor blade. The glass substrate should be washed with IPA and acetone to clean away any residual PDMS before attempting a second bonding.

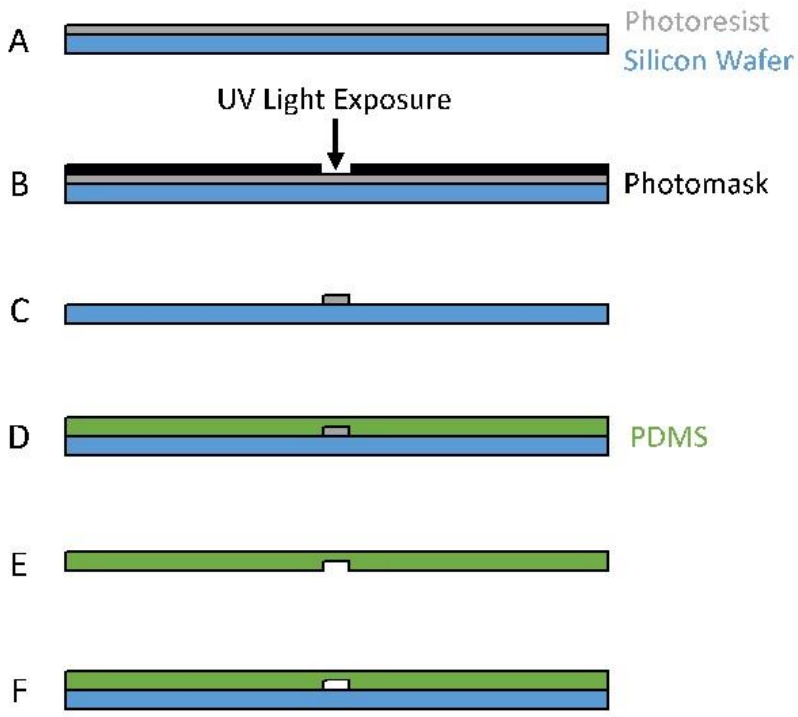

Figure B.1:PDMS-PDMS Microdevice Construction

1. Haubert, K., T. Drier, and D. Beebe, *PDMS bonding by means of a portable, low-cost corona system.* Lab on a Chip, 2006. **6**(12): p. 1548-1549.

C. Notes on ME Device Use

Experience has shown that there are many ways in which an ME separation can encounter difficulties. Below are the steps to diagnosing the most common problems.

1. Unstable Separation Voltage or Current

Changes in voltage or current during a separation can be the result of gradual evaporation from the sample and buffer wells. This evaporation can, in turn, change the ionic concentration and, consequently, the resistance of the ME system. However, sudden changes such as a spike or oscillation in current are indicative of the formation of bubbles (due to Joule heating) or a clogged channel. Should this occur once, it may only be necessary to clean the ME chip and replace the buffer. If bubbles are forming repeatedly, using a buffer of lower ionic strength may be necessary.

2. Spikes in Signal Output

Sudden signal spikes that are either too narrow to be genuine peaks or substantially higher in signal than the concentration would warrant can be caused by bubbles and/or particles in the channels. Both of these conditions can be quickly diagnosed by inspecting the channel under a microscope. Should particles be found during offline use, filtering the sample more thoroughly prior to injection using a 0.22 µm syringe filter is likely the best solution as sample volume is typically not a limiting factor. During online use, samples are filtered through the porous membrane of the microdialysis probe. Particles found in online samples could indicate that a

smaller pore size should be used. Despite this, particles will sometimes form in the channel itself due to, for instance, NDA precipitating from solution. This condition can sometimes be prevented by adding a small amount of ACN to the BGE.

Bubbles are typically indicative of one of two conditions. The first is that the ME device was not properly prepared before use. To ensure that no bubbles remain in the channel, continue to apply negative pressure to the waste port while adding the BGE. Visually inspect prior to use to verify that all bubbles have been removed. Should bubbles form during the run, it is likely due to Joule heating boiling the BGE inside the channel itself. Decreasing the applied potential or decreasing the ionic strength of the BGE (and thereby lowering the current draw) will prevent further bubble formation.

3. Gradual Increases in Baseline, No Peaks Detected

Gradual increases in the baseline are indicative of an unstable or nonexistent gate, therefore allowing fluorescent product to gradually enter the separation channel and accumulate. This can be diagnosed by visually inspecting the gate using a microscope and corrected by adjusting the ratio of HV potentials. Additionally, a parametric search for appropriate combinations of voltages using Comsol modeling can save considerable time when first using an ME device.

4. Short Circuit During Application of HV Potentials

Often, this is due to a thin layer of conductive liquid between wells on the chip. Should this be the case, carefully drying the surface using a Kimwipe® is often sufficient to resolve the problem. However, if a surfactant such as SDS is present in the buffer, a conductive monolayer can still be present. This monolayer can be removed using methanol. Finally, it is possible for high voltage arcing to occur within the chip itself if bonding of the two layers was incomplete.

5. Clogged or Blocked Channels

The micrometer channel dimensions in ME devices make them highly susceptible to clogging. If any particulates get into the channels or crystals form in the buffer, there can be a variety of effects on the separation. If no peaks are detected or if there are inconsistencies in the separation current and none of the previous issues are present, the channels should be examined with a microscope to see if any clogs are visible. Clogs are especially common near the sample reservoir inlets and at the electrokinetic gate, although they can occur anywhere within the microchip.

The easiest solution for clogs is to avoid them in the first place. Using lint-free paper any time it is necessary to physically wipe down the chip will help to avoid getting fibers in the wells. Additionally, any solution put into the device should be filtered to remove any particulate in the liquid. If the device is not in use for an extended length of time, the channels should be completely

filled with water and then stored within a beaker; this will prevent any evaporation within the channels leading to clogs.

6. Removing Clogs from Glass-Glass Microchips

Due to the length of time required to fabricate new all-glass microchips, cleaning a clog from one of these devices is often preferable to making a new one. Various solutions can be flowed through the channels via the application of negative pressure in order to reduce or completely dissolve clogs. We have previously used hydrochloric acid, nitric acid, sodium hydroxide, acetonitrile, isopropyl alcohol, and DMSO in order to clean clogs from chips. Unfortunately, there is no one specific solution that works more often than any other, so this process is mostly trial and error.

Sonicating the chip has also successfully removed clogs. In these cases, the channels were filled with water before being placed in a full beaker and placed in a sonicator bath. The vibrations can break down any blockages to the point at which they can be washed out. We have also had limited success using high temperatures to eliminate clogs. Putting a clogged glass-glass device in the kiln cycle for bonding has degraded blockages to the point where they can be easily washed out.

7. Removing Clogs from PDMS Microchips

It is often easier and faster to simply make a new PDMS device than to spend time clearing out clogs. If the PDMS is reversibly bound, it can be peeled off of the substrate and cleaned using a piece of clear tape. The substrate should also be wiped down with IPA to remove any detritus before attempting to re-apply the PDMS.

If the PDMS is irreversibly bound, the easiest way to remove a clog is briefly flowing IPA through the channels via the application of a negative pressure. IPA will slowly dissolve PDMS, so any particulate stuck on the channel walls can be washed away. However, this also means that repeated use can damage device features.

D. Recent advances in the analysis of therapeutic proteins by capillary and microchip electrophoresis

Jessica S. Creamer,[1,3] Nathan J. Oborny,[2,3] Susan M. Lunte[1,2,3]

[1]Department of Pharmaceutical Chemistry, University of Kansas, Lawrence, KS, USA

[2]Department of Bioengineering, University of Kansas, Lawrence, KS, USA

[3]Ralph N. Adams Institute for Bioanalytical Chemistry, University of Kansas, Lawrence, KS, USA

Susan M. Lunte, Ph.D.

Ralph N. Adams Professor of Chemistry and Pharmaceutical Chemistry

Ralph N. Adams Institute for Bioanalytical Chemistry

2030 Becker Dr. Lawrence, KS, 66044

slunte@ku.edu

Fax: 785-864-1916

Reproduced from "Recent advances in the analysis of therapeutic proteins by capillary and microchip electrophoresis", Analytical Methods, 2014, Vol 6, 5427-5449 [1] with permission from the Centre National de la Recherche Scientifique (CNRS) and The Royal Society of Chemistry.

List of abbreviations in alphabetical order:

1-vinyl-3-octylimidazolium ($ViOcIm^+$), 8-aminopyrene-1,3,6-trisulfonic acid (APTS), background electrolyte (BGE), bis-trifluoromethanesulfonylimide (NTf_2^-), bovine serum albumin (BSA), capillary electrochromatography (CEC), capillary electrophoresis (CE), capillary gel electrophoresis (CGE), capillary isoelectric focusing (CIEF), capillary isotachophoresis (CITP), capillary zone electrophoresis (CZE), diazoresin (DR), electroosmotic flow (EOF), electrospray ionization (ESI), erythropoietin (EPO), galactose-α-1,3-galactose (α1,3-Gal), gold nanoparticles (AuNP), graphene (G), graphene oxide (GO), hydrophilic interaction chromatography (HILIC), hydroxyproplymethylcellulose (HPMC), imaging capillary isoelectric focusing (iCIEF), ionic liquid (IL), isoelectric point (pI), laser-induced fluorescence (LIF), liquid chromatography (LC), mass spectrometry (MS), matrix-assisted laser desorption ionization (MALDI), microchip electrophoresis (ME), microchip gel electrophoresis (MGE), microchip isoelectric focusing (MIEF), molecular weight (MW), monoclonal antibodies (mAbs), nanoparticles (NP), N-glycolylneuraminic acid (Neu5Gc), N-methyl-2-pyrrolidonium methyl sulfonate ($[NMP]^+CH_3SO_3^-$), open-tubular capillary electrochromatography (OTCEC), pentaerythritol (PETA), phospholipid bilayers (PLB), polyamidoamine-grafted silica nanoparticles (PAMAM-SNP), polybrene (PB), polyethylene glycol (PEG), polyvinyl alcohol (PVA), post translational modifications (PTMs), pseudostationary phase (PSP), quaternized celluoses (QC), sodium dodecyl sulfate polyacrylamide gel electrophoresis (SDS-PAGE), silica nanoparticles (SNP), sodium dodecyl sulfate (SDS), stabilized phospholipid bilayer (SPB), sulfobutyl ether β-cyclodextrins (SBE β-CD)

Abstract

The development of therapeutic proteins and peptides is an expensive and time-intensive process. Biologics, which have become a multi-billion dollar industry, are chemically complex products that require constant observation during each stage of development and production. Post-translational modifications along with chemical and physical degradation from oxidation, deamidation, and aggregation, lead to high levels of heterogeneity that affect drug quality and efficacy. The various separation modes of capillary electrophoresis (CE) are commonly utilized to perform quality control and assess protein heterogeneity. This review attempts to highlight the most recent developments and applications of CE separation techniques for the characterization of protein and peptide therapeutics by focusing on papers accepted for publication in the in the two-year period between January 2012 and December 2013. The separation principles and technological advances of CE, capillary gel electrophoresis, capillary isoelectric focusing, capillary electrochromatography and CE-mass spectrometry are discussed, along with exciting new applications of these techniques to relevant pharmaceutical issues. Also included is a small selection of papers on microchip electrophoresis to show the direction this field is moving with regards to the development of inexpensive and portable analysis systems for on-site, high-throughput analysis.

1. Introduction

The characterization of protein therapeutics presents a unique analytical challenge due to the inherent heterogeneity of recombinant protein expression. Even small changes in the manufacturing process can lead to vastly different active pharmaceutical ingredients. Additionally, numerous physical and chemical degradation pathways can occur during manufacturing and storage that compromise protein integrity, leading to a potentially harmful, unstable product [2]. Thorough characterization of protein therapeutics is necessary at every step of the research and development process, from drug discovery to lot release.

Due to the potential complexity of product degradation during preformulation and formulation studies, additional separation techniques are needed to complement the more widely used column liquid chromatography (LC) methods. To address this issue, capillary electrophoresis (CE) has become a popular choice for the separation and analysis of therapeutic proteins and peptides.

CE provides several distinct advantages over LC. First, due to the faster separation times and the use of multi-capillary arrays, hundreds of samples can be processed by CE per day. Second, CE is capable of achieving very high efficiency separations due to the low diffusion coefficients of biomolecules. Lastly, the small dimensions of the capillary and the low sample volume requirements keep reagent and analyte use to a minimum, reducing the cost-per-test. The benefits of CE for the analysis of therapeutic peptides and proteins have been addressed in several excellent reviews to date [3-6].

This review is aimed at highlighting the advances made in the field of CE therapeutic protein analysis during 2012 and 2013 by expanding on a paper that was recently published by Zhao *et al.* [6]. Following brief descriptions of the working principles of the different CE separation and detection methods, the recent technological improvements and novel applications are discussed. Two additional sections have been included to further explore the use of CE for the determination of protein glycosylation and the comparison of biosimilars. Finally, a brief introduction into microfluidic approaches to protein analysis is given. Microchip electrophoresis (ME) has the additional advantages of increased speed, high-throughput capabilities, and portability for on-site analyses. Tables are presented in each section to highlight the relevant CE and ME application-based citations.

2. Techniques

Historically, capillary zone electrophoresis (CZE) has been the most commonly employed form of CE. Yet, the principles of electrophoretic separations and the benefits of capillary-based techniques are applicable to other CE separation modes as well. Protein analysis based on size can be accomplished by capillary gel electrophoresis (CGE), capillary isoelectric focusing (CIEF) can be used to determine isoelectric points and charge heterogeneity, and capillary electrochromatography (CEC), which combines the high efficiency electrophoretic separation with chromatographic retention, can be used for more selective separations and analysis of neutral species. Depending on the properties of the analyte and requirements of the assay, each of these separation modes can be coupled to a number of detection methods such as UV-Vis absorbance, laser-induced fluorescence (LIF), and mass spectrometry (MS).

2.1 Capillary zone electrophoresis

Of the electrophoresis-based separation techniques, CZE is most frequently used for the analysis of small molecules, carbohydrates, and peptides. It is simple, easy-to-use, and requires minimal reagents compared to chromatographic methods. Additionally, in CZE, the separation of analytes is based on their size-to-charge ratio making it well suited for separations of proteins with post-translational modifications (PTMs) or degradations that affect the charge of the molecule [7, 8] including deamidation, glycosylation, and phosphorylation.

One example of the use of CZE for the investigation of deamidation concerns the stability of oxytocin. Deamidation of Asn and Gln residues is the most common chemical degradation pathway for peptides and proteins [2]. This process leads to the production of an ionizable carboxylic acid from the neutral amide ($R\text{-}CONH_2 \rightarrow R\text{-}COOH$), facilitating a separation by CZE. However, if peptides, such as oxytocin, contain several labile Asn and Gln sites, multiple degradation products of the same size-to-charge ratio are produced and a straightforward separation becomes impossible. To distinguish between the seven desamino degradation products of heat-stressed oxytocin, Creamer *et al.* utilized sulfobutyl ether β-cyclodextrin (SBE β-CD) as a pseudo-stationary phase [9]. The negatively charged SBE β-CD forms an inclusion complex with the hydrophobic Tyr^2 residue of oxytocin, affecting the electrophoretic mobility of the peptides. A baseline separation of all eight peptides and a migration time RSD of less than 1.2% was achieved.

Unfortunately, reproducible separations of larger biomolecules using bare fused-silica capillaries are rare due to protein adsorption. Many proteins have large localized regions of positive charge that are electrostatically attracted to the negatively charged silanol groups at the capillary surface. Additional adsorption can be caused by hydrophobic and hydrogen bonding interactions. This adsorption process keeps CZE from obtaining the 10^6 theoretical plates that should be possible due to the very low diffusion coefficients of large proteins. [10, 11].

One strategy for minimizing protein adsorption is to alter either the charge density of the protein or the capillary wall by changing the pH or ionic strength of the background electrolyte (BGE). Another approach is to simply add a modifier to the BGE to reduce protein-wall interactions. The addition of surfactants, small amines, or anionic salts, such as phytic acid, to the BGE is common [12, 13]. In cases where modification of the run buffer does not obviate protein adsorption, dynamic and static capillary coatings have been used to create a barrier between the ionized silanol groups and the protein of interest.

2.1.1 Dynamic coatings

Dynamic coatings are buffer additives that adsorb to the surface of the capillary, shielding the silanol groups from analyte adsorption [14]. These noncovalent coatings are popular due to their simplicity, versatility, and ease-of-use. However, because of their impermanent nature, the coatings need to be continuously regenerated. This can be accomplished by refreshing the physically adsorbed layer at the capillary with rinses between runs, or adding a small amount to the BGE to prevent coating degradation during electrophoresis. A variety of such coatings have

been used for protein separations, ranging from small molecules such as ionic liquids (ILs), to larger molecules such as surfactants and polymers [15].

ILs have been previously explored as dynamic coatings for CZE protein separations [16-18]. ILs are salts made up of organic cations and inorganic or organic anions that are liquid at, or around, room temperature. Recently, a new IL, N-methyl-2-pyrrolidonium methyl sulfonate ($[NMP]^+CH_3SO_3^-$), was used to prevent basic protein (pI 9.0-10.7) adsorption to capillary walls during CE separation [19]. The $[NMP]^+$ moiety electrostatically adsorbs to the capillary surface, where it is able to hydrogen bond for additional stability (Figure D.1). Using this coating, the authors were able to achieve a baseline separation of four basic proteins (Table D.1) with an interday migration time RSD of less than 1.5%. The improvement in the separation after addition of only 0.02% w/v IL, compared to that obtained with phosphate buffer alone, is easily seen in Figure D.1D.

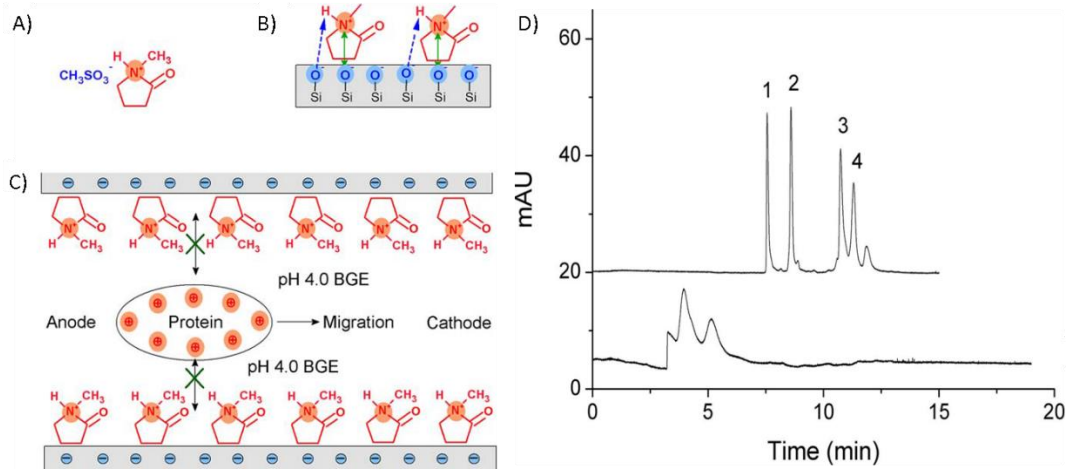

Figure D.1: A) The structure of the IL [NMP]+CH3SO3−, B) the interaction between [NMP]+ and the silica capillary inner wall, and C) the mechanism of separation of proteins using $[NMP]^+$ as dynamic coating material, D) Electropherograms of four basic proteins in bare silica capillary (bottom trace) and in the presence of 0.02% w/v IL (top trace). Running buffer: 40 mM pH 4.0 sodium phosphate; voltage: 18 kV; detection: 214 nm; peaks: (1) cytochrome c, (2) lysozyme, (3) ribonuclease A, (4) α-chymotrypsinogen A. Reprinted with permission from

Polysaccharides are also attractive candidates for dynamic coatings for protein separations because they are non-toxic, readily abundant, and biocompatible [20-22]. Two novel dynamic coatings based on the chemical substitutions of cellulose have recently been reported [23, 24]. The first, a positively charged quaternarnized cellulose (QC), was synthesized through a reaction of cellulose with 3-chloro-2-hydroxypropyltrimethylammonium chloride. The positive charge of the QC leads to the electrostatic adsorption of the compound to the capillary surface, reversing the electroosmotic flow (EOF). Addition of 5 µg/mL QC to the BGE prevented adsorption of model basic proteins leading to higher separation efficiencies [23]. To increase the reverse EOF by 10%, and further improve separation efficiency, additional substitution of the QC was made using hydrophobic hexadecyl groups [24]. Both QCs were evaluated with a separation of five basic proteins (Table D.1). In both cases, the modified capillaries produced a migration time reproducibility with RSD of less than 2.7%.

Table 1. CZE and capillary coatings

Analyte	Coating	Capillary	BGE	Voltage	Detection	Notes	Ref.
Therapeutic albumin	Semi-permanent coating with PEO	57 (50) cm, 50 µm id	50 mM HEPES, pH 7.5, 0.5 mM SDS	– 25 kV	UV 214 nm	Separation of human serum albumin isoforms	[6]
In-house IgG1 mAbs	Bare fused silica	30.2 (20) cm, 50 µm id	20 nM NaAc, 0.3% PEO, 2 mM triethylenetetraamine, pH 6.0	+ 30 kV	UV 214 nm	Rapid method to determine mAb charge variance	[7]
Oxytocin	Bare fused silica	50 (40) cm, 50 µm id	50 mM sodium phosphate pH 6.0,12.5 mM SBE β-CD, 10% v/v MeOH,	+ 22 kV	UV 214 nm	Separation of all oxytocin desamino products	[8]
Cytochrome *c*, lysozyme, ribonuclease A, and α-chymotrypsinogen A	Static coating with ionic liquid $[NMP]^+CH_3SO_3^-$	50 (41.5) cm, 75 µm id	40 mM sodium phosphate, pH 4.0, 0.3% w/v ionic liquid	+ 15 kV	UV 214 nm	Minimize protein adsorption	[18]
(1,2) Chymotrypsinogen, ribonuclease A, cytochrome *c*, trypsin inhibitor, lysozyme	(1) QC (2) HMQC	47 (40) cm, 75 µm id	25 mM sodium phosphate over a range of pH 3.0-8.0	+ 12 and – 12 kV	UV 214 nm	The hydrophobic QC provided a more effective for coating	QC [22] HMQC [23]
Purchased mAbs	Various commercial and in-house coatings	64.5 (56) cm, 50 µm id	Various BGE composition, pH, and additives	+ 30 and – 30 kV	UV 200 nm	Comparison of static capillary coatings	[26]
Enhanced green fluorescent protein and R-phycoerythrin	Polymerize phospholipid bilayer	42 (32) cm, various µm id	Various BGEs over a range of pH 4.0-9.3	+ 24 kV	LIF	Best coating stability in capillaries with id of ≤ 50 µm	[28]
(1,2) Lysozyme, cytochrome *c*, BSA (2) amyloglucosidase, myoglobin	(1) PVA or (2) PEG and diazoresin	50 (41) cm, 75 µm id	40 mM sodium phosphate over a range of pH 3.0-9.0	+ 15-18 kV	UV 214 nm	Easy to form covalently bonded capillary coatings	PVA [29] PEG [30]

Capillary: actual length (effective length), inner diameter
Bovine serum albumin (BSA), Hydrophobically modified QC (HMQC), N-methyl-2-pyrrolidonium methyl sulfonate IL ($[NMP]^+CH_3SO_3^-$), Polyethylene glycol (PEG), Polyethylene oxide (PEO), Polyvinyl alcohol (PVA), Quaternized celluloses (QC), Sulfobutyl ether β-cyclodextrin (SBE β-CD)

Table D.1: CZE and Capillary Coatings

Despite their simplicity, buffer additives and dynamic coatings are not always the best approach to eliminate protein adsorption. If the modifier is highly charged, band broadening can occur due to high separation currents and Joule heating. Additionally, some buffer modifiers can interfere with protein binding assays [25], disrupt protein stability [26], or be incompatible with downstream detection methods such as MS. In cases where greater stability and reproducibility are needed, static coatings have been used [14].

2.1.2 Static coatings

Static coatings are chemically linked to the capillary wall and do not need to be added to the run buffer to achieve reproducible separations. Therefore, they have the potential for large-scale production and can be made commercial available. Several companies are already selling coated capillaries for protein separations including GL Sciences (FunCap®), Target Discovery (UltraTrol™), MicroSOLV (CElixer™), and Beckman Coulter (eCAP™).

Gassner et al. performed a thorough comparison of both commercially available and lab-generated static coatings in 2013 [27]. Eight coatings were selected—four positive: FunCap®-type A, UltraTrol™ HR, Hexadimethrin bromide (polybrene) (PB)-dextran sulfate-PB, and polyethylenimine; and four neutral: FunCap®-type D, UltraTrol™ LN, hydroxypropylcellulose, and polyvinyl alcohol (PVA). The coatings were evaluated for the protein recovery, isoform resolution, and migration time reproducibility of two monoclonal antibodies (mAbs).

For the positively charged coatings, the separation was run in negative polarity. With these capillaries it was determined that the slower the EOF, the better the resolution. Yet, while UltraTrol™ HR had the slowest EOF, it had poor reproducibility (8.9% RSD) and was discarded from the study. For the neutral coatings run in normal polarity, the largest factor for protein adsorption was the presence of residual silanol groups. This was apparent by the fact that some EOF was still generated in the capillary. Of the four neutral coatings in this study, both commercial options, FunCap®-type D and UltraTrol™ LN, generated a small amount of EOF at pH 7.0, indicating that the coating was not uniform and there were still potential sites for protein adsorption. However, it is important to note that the separation performance of each coating was

highly dependent on the pH and composition of the BGE. Consequently, care should be taken during method development to fully optimize the BGE for the selected coating.

Due to the varied performance of the commercially available products, new coatings for the separation of basic and hydrophobic proteins are still under development. One particularly attractive choice for static coatings is phospholipid bilayers (PLB) because of the protein resistant nature of the hydrophobic phosphoylcholine polar headgroup. However, the limiting factor for these coatings is their poor long-term chemical and physical stability. This can be remedied by cross-linking the PLB with bis-SorbPC which produces a stabilized phospholipid bilayer (SPB) at the capillary surface [28]. In a recent report, it was shown that the SPB produced a stable coating over a pH range from 4.0–9.3 [29]. Over the course of 45-days dry storage the migration time reproducibility for both model proteins (Table D.1) was marginally affected and the overall RSD for the EOF was only changed by 1.1%.

To reduce the preparation time for the preparation of static coated capillaries, self-assembled bilayers and photoinitiated polymerization can be used. An example of such a process was described by Yu *et al.* using a photosensitive diazoresin (DR) in combination with either PVA [30] or polyethylene glycol (PEG) [31]. After exposure to 365 nm light, both the DR/PVA and DR/PEG coatings were able to prevent protein adsorption and achieve an efficient separation of several model basic proteins (Table D.1) with a migration time precision less than 4% RSD.

2.1.3 Evaluation of capillary coating performance

Prior to assay development, the determination of capillary coating performance is extremely important. A previous analytical approach to determine protein adsorption in capillaries involves flushing the capillary with the protein of interest to allow adsorption and then measuring desorption on a subsequent rinse [32-34]. However, with this method, only irreversibly bound proteins are measured. As an alternative, de Jong *et al.* recently developed a more direct method using pressure-driven flow [35]. Briefly, a plug of sample is pressure injected into a capillary at a low flow rate (0.5 psi) and the Taylor dispersion of the plug is measured at two different detection points along the capillary. Based on these measurements, the magnitude of the protein adsorption can be estimated (Figure D.2).

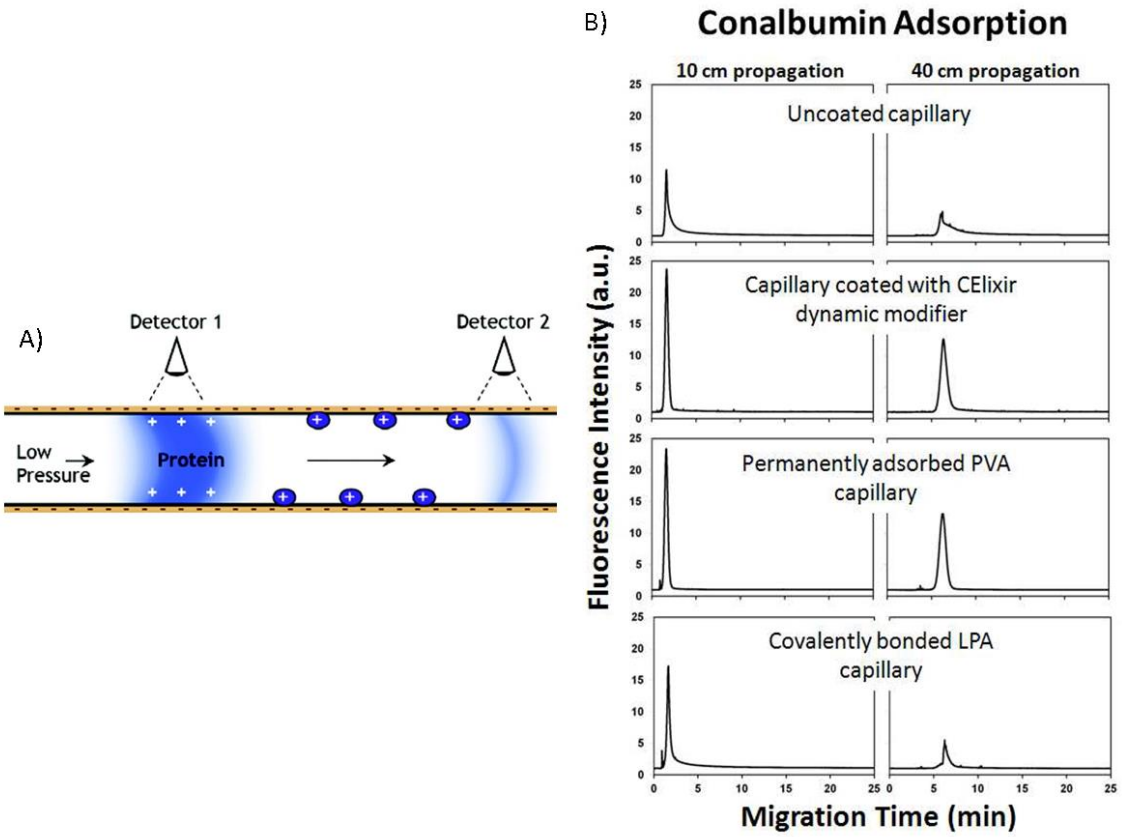

Figure D.2: A) Diagram of the set-up for the dual detection pressure-based technique for assessing protein adsorption. B) Pressure-driven propagation of 5.3 μM chromeo-labeled conalbumin detected at 10 and 40 cm. Better protection against adsorption can be seen in both the capillary coated with CElixir dynamic modifier and the capillary with a permanently adsorbed PVA coating. Reprinted with permission from ref. 34

2.2 Capillary gel electrophoresis

The most commonly used analytical method for size determination, purity assessment, and quality control of therapeutic recombinant proteins is sodium dodecyl sulfate polyacrylamide gel electrophoresis (SDS-PAGE). SDS is used to coat the proteins, resulting in a uniform negative charge proportional to their size. Under an electric field the proteins are then separated through a sieving gel matrix, allowing for estimation of protein molecular weight (MW). However,

conventional SDS-PAGE can be time-consuming, tedious, and yield irreproducible results with limited quantitative abilities [36, 37].

Table 2. CGE and MGE

Analyte	Mode	Gel	Capillary	Voltage	Detection	Notes	Ref.
In-house IgG2λ, IgG2κ, and IgG1κ mAbs	Nonreducing	Beckman Coulter SDS-MW gel buffer	30 (20) cm, 50 µm id	15 kV	UV 220 nm	Monitor disulfide reduction during production	[36]
In-house IgG1 mAbs	Reducing and nonreducing	Agilent High Sensitivity Protein 250 Kit	Agilent 2100 Bioanalyzer	NR	LIF	Characterization of size variants	[37]
In-house IgG1 and IgG4 mAbs	Reducing and nonreducing	Beckman Coulter SDS-MW gel buffer	31.2 (20) cm, 50 µm id	-15 kV	LIF ex. 488 nm / em. 600 nm	Impurity analysis	[38]
IgG 1 mAb	Reducing	Beckman Coulter SDS-MW gel buffer	30.2 (20) cm, 50 µm id	-15kV	PDA	Comparison of SDS-CGE to SDS-PAGE	[39]
Myoglobin, carbonic anhydrase I, ovalbumin, BSA	Nonreducing	Beckman Coulter SDS-MW gel buffer	33 (24.5) cm, 50 µm id	-16.5 kV	220 nm	Demonstration of improved precision	[40]
In-house Fc-fusion proteins, and IgG1 and IgG2 mAbs	Reducing and nonreducing	Beckman Coulter SDS-MW gel buffer	30 (20) cm, 50 µm id	15 kV	220 nm	Automated sample preparation	[41]
In-house vaccine proteins	Reducing	ProteinSimple separation matrix	12-capillary cartridge; 5 cm, 100 µm id	250 V	Chemiluminescence from secondary antibody	Automated separation and Western blot	[42]
Ricin A-chain immunotoxins	Reducing and nonreducing	Bio-Rad CE-SDS run buffer	24 (19.5) cm, 50 µm id	5 or 15 kV	UV 220 nm and MALDI-TOF-MS	CGE-MALDI-TOF-MS of ricin proteins	[45]
In-house mAbs and proteins	MGE Reducing and nonreducing	HT Protein Express gel matrix	LabChip GXII	NR	Indirect and direct LIF ex. 620 nm / em. 700 nm	MGE methods for high-resolution and high-sensitivity	[138]
Actin, carbonic, anhydrase II, and, lysozyme	MGE Nonreducing	Beckman Coulter SDS-MW gel buffer	2 cm glass microchip	480 kV	Western blot	MGE separation with off-chip Western blot detection	[140]

Capillary: actual length (effective length), inner diameter
Bovine serum albumin (BSA), Not reported (NR)

Table D.2: CGE and MGE

To improve on this important technique, the CGE equivalent, SDS-CGE, has been developed and utilized for the determination of size heterogeneity of therapeutic proteins [38-40]. Here the sieving gel is placed inside the capillary through which the negatively charged SDS-coated proteins are separated. SDS-CGE has many advantages over SDS-PAGE, including high efficiency separations, more accurate MW and concentration determination, and the ability to automate the process for high-throughput analysis.

Shi *et al.* demonstrated these advantages of SDS-CGE over SDS-PAGE, along with the improved precision of migration time and peak area, for the analysis of the light chain, nonglycosylated heavy chain, and heavy chain fragments of a mAb [41]. Using the capillary format, the authors were able to achieve RSDs of less than 0.5% for migration time and less than 5% for corrected peak area. However, for quality control of biopharmaceuticals, the precision for a quantitative assay needs to be lower than 2% RSD. By switching from hydrodynamic rather than electrokinetic injection, along with increased sample concentration, the precision of a standard SDS-CGE assay was improved to 0.2% RSD for migration time and between 1 and 2% RSD for peak area ratio [42].

Another method to improve assay precision for the SDS-CGE assay is through automation of the sample preparation process. A large number of samples are generated during the development of high-quality biologics. These samples originate from every step of the development process and are presented for analysis in a variety of matrices. The use of an automatic robotic platform for sample preparation can help mitigate user error introduced in the multi-step sample preparation process. The PhyNexus Micro-Extractor Automated Instrument uses a ProA resin column to bind mAb samples prior to separation. Once bound, the instrument performs sample concentration normalization, removal of contaminates, desalting, and mixing with appropriate SDS-CGE buffers**.** With this method, protein recovery of Fc-fusion proteins, and IgG1 and IgG2 mAbs was increased to 90% [43].

UV absorbance and LIF spectroscopy are the dominant detection methods for SDS-CGE. However, for detection of specific mAbs, Western blot immunoassay detection has also been

utilized. The ProteinSimple Simple Western™ (or Simon™) automates the immunoassay detection procedure by performing all separation steps and washes in-capillary. Following a SDS-CGE separation, the proteins are photochemically cross-linked to the capillary wall, where they are exposed to a horseradish peroxidase-conjugated secondary antibody for whole-capillary chemiluminescence imaging (Figure D.3). Simon™ also makes quantitative Western blots possible. Using this instrument, a standard curve was generated for a vaccine candidate protein with linearity from 0.45–7 µg/mL and R^2 values of 0.990 or greater for five experiments [44].

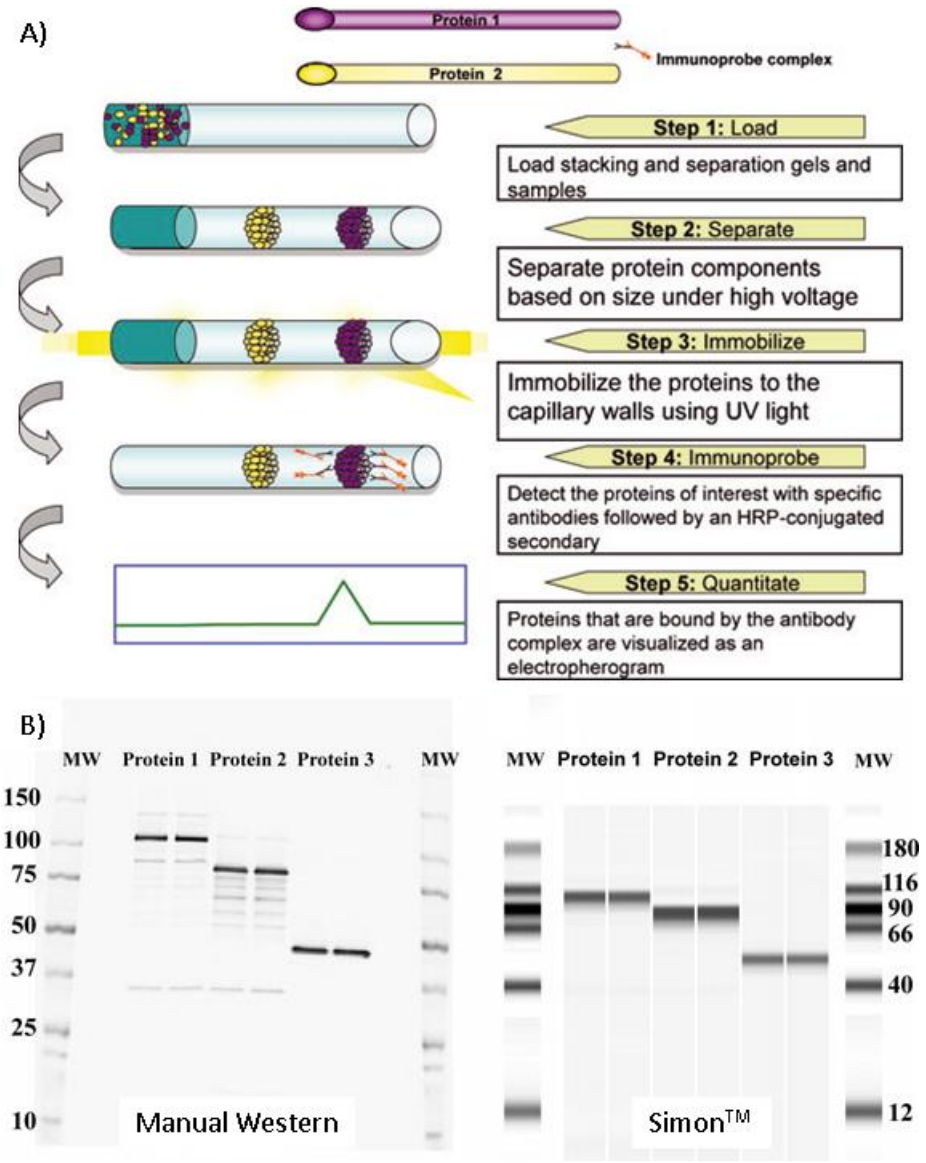

Figure D.3: A) Step-by-step overview of the Simon™ operational procedure. B) Comparison between the manual Western and Simon™ for duplicate runs of three proteins. Experimental details for protein and antibody conditions in ref. 31. Reprinted with permission from ref. 42

Immunoassay detection methods for CGE are useful because coupling CGE with MS by electrospray ionization (ESI) is difficult due to the presence of nonvolatile BGE. However, CGE-SDS has been coupled successfully to matrix-assisted laser desorption ionization (MALDI) MS by moving a poly(tetrafluoroethylene) membrane past the end of the capillary to collect the peaks as

they leave the capillary [45]. CGE-MALDI-MS has been utilized for the direct mass measurement of recombinant proteins [46, 47] and neoglycoproteins [48].

2.3 Capillary isoelectric focusing

Another capillary-based technique that was adapted from its original slab-gel format is capillary isoelectric focusing (CIEF). Like SDS-CGE, performing IEF in a capillary exhibits the benefits of faster analysis times, higher resolutions (up to 0.005 pH units [49]), lower limits of detection, and the capacity for high-throughput analysis [50].

CIEF separates proteins based on their isoelectric point (pI) and can be used to determine charge heterogeneity of biogenic products [51]. The assay is typically performed in a coated capillary to eliminate EOF. A pH gradient is self-assembled under an electric field using a mixture of mobile carrier ampholytes with a distribution of pIs. The anodic end of the capillary is then placed in an acidic solution and the cathodic end in a basic solution. Under the applied electric field, the protein will migrate through the ampholyte solution toward the oppositely charged electrode until the pH environment equals its pI.

UV detection at 280 nm is typically used with CIEF because the ampholytes exhibit strong absorbance at wavelengths below 240 nm [52]. Optical detection for CIEF can be accomplished either by a two-step method that requires mobilization after focusing to bring the analyte bands past a small detection window or using whole-capillary imaging CIEF (iCIEF) within a transparent capillary.

An important application of CIEF for the analysis of biologics is for the characterization of charge heterogeneity, as it is possible to identify proteins based on their unique charge profile [53] (Table D.3). Variations in this charge profile are often used to determine protein stability [54, 55] and identify degradation products or PTMs that change the charge of the protein, such as glycosylation and deamidation [56].

Table 3. CIEF and microchip IEF (mIEF)

Analyte	Mode	Capillary coating	Capillary	Detector	Ampholyte	Catholyte	Anolyte	Notes	Ref
In-house EPO, Fc-fusion protein, and IgG mAb	iCIEF	Fluorocarbon (ProteinSimple)	iCE280 Analyzer; 50 mm, 100 µm id	UV 280 nm	Pharmalyte pH 3-10, 4-6.5, 5-8, and 8-10.5	0.1 M NaOH in 0.1% MC	0.08 M phosphoric acid in 0.1% MC	Wide range of therapeutic protein applications	[51]
In-house noninfectious virus-like particles	iCIEF	Fluorocarbon (ProteinSimple)	iCE280 Analyzer; 50 mm, 100 µm id	UV 280 nm	Pharmalyte pH 2.5-5 and 3-10	0.1 M NaOH in 0.1% MC	0.08 M phosphoric acid in 0.1% MC	Charge characterization of virus-like particles	[52]
In-house vaccine carrier protein	iCIEF	Fluorocarbon (ProteinSimple)	iCE280 Analyzer; 50 mm, 100 µm id	UV 280 nm	Pharmalyte pH 3-10 and 4-6.5	0.1 M NaOH in 0.1% MC	0.08 M phosphoric acid in 0.1% MC	Characterization of polysaccharide vaccine carrier protein	[53]
In-house IgG2κ mAb	CIEF	PDMA	180 mm, 50 µm id	LIF ex. 543.5 nm / em. 590 nm	Pharmalyte pH 3-10, 0.001% BSA	20 mM NaOH	20 mM phosphoric acid	Determination of deamidation rates in mAb	[54]
Trypsinogen, β-lactoglobulin, BSA, and ovalbumin	CIEF	4% acrylamide 0.6% cross-linker	Various capillary lengths and id	LIF ex. 488 nm	BioRad pH 3-10	20 mM NaOH	10 mM phosphoric acid	Microchip interface for 2D CIEF and CGE separations	[55]
β-lactoglobulin A, hemoglobin A, myoglobin, α-chymotrypsinogen A, ribonulcease A, cytochrome *c*, lysozyme	CIEF		Seven PEEK tubing segments, 1.55 cm, 395 µm id connected by Nafion membrane 0.2 cm, 330 µm id	TOF and Orbitrap	Various MS-compatable carrier ampholytes	Various electrolytes at each Nafion junction modified the local pH of the carrier ampholyte		Segmented capillary for selective mobilization	[60]
Insulin receptor and protein tryptic digests	CIEF	LPA	50 cm, 50 µm id	Sheath flow ESI-Orbitrap-MS	Glutamate, asparagine, glycine, proline, histidine, and lysine	0.1% Formic acid, pH 2.5	0.3% ammonium hydroxide, pH 11	Amino acids used as low MW ampholyte	[64]
In-house IgG mAb	iCIEF	Proprietary photoreactive layer	12-channel cartidge; 50 mm, 100 µm id	Chemiluminescence from secondary antibody	Pharmalyte pH 5-8 (30%) and pH 8-10.5 (70%)	0.1 M NaOH in 0.1% MC	0.08 M phosphoric acid in 0.1% MC	CIEF with immunoassay detection	[65]
Donated mAb products	imIEF	Uncoated quartz	MCE-2010 system, 2.7 cm	UV 280 nm	Protein imple pH 3-10, 5-8, and 8-10.5	300 mM NaOH, 0.4% HPMC	200 mM phosphoric acid, 0.4 % HPMC	mIEF of mAb charge variants	[141]
Model Proteins	iMIEF		100 µm id	Immunoblot	Polyprotic carboxylic amino acids	20 mM lysine	20 mM arginine	Integrated microchip for separation and immunoblot	[142]

Capillary: actual length, inner diameter
Bovine serum albumin (BSA), Linear polyacrylamide (LPA), Methylcellulose (MC), Polydimethylacrylamide (PDMA), Polyvinyl alcohol (PVA),

Table D.3: CIEF and microchip IEF (mIEF)

As mentioned earlier, deamidation can be a major pathway of protein and peptide degradation. The rate of deamidation depends on both the primary and secondary structure surrounding the Asn or Gln residue in question [2]. Typically, characterization of deamidation sites is accomplished

through peptide mapping and MS analysis. However, this process can be complicated, sometimes impossible when a fragment contains multiple desamino sites. Shimura *et al.* used CIEF and site-directed mutagenesis to determine the rates of deamidation in Fab fragments of mouse IgG1-κ [56]. The rate of disappearance of the parent peak of each mutant was compared to that of the wild type to obtain the single-residue deamidation rates. By monitoring the CIEF charge profile of the six Fab mutants for the additional acidic peaks, a third, previously unknown deamidation hotspot for the mouse IgG1-κ was identified.

CIEF can be even more powerful when run in combination with an orthogonal separation technique such as SDS-CGE [57] or reversed-phase LC, or in tandem with MS. CIEF has been coupled to MS through both ESI [58, 59] and MALDI interfaces [60, 61]. Due to the presence of the non-volatile ampholytes in the separation buffer, coupling CIEF with ESI can be complicated by ion-suppression and source contamination. To cut down on the intensive sample preparation needed to desalt protein samples from gels, a segmented capillary has been described. In this design, seven segments of PEEK capillary were connected by Nafion joints, each with its own buffer reservoir (Figure D.4) [62]. This allowed analytes in the capillary segments to be selectively mobilized after focusing, creating an online fractionator prior to additional analysis by LC, CE, or MS.

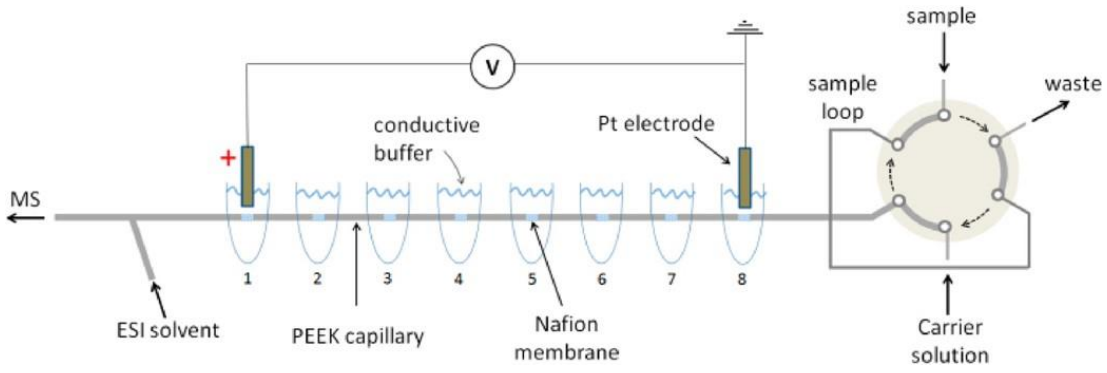

Figure D.4: Schematic layout of the on-line multiple junction CIEF setup; the six-port injector is shown in the sample-loop loading position. Reprinted with permission from ref. 60

Additional technological advances in CIEF-MS interface development have been reported by Zhong *et al.* [63] and Wang *et al.* [64]. Their work is discussed further in the MS detection section of this review. Along with the development of new interfaces, several straightforward BGE buffer modifications have been described in the literature to solve the problems of high backgrounds and ion suppression [37, 65].

As with SDS-CGE, detection of proteins by immunoassay following separation by CIEF can be used to improve detection limits and specificity without the need for an MS. For example, Michels *et al.* have described the first multiplexed iCIEF immunoassay for investigation of the charge heterogeneity of mAbs [66]. Once the mAbs were focused, they were then photochemically immobilized to the capillary wall where they were then exposed to a secondary antibody, conjugated with horseradish peroxidase, and detected by chemiluminescence (Figure D.5). The resulting LOD of this assay was 6 ng/mL, which was a 1000-fold increase over UV detection.

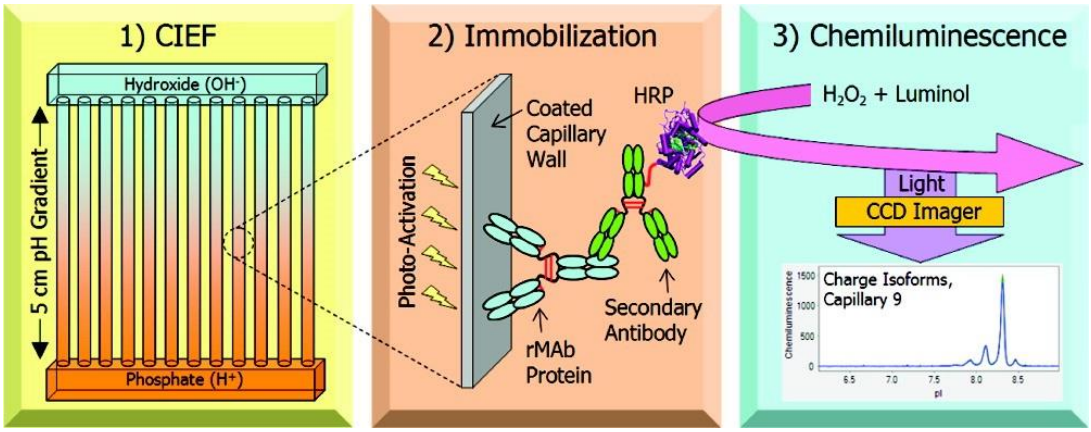

Figure D.5: Schematic of the Nanopro three-step process 1) Separation by CIEF, 2) immobilization of the antibody to the capillary wall, 3) detection with secondary antibody by chemiluminescence. Reprinted with permission from ref. 65

2.4 Capillary electrochromatography

Capillary electrochromatography (CEC) is a technique that uses both chromatographic retention and electrophoretic migration for the separation of analytes, with bulk fluid flow created by the EOF. This combination enhances the selectivity and efficiency of the separation, drastically lowers the reagent use compared to LC, and enables the separation of neutral species not possible with CZE.

In the first applications of CEC to proteins, capillaries packed with porous particles were utilized because of their similarity to the stationary phase materials used for conventional LC, and the commercial availability of particles with a variety of functionalities. However, the packed CEC columns have significant limitations in terms of stability and fabrication reproducibility and are not yet able to match the robust performance of nano-LC [67]. This limits their usefulness for routine protein assays on a larger industrial scale. In its place, the use of nanoparticles (NP) as a

pseudostationary phase (PSP), open-tubular CEC (OTCEC), and monolithic columns have gained momentum.

The use of NP as a PSP for CEC has been thoroughly reviewed [68]. In the BGE, the NP can interact with the proteins during the separation, changing their electrophoretic mobility and generating a separation based on the difference in affinity between the analytes for the NP. A wide range of materials have been investigated for PSP-CEC, including polymer NP, carbon nanotubes, gold NP, and silica NP (SNP) [68]. To improve the stability and functionality of SNP, Gao *et al.* synthesized polyamidoamine-grafted SNP (PAMAM-SNP) and utilized them for a separation of basic and acidic proteins [69] (Figure D.6). With 0.01% PAMAM-SNP in the BGE, a complete separation of all four model proteins (Table D.4) was possible. Additionally, the PAMAM-SNP were able to effectively reduce the adsorption of basic proteins to the capillary wall.

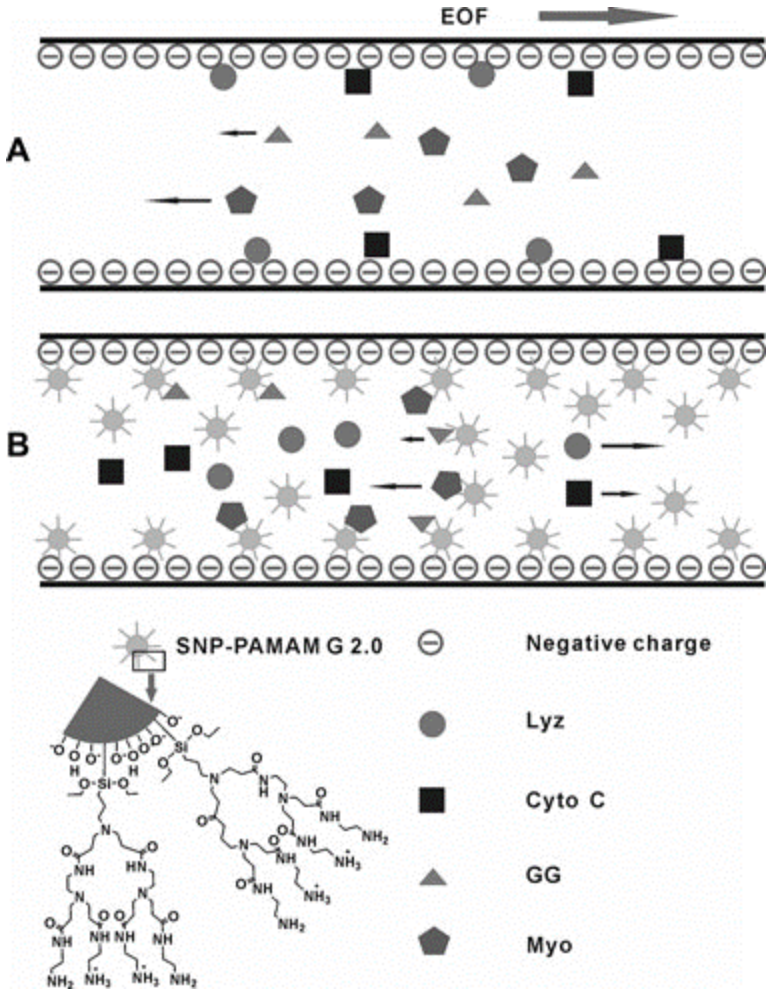

Figure D.6: A) Diagram of the separation of four proteins without and B) with the pseudostationary phase effect of the polyamidoamine (PAMAM)-grafted silica nanoparticles (SNP). Reprinted with permission from ref. 68

OTCEC columns are a popular alternative to packed columns because of their ease of fabrication and excellent separation efficiency [70]. These OTCEC columns can be made by either physically bonding the stationary phase to the capillary wall or several layered coatings. In one report, OTCEC columns were fabricated through the immobilization of gold NP (AuNP) on the surface of the capillary that had been pretreated with a sol-gel. The gold immobilized in the sol-gel participates in noncovalent interactions with thiol and amino groups of proteins, increasing

their capacity factor. Using this technique, Miksik *et al.* were able to separate the peptides generated by the tryptic digestion of native and glycosylated bovine serum albumin (BSA) and human transferrin [71]. Unfortunately, preparation of the AuNP modified columns required several days and many reaction steps, which limited its utility. To alleviate this problem, a new method for AuNP immobilization to the capillary wall through covalent binding using (3-aminopropyl)triethoxysilane has been described [72]. This procedure creates a stable coating that could be reused over 900 times with migration time RSDs less than 1.7% for model proteins (Table D.4).

Table 4. CEC

Analyte	Column type	Column material	Capillary	BGE	Voltage	Detection	Notes	Ref.
Cytochrome *c*, myoglobin, gamma globulin, and lysozyme	Pseudostationary phase	Polyamidoamine-grafted SNP	48 (38) cm, 75 µm id	12.5 mM tetraborate/ phosphate, pH 9.1, 0.01% SNP	+ 15 kV	UV 214 nm	Improved SNP stability	[68]
Tryptic digests of BSA and human transferin	Open-tubular	Bare AuNP on sol-gel modified surface	47 (40) cm, 50 µm id	100 mM sodium phosphate, pH 2.5	+ 10 kV	UV 214 nm	AuNP OT column for tryptic digests of native and glycated proteins	[70]
Bradykinin, LHRH, oxytocin, angiotensin I, met-enkephalin, and HSA tryptic digest	Open-tubular	AuNP on (3-aminopropyl) triethoxysilane modified surface	41.2 (31) cm, 75 µm id	20 mM potassium phosphate, pH 8.0	+ 12 kV	UV 214 nm	New preparation of AuNP OT column with improved stability	[71]
Egg while proteins	Open-tubular	Graphene oxide and graphene	60 (50) cm, 75 µm id	5 mM sodium phosphate, pH 7.0	+ 20 kV	UV 214 nm	Separation was only possible with the GO column	[72]
Egg while proteins	Open-tubular	Ionic adsorption of GO to surface modified with PDDA	60 (50) cm, 75 µm id	5mM sodium phosphate, pH 7.5	+ 20 kV	UV 214 nm	Improved assembly and stability of GO OT columns	[73]
Cytochrome *c* and BSA	Open-tubular	Mixture of four monomers in the presence of 1-propanol as sole porogen	35 (25) cm, 75 µm id	5 mM sodium borate, 45% ACN, pH 9.04 and 10 mM Tris-HCl, 0.4% PVP, pH 8.86	– 10 kV	UV 214 nm	Improve retention of proteins in OTCEC	[74]
Many model proteins and tryptic digests of cytochrome *c*	Monolith	C-8, -12, and -16 methacrylate with pentaerythritol triacrylate	27 (20) cm, 100 µm id	1-10 mM sodium phosphate, ACN, pH 7.0	+ 15 kV	UV 214 nm	Neutral monoliths to reduce adsorption	[75]
Cytochrome *c*, equine myoglobin, lysozyme, and BSA	Monolith	Cationic ionic liquid ViOclm$^+$ with various anions: Br^-, BF_4^-, PF_6^-, and NTf_2^-	32 (20) cm, 100 µm id	20% ACN, 30 mM sodium phosphate/citric acid buffer, pH 2.5-4.0	– 10 kV	UV 210 nm	Only the anion NTf_2^- was able to achieve separation of proteins	[77]

Capillary: Actual length (effective length), inner diameter
1-vinyl-3-octylimidazolium (ViOclm$^+$), Bovine serum albumin (BSA), Gold nanoparticles (AuNP), Graphene oxide (GO), Human serum albumin (HSA), Ionic liquid anions (bromide, Br^-; tetrafluoroborate, BF_4^-; hexafluorophosphate, PF_6^-; and bis-trifluoromethanesulfonylimide, NTf_2^-) Open-tubular (OT), Luteinizing-hormone-releasing hormone (LHRH), Poly(diallydimethylammonium chloride) (PDDA), Polyvinylpyrrolidone (PVP), Silica nanoparticles (SNP)

Table D.4: CEC Methods

Another novel OTCEC column was described by Qu *et al.* and was produced by immobilizing graphene (G) and graphene oxide (GO) sheets to the capillary wall to act as the stationary phase. It was found that between the two coatings, only the GO exhibited a reproducible EOF over the pH range of 3–9 and separate a mixture of egg white proteins [73]. The separation was achieved due to the reverse-phase-like interaction between the graphene coated surface and the proteins. To improve the stacking of GO at the capillary wall, a layer-by-layer technique to produce the GO-modified OTCEC column was reported. In this case, GO nanosheets were adsorbed on a poly(diallydimethylammonium chloride)-treated capillary by electrostatic interaction. This created a stable coating for over 200 runs [74]. Both methods for column fabrication produced excellent run-to-run, day-to-day, and column-to-column reproducibility with less than 3% RSD for the EOF.

Often, OTCEC separations suffer from low capacity factors because of the small active surface area and fewer available functional sites. This also can lead to poor separation efficiency and co-eluting peaks. In an attempt to improve peak capacity, a new porous layer for OTCEC has been described that uses the in situ polymerization of a mixture of monomers in the presence of porogen for higher separation efficiencies [75]. A column generated from the porogen, 1-propanol, was able to generate a high abundance of micropores and mesopores, resulting in a large specific surface area. This generated an efficient separation of the two model proteins, BSA and cytochrome-*c*.

Another widely explored approach for the implementation of CEC is the use of monolithic columns. Monoliths have high permeability, a fast mass transfer rate, and high loading capacity. Many commercially available monoliths are made from silica leading to a risk of band broadening

and sample loss due to protein adsorption. Therefore, to minimize protein adsorption during CEC and improve separation efficiencies, neutral and cationic monoliths have been developed.

A series of neutral nonpolar monolithic columns were manufactured and tested for the separation of both intact proteins and peptides from protein tryptic digest. To produce the monoliths, various ratios of monomers C8-methacrylate, C12-methacrylate, and C16-methacrylate were mixed with the crosslinking polymer pentaerythritol (PETA) [76]. In these experiments, it was determined that when the ratio of monomer to PETA was kept constant, the C8 monolith gave the best separations for intact proteins. The C16 column exhibited the best efficiencies for smaller peptides. In their report, Puangpila *et al.* claim that, even in the absence of a charged surface, there is EOF generated by adsorption of BGE ions to the monolith and it can be controlled by changes in the pH and ACN content of the mobile phase.

Cationic monolithic columns can also be used to reduce electrostatic interaction of basic proteins to the monolithic and capillary surface. Wang *et al.* developed a novel monolithic IL column that was made by a simple "one pot" approach using thermal free radical copolymerization [77]. Using this method, several counterions (bromide, tetrafluoroborate, hexafluorophosphate, and bis-trifluoromethanesulfonylimide (NTf_2^-)) were tested with the cation 1-vinyl-3-octylimidazolium ($ViOcIm^+$) to create an IL monolith capillary columns [78]. Each IL monolith was capable of generating a consistent reverse EOF over the pH range 2.9–12.0. However, only the $ViOcIm^+NTf_2^-$ was able to achieve baseline resolution for all proteins in a standard mix (Table D.4).

3 Detection methods

3.1 Spectroscopic detection

Spectroscopy is the most common detection method for proteins and peptides separated by CE. UV absorbance tends to be favored over fluorescence spectroscopy due to a natural absorbance of the amide bonds and aromatic residues in the near UV (214 and 280 nm). However, this approach suffers from poor limits of detection due to the micrometer pathlengths characteristic of CE and high background from the UV source. Additionally, BGE composition, pH, and ionic strength can have a significant effect on background. Approaches such as increasing the pathlength through modification of the detection window using Z-shaped capillaries and bubble-cells have been successful in decreasing the LOD by an order of magnitude or greater [79, 80].

Fluorescence detection of proteins can be accomplished based on the native fluorescence of tryptophan, phenylalanine, and tyrosine residues in proteins using a deep UV light sources [81-83]. However, with native fluorescence based detection, the signal is dependent on the number of excitable residues as well as their accessibility within the tertiary structure of the protein. Therefore, the applicability of this technique varies from protein to protein. To improve the LODs for native fluorescence detection of erythropoietin (EPO), Wang *et al.* utilized a magnetic bead-based extraction system for pre-concentration. Using this procedure, it was possible to obtain an LOD of 10 nM, two orders of magnitude lower than what was possible with UV absorbance at 214 nm [84].

Low limits of detection achievable by LIF can also be obtained through derivatization of the protein or peptide of interest with a fluorophore [85]. The most common derivatization sites for proteins are the primary amines and cysteine residues. These can be tagged with a variety of agents including Alexa Fluor-based dyes, naphthalene-2,3-dicarboxaldehyde, fluorescein isothiocyanate, and many others. A major disadvantage of pre-separation derivatization for proteins is the complexity of the derivatization process. This approach requires not only that the tag is specific for the functional group on the analyte of interest but also that it does not interfere with the separation by introducing additional fluorescent by-products. Proteins typically have several reactive sites that can be labeled which leads to multiple peaks for one analyte, complicating data analysis [86].

3.2 Mass spectrometry

CE-MS is a powerful combination of high efficiency separations with selective and sensitive detection. This technique can provide important information on identity, glycoforms, degradation, and impurities of protein therapeutics [87, 88]. It is possible to couple CE to MS using different ionization techniques, as has been described in several excellent reviews [89, 90]. For this review, only the recent advances regarding the development and application of the ESI interfaces will be highlighted. CE was first interfaced with MS by ESI in 1987 [91] and it remains the most popular ionization method due to its broad applicability and commercialization.

ESI is a robust soft-ionization technique that produces multiply charged ions for proteins in the gas phase. However, there are many considerations that must be taken into account when coupling it with CE. Primarily, the use of run buffers containing non-volatile salts and additives

can lead to their deposition within the instrument, and subsequent contamination of the source. While formic acid and acetate buffers have been used as BGEs for the separation of proteins by CE, they are not always ideal because of inadequate resolution and possible protein instability at low pH. Additionally, the voltages typically applied to the capillary for separation are 2–3 orders of magnitude higher than what is used for ESI. Toward this end, researchers have developed three general approaches for coupling CE to MS with ESI: sheath-liquid, sheathless, or junction-at-the-tip interfaces.

The most widely used and commercially available option is the sheath-liquid interface. This is accomplished by placing the outlet of the CE capillary coaxially within a tube. The tube delivers a MS-compatible sheath liquid (Figure D.7A) that provides easy electrical connections and a flow rate to the ESI of μL/min. This is beneficial because the EOF of the CE is generally much slower (nL/min) than what is compatible for a stable spray.

The compatibility of separation and detection parameters for CE-ESI-MS with a sheath-liquid interface was evaluated for eight model proteins and several EPO isoforms [92]. It was found that the BGE composition and capillary coating play the largest role in the quality of the separation. For all analytes, the best signal was obtained with a sheath flow rate between 2-5 μL/min and a sheath flow liquid composed of 1% acetic acid in 1:1 organic:water; in this study, 2-propanol was chosen over MeOH or ACN. The optimal gas pressure was determined to be 0.2 bar, since anything lower lead to a loss of analyte intensity and anything higher was shown to affect the resolution of the separation. As an added benefit, the nebulizer gas pressure can create suction at the capillary outlet, increasing the CE flow rate for separations performed in neutral capillaries.

An obvious disadvantage of the sheath-liquid interface is the loss in detector sensitivity from dilution of the eluting peaks. To improve detection limits, a sheathless interface was developed. The largest downside of this approach is the difficulty in properly completing the electrical circuits for the CE and the ESI. While many attempts have been made, these interfaces were limited by stability and ease of application [90, 93].

Recently, Moini and Whitt developed a sheathless interface based on a porous junction [94, 95]. In this interface, the end of the capillary was made porous to small ions by drilling a well into the polyamide coating and etching the remaining material with hydrofluoric acid. The capillary was then placed within an existing ESI needle filled with BGE, allowing electrical connection to both the CE and ESI (Figure D.7B). The tip of the capillary could then be used for electrospray when voltage is applied. The only drawback to this technique was the difficulty in reproducibly etching the capillary end. To improve the applicability and availability of the Moini and Whitt sheathless interface, Beckman Coulter developed a prototype that has been successfully applied to the analysis of intact proteins [96], protein glycoforms [97], and protein tryptic digests [98, 99].

In a recent report, both CE- and LC-MS were compared for the analysis of a particular therapeutic mAb [99]. With LC-MS, 11 small peptides eluted in the void volume and could not be detected, including two fragments that were critical for the identification of the binding domain of the mAb. The same digest was analyzed by CE-MS employing both a traditional sheath-liquid interface and the Beckman Coulter sheathless interface using a BGE consisting of 10% acetic acid

at pH 2.3. Sixty of 61 peptides were detected with the sheath-liquid interface, while all 61 peptides were detected with the sheathless system with higher separation efficiencies and better sensitivity.

Another alternative to the sheath-liquid interface is the junction-at-the-tip design developed by Chen's group. In this interface, the capillary end is placed within a hollow needle that forms a "flow-through microvial" [100] (Figure D.7C). The hollow needle is filled with a chemical modifier that provides the necessary electrical contacts for the separation and ESI voltages. Similar to a sheath-liquid interface, this modifier increases the CE BGE compatibility with the ESI. However, because the flow rates are much lower (< 1 µL/min), the dilution factor is not significant. Chen's group has extensively characterized the performance of this interface in several publications [63, 100-103].

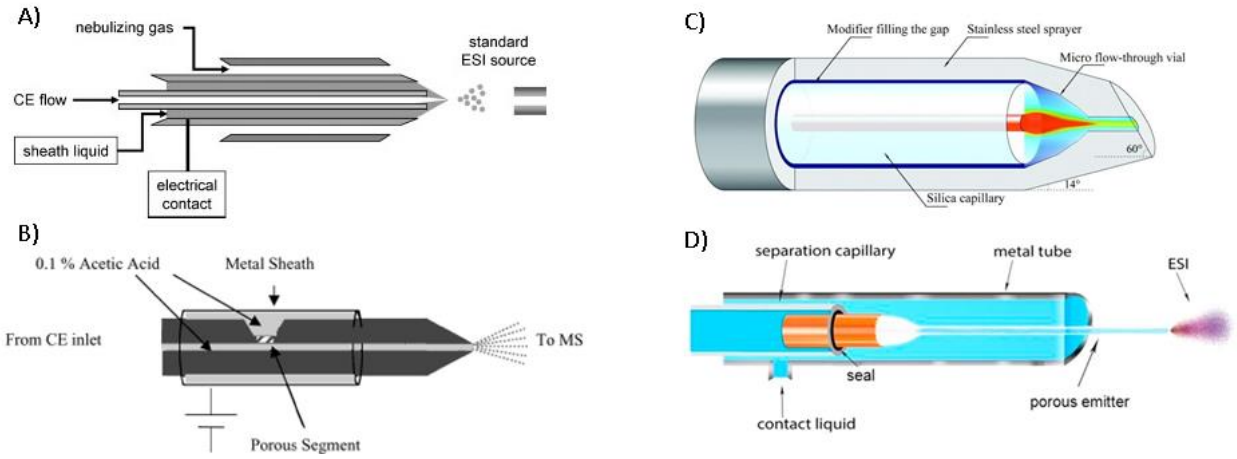

Figure D.7: Diagrams of four CE-ESI-MS interfaces. A) Sheath-flow, B) Moini and Whitt sheathless flow, C) Chen junction-at-the-tip, D) sheathless interface for CITP/CZE-nanoESI-MS. Reprinted/adapted with permission from ref. 89, 94, 102, 62 respectively

Perhaps the most exciting new use of these interfaces is in coupling MS to more complex CE modes, such as CIEF and capillary isotachophoresis (CITP) which require high concentrations of non-volatile components to achieve a separation. In 2011, Zhong *et al.* described a CIEF-MS approach for the analysis of several model peptides and proteins using the junction-at-the-tip interface with coated and uncoated capillaries [103]. Unfortunately, the ampholytes used for the separation were still able to reach the detector, leading to high backgrounds and ion suppression. To prevent this from occurring, a new sheathless interface was developed by Wang *et al.* that uses a large bore separation capillary for sample loading and a sheathless interface with a porous emitter for its application with CITP [64] (Figure D.7D). This system was then utilized for the analysis of test peptides spiked into tryptic digests of BSA (Table D.5). They were able to obtain a linear range over 4.5 orders of magnitude and a five-fold sensitivity improvement compared to the sheath-liquid interface for two test peptides, kemptide and angiotensin II.

Table 5. CE-MS and ME-MS

Analyte	Mode	Interface	Sheath flow	BGE	Capillary coating	MS	Notes	Ref.
Lysozyme, β-lactoglobulin A, cytochrome *c*, RNase A, myoglobin, RNase B, trypsin inhibitor, carbonic anhydrase, and EPO glycoforms	CZE	Agilent sheath-liquid	2-propanol /water (1:1), 1% acetic acid	0.5-2 M acetic acid	Various coating solutions and permanently coated capillaries	TOF	Comparison of coatings. Emphasis on intact protein analysis	[91]
EPO and interferon-β glycoforms	CZE	Beckman Coulter sheathless		0.5 mM - 2.0 M acetic acid	Beckman Coulter neutral bilayer	TOF	Glycoprofiling of pharmaceutical products	[96]
Tryptic digest of Trastuzumab	CZE	Beckman Coulter sheathless		10% acetic acid	Bare fused silica	TOF	Rapid characterization of therapeutic mAbs	[97]
Tryptic digests of in-house mAbs	CZE	(1) Agilent sheath-liquid (2) Beckman Coulter sheathless	(1) 0.1% acetic acid	10% acetic acid	(1) PVA-coated and bare silica (2) Bare fused silica	TOF	Improving detection of small peptides from tryptic digrests	[98]
Bradykinin, angiotensin I, neurotensin, fibrinopeptide, substance P, kemptide, leu-enkephalin, angiotensin II, melittin, and renin spiked in tryptic digests of BSA	CITP	In-house sheathless		0.1 M acetic acid (90%), MeOH (10%) LE: 25 mM ammonium acetate, pH 4	HPMC	TQ	Five fold sensitivity improvement from the sheath-liquid interface	[62]
Trypticdigest of in-house IgG2 mAb	LC-ME	Microchip		50% ACN, 0.1% formic acid	APTES	TOF	UPLC followed by MCE and on-chip ESI-MS interface	[146]

Capillary: Actual length (effective length), inner diameter
Aminopropyltriethoxysiland (APTES), Bovine serum albumin (BSA), Capillary isotacholphoresis (CITP), Hydroxypropyl cellulose (HPMC), Leading electrolyte (LE), Polyvinyl alcohol (PVA), Triple quadrupole (TQ)

Table D.5: CE-MS and ME-MS

4. Applications

In addition to assessing protein pharmaceutical products based on their size and charge heterogeneity and the presence of impurities, the analysis of biologics poses two additional analytical challenges: 1) how to characterize and better understand the complicated cellular process of glycosylation, and 2) preparing for the onset of biosimilar drugs to the market and how to best prove their similarity to the innovator product.

4.1 Glycosylation

Glycosylation is one of the most prevalent PTMs of therapeutic proteins. *In vivo*, glycosylation plays several important roles, including protection against degradation and non-specific interactions as well as orientation for the binding domain. The two major types of glycosylation that occur involve N-linked and O-linked carbohydrates. N-linked glycans are attached to the protein backbone at the amine side of Asn and are found in the well-defined amino acid sequence of Asn-X-Ser/Thr, where X is any amino acid but proline. O-linked glycans are not sequence-specific and are found attached to the protein backbone at the OH group of Ser or Thr.

Monoclonal antibody-based therapeutics of the IgG1 sub-type make up a 100 billion dollar annual market [104]. These mAbs consist of 2–3% carbohydrate by mass. Most of the glycosylation occurs as N-linked glycans located on the Asp^{297} in the C_H2 domain of the Fc region of each heavy chain. A number of factors can affect the composition, structure, and frequency of

these glycans, posing an interesting challenge for the manufacturing of a homogeneous product. To ensure a homogeneous product and avoid potentially immunogenic glycans, each step of biotherapeutic production from clone selection to lot release needs to be well characterized. This characterization requires fast, high-throughput analytical methods to accurately screen the numerous samples generated per day.

The size and charge characterization of glycoproteins can be accomplished by the various electrophoretic separation techniques mentioned in the previous sections of this review. Several methods and protocols for CZE, SDS-CE, and CIEF separations of glycoproteins have been compiled by Rustandi *et al.* [105]. A typical downside to CE-based methods is the characteristic migration time irreproducibility. To address this, freely available software, glyXalign, was developed based on a set of rapid algorithms that enables automatic correction of distortions in CGE-LIF data to improve peak identification [106].

For further understanding of the nature, location, and composition of the glycans, methods for the removal and analysis of the sugars themselves are also needed. The majority of these carbohydrate analyses are performed by LC. In particular, hydrophilic interaction chromatography (HILIC) coupled to LIF and MS detection has been useful for the sensitive analysis of glycans [107].

CE-LIF is an excellent orthogonal technique to HILIC-LIF for separation of glycans, and in a comparative study it was shown that they were able to detect an equal number of glycans removed from an IgG [108]. An advantage of CE-LIF for glycan analysis is that it can be used to distinguish

both lineage and positional isomers [109, 110]. Using CZE-LIF, carbohydrate sequencing can be performed by both top-down digestion and bottom-up identification using a series of sugar-specific exoglycosidases. Typically, glycans are enzymatically removed, fluorescently labeled, and separated by size or charge. There are several charged fluorescent reagents commercially available for tagging glycans. The most common reagent used in conjunction with CE-LIF is 8-aminopyrene-1,3,6-trisulfonic acid (APTS). However, recently, Kuo *et al.* published a rapid method for labeling aldoses with 2,3-naphthalenediamine to produce highly fluorescent naphthimidazole derivatives [111]. Using this reagent, it was possible to perform composition analysis and enantioseparation of the glycans using CE with cyclodextrin in the BGE.

An important advantage of CE-LIF over HILIC-LIF is the ability to multiplex 48- and 96-capillary arrays for high-throughput analysis. Callewaert *et al.* were the first to perform glycan analysis using a commercially available multiplexed CE-based DNA analyzer [112]. Later, this same technique was used along with a 48-capillary array to perform high-throughput analysis of glycans from IgG. In this application, glycans were removed by digestion and labeled with APTS in 96-well plates and then subjected to simultaneous analysis by capillary array. This approach made it possible to run 3000 samples in a single day [113] (Table D.6).

Table 6. CE-based analysis of protein glycosylation

Analyte	Mode	Capillary	BGE	Detection	Label	Notes	Ref.
N-glycans of mAb1	CGE	48 capillary array, 50 cm each	Applied Biosystems Pop-7™	LIF ex. 473 nm / em. 520 nm	APTS	High-throughput glycan analysis	[112]
(1) Neu5Gc and (2) α1,3-Gal containing N-glycans	Partial-filling CE	40 (30) cm, 50 μm id DB-1 capillary	100 mM Tris-acetic acid, 0.05% HPC, pH 7.0	LIF ex. 488 nm / em. 520 nm	APTS	Reaction with (1) anti-Neu5Gc or (2) α-galactosidase inject prior to sample	[115]
Non-human N-glycans	CGE	40 (30) cm, 100 μm id DB-1 capillary	100 mM Tris-borate, 5% PEG, pH 8.3	LIF ex. 325 nm / em. 405 nm	2-AA	Analysis of commercially available mAbs	[116]
α1,3-Gal containing N-glycans	CGE	60 (50) cm, 50 μm id eCAP NCHO coated	Beckman Coulter Carbohydrate Separation Gel Buffer-N	LIF ex. 488 nm / em. 520 nm	APTS and AMAC	Ultrasensitive detection method	[117]
N-glycans of mAb	CGE	50 (40) cm, 50 μm id PVA coated	Beckman Coulter Carbohydrate Separation Buffer Or 40 mM EACA-acetate, 0.2% HPMC	LIF ex. 488 nm / em. 520 nm	APTS	Glycans of mAbs from NS0 cells	[118]
N-glycans of fusion protein	CE	90, 60, or 43 cm	0.7 M ammonia and 0.1 M EACA in 70% MeOH	TOF-MS	APTS	Alkaline CE-MS method	[119]
N-glycans	(1) CGE (2) CE	Various capillary lengths and coatings	(1) Beckman glycan separation buffer or POP-7 polymer (2) 40 mM EACA, 131 mM acetic acid, pH 4	(1) LIF ex. 488 nm / em. 512 nm (2) TOF-MS	APTS	CGE-LIF and CE-MS methods compared to the CE-MS method in ref [119]	[120]
N-glycans of mAbs	CE	50 (40) cm, 50 μm id N-CHO coated	Beckman Coulter Carbohydrate Separation Gel Buffer	LIF ex. 488 nm / em. 520 nm	APTS	CE-LIF as an orthogonal technique to MS	[121]

Capillary: Actual length (effective length), inner diameter, coating
2-aminoacridone (AMAC), 2-aminobenzoic acid (2-AA), 9-aminopyrene-1,3,6-trisulfonic acid (APTS), ε-aminocaproic acid (EACA), Galα1–3Gal (α1,3-Gal), Hydroxypropyl cellulose (HPC), Hydroxypropylmethylcellulose (HPMC), N-Glycolylneuraminic acid (Neu5Gc), Polyvinyl alcohol (PVA), Poly(ethylene glycol) (PEG),

Table D.6: CE-based analysis of protein glycosylation

In the research and development of mAbs, a particular area of interest is the study of immunogenic non-human glycans. The frequency and type of non-human glycans attached to the therapeutic protein during production differ from cell line-to-cell line [114]. It is well known that the non-human oligosaccharides galactose-α-1,3-galactose (α1,3-Gal) and N-glycolylneuraminic acid (Neu5Gc) can illicit an immune response. In fact, in response to enteric bacteria, approximately 1% of all human antibodies are against the α1,3-Gal epitope [115].

Detection of both α1,3-Gal and Neu5Gc non-human glycans was performed by partial filling affinity CE. In this method, a plug of either anti-Neu5Gc antibody or α-galactosidase (dissolved in BGE) was injected on capillary prior to injection of the APTS-labeled glycans (removed from

the target antibody) [116]. Once the electric field was applied, the higher mobility sugars in the sample pass through the antibody or enzyme plug, causing a reaction. This reaction produced additional product peaks upon LIF detection, allowing specific detection and quantification of the two immunogenic sugars.

In another study, six commercially available mAb pharmaceuticals produced in nonhuman mammalian cell lines were analyzed by CZE-LIF, in parallel with LC-ESI-TOF-MS, to determine the presence of nonhuman N-glycans [117]. By CZE, forty-six fluorescently labeled N-glycans were separated using a tris-borate BGE containing 5% PEG to slow the EOF. Of the six mAb pharmaceuticals, three were found to contain nonhuman N-glycan residues. To obtain additional information regarding the attachment of nonhuman N-glycans to therapeutic proteins, CZE-LIF with exoglycosidase digestion and fluorescent tagging was used to achieve LODs of 1 μg allowing characterization of the low-abundance α1,3-Gal epitope [118].

CE-MS can also be used in conjunction with CGE-LIF [119] to obtain additional structural information and identify unknown glycans [3]. For example, Bunz *et al.* described both alkaline and acidic BGE systems that could be used for the determination of APTS-labeled mAb glycans by CE-TOF-MS [120, 121]. The CE-MS methods were then compared against to two CGE-LIF methods commonly used for routine glycan analysis. While both CE-MS and CGE-LIF were able to resolve and detect the glycans, because of the difference in the separation mechanisms they had different migration orders, making it difficult to directly compare the two electropherograms obtained for a complex sample.

The downside of glycan analysis by MS is the likelihood of unwanted fragmentation of sugars during the ionization process. This can lead to large amounts of difficult-to-interpret data and misidentification [122]. For this reason, it is important not only to insure careful optimization during MS method development but to provide orthogonal analyses such as CZE-LIF or CGE-LIF to validate the findings.

4.2 Biosimilars

Follow-on biologics, also known as biosimilars or biobetters, is the term for the "generic" biopharmaceuticals that have recently entered the market. The European Medicines Agency published regulatory guidelines for biosimilars in 2005, and by 2012 there were 14 products approved for sale in Europe [123]. In 2013 the first mAb biosimilar, Hospira's Inflectra, hit the European market, and more than a half-dozen prospective biosimilars are in the pipeline. In 2015, as the majority of the leading biologics go off patent, there will be ample opportunity for established and start-up companies to begin producing biosimilars.

While production of biosimilars is an inherently less risky venture, due to the established market and tested safety of the innovator product, proving comparability to regulatory agencies still poses a significant challenge. Unlike chemical synthesis of small molecule generics, the composition of biologics is highly dependent on the manufacturing process. Small changes in production can have significant implications on the quality. In particular, the addition of impurities, aggregation products, and/or PTMs such as glycans can cause the protein to be

immunogenic. Without detailed knowledge of how the innovator was produced, it can be very difficult to create an identical product.

Fortunately, dozens of analytical techniques exist to verify the physicochemical and functional comparability of the biosimilar to the innovator [124]. As discussed in the previous sections of this review, electrophoretic techniques are widely used for characterization of size and charge heterogeneity, product degradation, and PTMs. The appropriate method is generally chosen based on protein complexity, which varies from small non-glycosylated proteins like insulin and HGH to large, heterogeneous glycoproteins and mAbs [125].

EPO is a glycoprotein with approved biosimilars making up 12% of its market [123]. EPO has three complex N-glycosylation sites and one O-glycosylation site, which introduce a high level of heterogeneity into the protein. To be able to differentiate between the various formulations of EPO, or prove similarity between innovator and biosimilar, Taichrib *et al.* evaluated two multivariate statistical approaches for the analysis of CE-MS data [126] (Table D.7). The data were generated using a CE-ESI-TOF-MS method developed previously that exhibited high separation efficiencies and high selectivity for 14 commercially available preparations of EPO [92]. Both statistical approaches proved useful for analyzing the similarity or difference between large sets of glycosylated biologics that were generated under different production conditions, cell lines, and various batch numbers.

Table 7. CE-based analysis of biosimilars

Analyte	Mode	Capillary	Coating	BGE	Detection	Notes	Ref.
EPO glycoforms	CZE	60 cm, 50 µm id	UltraTrol™ LN	1 M acetic acid	TOF-MS	Multivariate statistical approach for glycoform analysis	[125]
(1) Rituximab. trastuzumab, and ranibizumab (2) Infliximab and bevacizumab	CZE	40.2 (30.2) cm, 50 µm id	Polyacrylamide	(1) 200 mM EACA-acetic acid, 30 mM lithium acetate, 0.05% HPMC, pH 4.8 (2) 150 mM EACE-acetic acid, 20 mM lithium acetate, 0.05% HPMC, pH 5.5	UV 214 nm	CZE methods tested against orthogonal techniques for mAb characterization	[126]
Rituximab	CGE	NR	NR	NR	UV 214 nm	Size heterogeneity of mAbs	[127]
Anti-α1-antitrypsin mAb	iCIEF	iCE280 Analyzer; 50 mm, 100 µm id	Fluorocarbon (ProteinSimple)	Pharmalyte pH 5-8	UV 280 nm	Interlaboratory study for robustness	[128]

Capillary: Actual length (effective length), inner diameter
ε-aminocaproic acid (EACA), Hydroxypropylmethyl cellulose (HPMC), Not reported (NP)

Table D.7: CE-based analysis of biosimilars

With the upcoming mAb biologic patent cliff, much of the biosimilar research has focused on the comparability of antibodies from various sources. Towards this end, CZE [127] and SDS-CGE [128] techniques can be used to determine charge heterogeneity of mAbs. Using CZE, rituximab (Kikuzubam® and Reditux®) and trastuzumab biosimilars were analyzed with respect to existing commercial products, Mabthera® and Herceptin®, respectively [127]. The CZE methods were then compared to existing CIEF and chromatographic methods (HILIC and cation exchange chromatography). They found that, not surprisingly, a single method was not sufficient to resolve and characterize a protein, putting the emphasis on orthogonal techniques. However, they did report that CZE and CIEF gave better resolution of the mAbs than either HILIC and cation exchange chromatography, especially when using coated capillaries, since protein adsorption tends to lead to band broadening.

With the multitude of assays that exist, reproducibility and ruggedness is essential for widespread biosimilar production and regulation. The innovator, the biosimilar manufacturer, and

the regulatory agency need to be certain that, despite the various laboratory conditions, the experimental results are comparable. To help facilitate this, Salas-Solano *et al.* evaluated an iCIEF method in 12 different laboratories across the world using several analysts, a variety of ampholytes, and multiple instruments [129]. The combined precision for the 12 labs was 0.8% RSD for the pI determination and 11% RSD for the percent peak area values for the charge variants of a therapeutic mAb. This study compared these values to those obtained using conventional CIEF, where the RSDs for pI and peak area were of 0.8% and 5.5%, respectively [130].

5. Microchip electrophoresis

Many aspects of CE, such as low sample volume requirements, speed, efficiency, and the ability to use physiologically appropriate BGEs, make it an attractive method for the analysis of biopharmaceuticals. The advantages CE offers over chromatography are a function of the small inner diameter of the capillary. Consequently, there has been an effort to further miniaturize bench-top CE instrumentation to a microfluidic format. This has decreased samples sizes needed for analysis from mL to µL, reduced analysis times from minutes to seconds, increased separation efficiencies, decreased costs, and added the ability for portable point-of-care analysis. Additionally, multiplex ME systems can be designed to handle high-throughput analysis on a greater scale than CE systems, making them an attractive technology for drug discovery and analysis [131, 132].

While most CE separation modes can be transferred to ME, the majority of the current published assays have dealt with analysis of biomarkers and small molecule drugs. Recent

advances in N-glycan profiling by ME have also been made for clinical chemistry applications [133, 134]. However, as the field of protein analysis on-chip grows, so does the possibility that the use of these devices will soon be accepted by the FDA as a validated method, allowing them to be incorporated into industry protocols.

5.1 Microchip gel electrophoresis

The LabChip® GXII, a commercially available microchip gel electrophoresis (MGE) system from PerkinElmer, is used frequently in the pharmaceutical industry [135, 136]. The commercial procedure, which uses indirect fluorescence and a HT Protein Express gel matrix [137], was compared against two new SDS-MGE methods, one for "high-sensitivity" and the other for "high-resolution" [138]**.** In the "high-sensitivity" method, direct LIF detection of fluorescently labeled proteins was investigated. Two labeling schemes were compared, and it was reported that performing the labeling step prior to protein denaturation improved the signal up to 50-fold for a loading concentration LOD of 1 ng/mL. In the "high-resolution" method, the sieving effect of the commercial gel was increased by the addition of a 6% poly(N,N-dimethylacrylamide) (PDMA) solution. With an optimal ratio of 2:1, gel:PDMA, the assay achieved resolution between Fab heterodimers without increasing the separation time. Additional high-throughput analysis is available to process 96 samples in less than an hour.

SDS-MGE has also been integrated with Western blot immunoassay detection [139]. The separation of a series of test proteins with a MW range of 11–155 kDa (Table D.2) was performed on-chip by Jin *et al.* [140]. Following the separation, the sample was eluted from the chip onto the Western blot membrane. In order to maintain the discrete zones accomplished during the

separation, the chip was held in place vertically while the membrane moved below the outlet on an X-Y stage for spotting (Figure D.8). By carefully controlling the membrane spotting rate and the flow from the SDS-MGE chip, separation efficiencies of 40,000 theoretical plates were possible. With this set-up, the throughput capabilities were improved with a total analysis time of less than 32 min for the separation and immunoassay. This is a dramatic improvement over the traditional Western assay that takes several hours to complete.

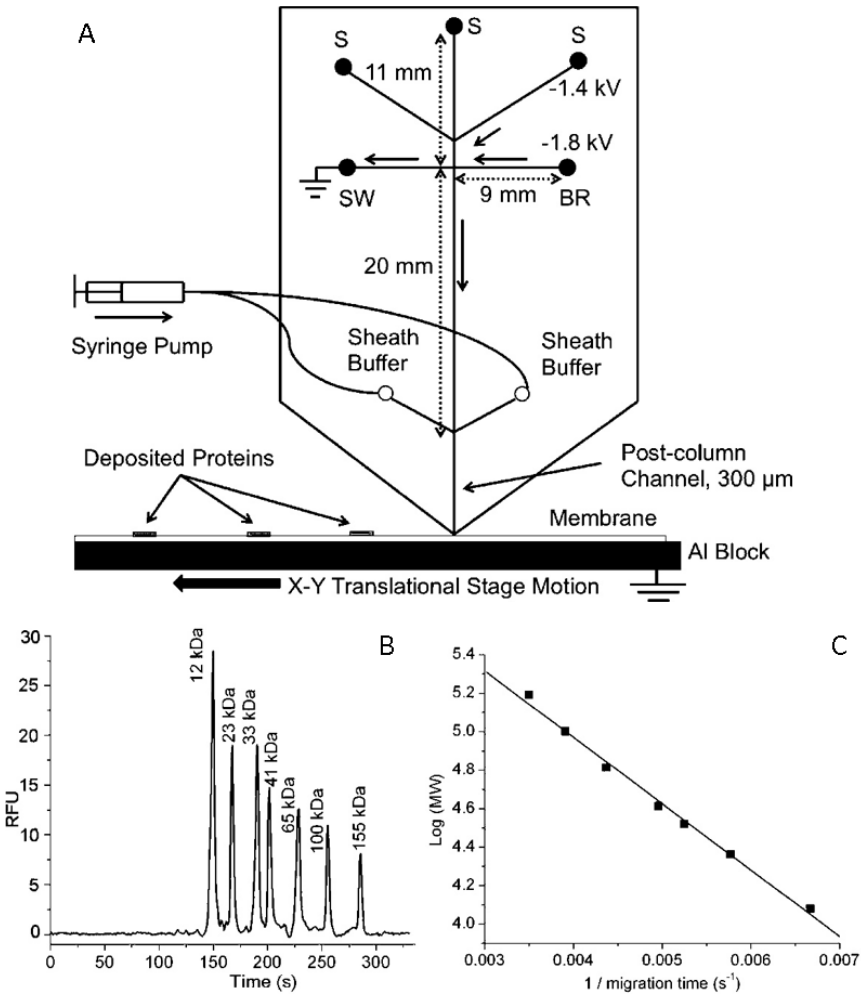

Figure D.8: A) Microchip overview. Samples are Samples are loaded in different sample reservoirs (S). Samples are injected by floating the buffer reservoir (BR) and sample waste (SW) with voltage applied between the desired sample reservoir and the Al block at the exit. During separation, flow from the sample reservoir is gated to the sample waste reservoir (SW) using the voltages as shown. During these operations, other sample reservoirs are floating. Sieving media is pumped through the sheath channels to give stable current. Channel lengths are indicated by double arrow lines and direction of flow during separation is indicated by solid, single arrows. B) Size-dependent separation of FITC-labeled protein ladder in microchips. Detection window was set at the end of separation channel, 300 µm away from the chip outlet. Electric field during separation was 240 V/cm. C) Relationship of MW to migration time. Reprinted with permission from ref. 140

5.2 Microchip isoelectric focusing

ME-based systems have also been used to verify the charge heterogeneity of mAbs with microchip isoelectric focusing (MIEF). Using a commercially available MCE-2010 system with whole-channel imaging from Shimadzu, Kinoshita *et al.* were able to analyze the charge variants of several mAbs [141]. The microchip consisted of two sample wells, one containing an anolyte and the second containing a catholyte, separated by a 2.7 cm channel. Following the separation, the whole channel was imaged with UV detection. To reduce the EOF, 0.2% hydroxyproplymethylcellulose was added to the BGE allowing greater focusing while preventing the non-specific adsorption of protein to the capillary wall. Using the optimized conditions, the authors were able to separate charge variants of three commercially available mAbs (bevacizumab, trastuzumab, and cetuximab) within 200–300 s. These separations were very reproducible (< 0.5% RSD) and were roughly 10 times faster than the corresponding CIEF assay.

To further improve the utility and throughput of MIEF assay a single-channel microchip device where separation, immobilization, and subsequent immunoblot rinse steps could all be performed has been reported [142]. Once the proteins were separated within the pH gradient they were exposed to UV light and covalently cross-linked to a light-activated volume-accessible gel present in the microchip. This technique gave similar capture efficiencies (≈ 0.01%) to previous reports where proteins were immobilized on the inner surface of the capillary [44, 143]. Wash steps were performed by electrophoretic transport on the immobilized protein without concern of sample loss. Using this technique, it was possible to complete an isoform assay in less than 120 min, up to 15x

faster than the conventional slab-gel followed by Western blot. Such rapid purity assays illustrate the significant advantage ME has over CE and other techniques.

5.3 Microchip electrophoresis-mass spectrometry

As with CE, even more specific and selective detection of analytes is possible by coupling ME to MS. The most common ionization interface for ME with MS is ESI, but MALDI is also possible [144]. The major benefit of ME-ESI-MS is that the flow rate on-chip is compatible with ESI and can therefore be seamlessly interfaced without disrupting the electrophoretic separation. When constructing an ME-MS interface, the geometry of the outlet and flow rate through the capillary must be taken into account given their monolithic construction and integration.

An advantage of ME over CE is that sample preparation and multiple separation methods can be integrated onto a single device prior to the ESI interface. Therefore, the excess dead volumes that are characteristic of conventional systems are eliminated, reducing the band broadening and sample dilution. The Ramsey group reported a fully integrated LC/CE microchip that terminated in an ESI source off the corner of the device in 2011 [145]. The potential combination of LC and ME for a more selective and specific separation is very powerful. In addition, the microchip flow rates are compatible with the ESI. However, a major disadvantage of fully integrated microchips is that the increased complexity of the device makes them difficult to fabricate.

As noted in a subsequent Ramsey paper, the fully integrated chip described above could not handle pressures over 200 bar. Therefore, to improve on the earlier design, a glass microchip that could be integrated with an off-chip UPLC was designed (Figure D.9) [146]. This allowed higher

pressures to be reached than were possible with the LC on-chip. The new device produced significant improvements in reproducibility and peak capacity when evaluated for the analysis of digested N-glycosylated proteins. Additionally, the authors point out the utility of the new design in its ability to integrate to existing LC equipment that is already ubiquitous in industry.

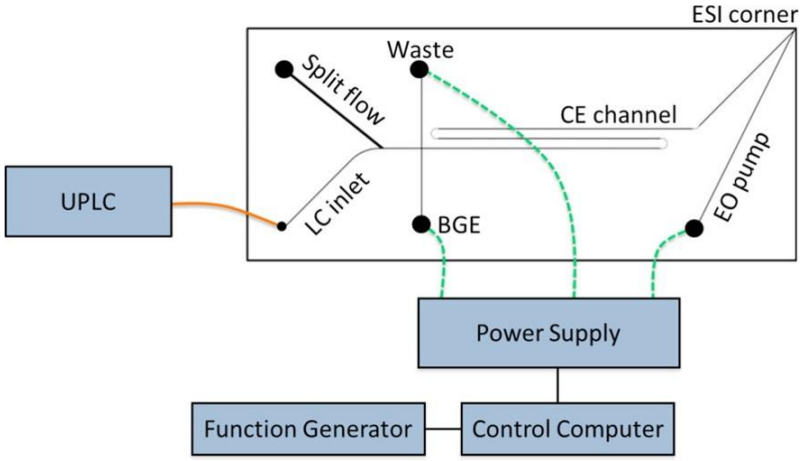

Figure D.9: Schematic of the hybrid capillary LC microchip CE-ESI experimental setup. The orange line represents a transfer capillary connecting the LC column to the microfluidic device. The dashed green lines represent electrical connections between the high voltage power supply and the microfluidic reservoirs. Reprinted with permission from ref. 146

6. Conclusions and future perspectives

The development of protein and peptide therapeutics is a complex and high-risk venture, as products produced by recombinant expression are inherently heterogeneous. However, with advances in analytical techniques, thorough protein characterization is possible. In particular, CE-based separation techniques such as CZE, CGE, CIEF, and CEC provide versatile, efficient, and fast analyses of proteins. Additionally, CE-based techniques have the potential for high-throughput analysis using capillary arrays. The wide range of capillary-based separations can assess many

aspects of protein stability, process impurities, and PTMs such as glycolysis, each of which is essential in providing a safe, effective, and quality product.

Microchip based formats have the potential for increased speed, higher throughput, and portability of CE. While the development of ME devices is still primarily an academic research area, there is considerable promise for this miniaturized technique in the future of on-site pharmaceutical analysis. Pharmaceutical applications of ME and CE to therapeutic protein analysis will be further expanded through the development and commercialization of specialty capillaries, BGEs, and detection techniques. This is especially true for CE-MS and ME-MS interfaces. With numerous reviews already existing on this topic alone, coupling of MS with these techniques show great promise in the future for therapeutic protein analysis.

7. Acknowledgments

The authors would like to thank the University of Kansas for continued support and Nancy Harmony for proofreading and editorial assistance. We gratefully acknowledge funding from the National Institutes of Health, grant number NINDS R56-NS042929. Additionally, JSC and NJO were participants of the Biotech Training Grant NIGMS T32-GM008359.

The authors declare no conflicts of interest.

8. References

1. Creamer, J.S., N.J. Oborny, and S.M. Lunte, *Recent advances in the analysis of therapeutic proteins by capillary and microchip electrophoresis.* Analytical Methods, 2014. **6**(15): p. 5427-5449.
2. Manning, M.C., et al., *Stability of protein pharmaceuticals: an update.* Pharm Res, 2010. **27**(4): p. 544-75.
3. Fekete, S., et al., *Analytical strategies for the characterization of therapeutic monoclonal antibodies.* TrAC, Trends Anal. Chem., 2013. **42**: p. 74-83.
4. Little, M.J., D.M. Paquette, and P.K. Roos, *Electrophoresis of pharmaceutical proteins: status quo.* Electrophoresis, 2006. **27**(12): p. 2477-2485.
5. Staub, A., et al., *Intact protein analysis in the biopharmaceutical field.* J. Pharm. Biomed. Anal., 2011. **55**(4): p. 810-822.
6. Zhao, S.S. and D.D.Y. Chen, *Applications of capillary electrophoresis in characterizing recombinant protein therapeutics.* Electrophoresis, 2014. **35**(1): p. 96-108.
7. Marie, A.-L., et al., *Capillary zone electrophoresis and capillary electrophoresis-mass spectrometry for analyzing qualitative and quantitative variations in therapeutic albumin.* Anal. Chim. Acta, 2013. **800**: p. 103-110.
8. Shi, Y., et al., *Development and validation of a rapid capillary zone electrophoresis method for determining charge variants of mAb.* J. Chromatogr. B: Anal. Technol. Biomed. Life Sci., 2012. **906**: p. 63-68.
9. Creamer, J.S., S.T. Krauss, and S.M. Lunte, *Capillary electrophoresis separation of the desamino degradation products of oxytocin.* Electrophoresis, 2013: p. Ahead of Print.
10. Jorgenson, J.W. and K.D. Lukacs, *Capillary zone electrophoresis.* Science, 1983. **222**(4621): p. 266-72.
11. Lukacs, K.D. and J.W. Jorgenson, *Capillary zone electrophoresis: effect of physical parameters on separation efficiency and quantitation.* HRC CC, J. High Resolut. Chromatogr. Chromatogr. Commun., 1985. **8**(8): p. 407-11.
12. Corradini, D., *Buffer additives other than the surfactant sodium dodecyl sulfate for protein separations by capillary electrophoresis.* J. Chromatogr. B: Biomed. Sci. Appl., 1997. **699**(1 + 2): p. 221-256.
13. Watzig, H., M. Degenhardt, and A. Kunkel, *Strategies for capillary electrophoresis: method development and validation for pharmaceutical and biological applications.* Electrophoresis, 1998. **19**(16-17): p. 2695-752.
14. Stutz, H., *Protein attachment onto silica surfaces - a survey of molecular fundamentals, resulting effects and novel preventive strategies in CE.* Electrophoresis, 2009. **30**(12): p. 2032-2061.
15. Lucy, C.A., A.M. MacDonald, and M.D. Gulcev, *Non-covalent capillary coatings for protein separations in capillary electrophoresis.* J. Chromatogr. A, 2008. **1184**(1-2): p. 81-105.
16. Corradini, D., I. Nicoletti, and G.K. Bonn, *Co-electroosmotic capillary electrophoresis of basic proteins with 1-alkyl-3-methylimidazolium tetrafluoroborate ionic liquids as non-covalent coating agents of the fused-silica capillary and additives of the electrolyte solution.* Electrophoresis, 2009. **30**(11): p. 1869-1876.
17. Li, J., et al., *Polymeric ionic liquid as a dynamic coating additive for separation of basic proteins by capillary electrophoresis.* Anal. Chim. Acta, 2010. **674**(2): p. 243-248.

18. Wu, X., et al., *Simultaneous separation of basic and acidic proteins using 1-butyl-3-methylimidazolium-based ion liquid as dynamic coating and background electrolyte in capillary electrophoresis.* Electrophoresis, 2008. **29**(11): p. 2356-2362.
19. Guo, X.-F., et al., *N-methyl-2-pyrrolidonium methyl sulfonate acidic ionic liquid as a new dynamic coating for separation of basic proteins by capillary electrophoresis.* Electrophoresis, 2013. **34**(24): p. 3287-3292.
20. Cao, F., et al., *Hydroxyethylcellulose-graft-poly(2-(dimethylamino)ethyl methacrylate) as physically adsorbed coating for protein separation by CE.* Electrophoresis, 2011. **32**(10): p. 1148-1155.
21. Fu, X., et al., *Carboxymethyl chitosan-coated capillary and its application in CE of proteins.* Electrophoresis, 2007. **28**(12): p. 1958-1963.
22. Kato, M., et al., *Cationic amylopectin derivatives as additives for analysis of proteins in capillary electrophoresis.* Electrophoresis, 2006. **27**(10): p. 1895-1899.
23. Zhao, L., et al., *Quaternized celluloses as new dynamic coatings in capillary electrophoresis for basic protein separation.* Electrophoresis, 2012. **33**(12): p. 1703-1708.
24. Zhao, L., et al., *Hydrophobically modified quaternized celluloses as new dynamic coatings in CE for basic protein separation.* Electrophoresis, 2013. **34**(11): p. 1593-1599.
25. de Jong, S., et al., *A semipermanent coating for preventing protein adsorption at physiological pH in kinetic capillary electrophoresis.* Electrophoresis, 2012. **33**(16): p. 2584-2590.
26. Cooper, B.T., R.D. Sanzgiri, and S.B. Maxey, *Probing the conformational behavior of a monoclonal antibody with surfactant affinity capillary electrophoresis (SurfACE).* Analyst (Cambridge, U. K.), 2012. **137**(24): p. 5777-5784.
27. Gassner, A.-L., S. Rudaz, and J. Schappler, *Static coatings for the analysis of intact monoclonal antibody drugs by capillary zone electrophoresis.* Electrophoresis, 2013. **34**(18): p. 2718-2724.
28. Mansfield, E., E.E. Ross, and C.A. Aspinwall, *Preparation and Characterization of Cross-Linked Phospholipid Bilayer Capillary Coatings for Protein Separations.* Anal. Chem. (Washington, DC, U. S.), 2007. **79**(8): p. 3135-3141.
29. Adem, S.M., et al., *Practical considerations for preparing polymerized phospholipid bilayer capillary coatings for protein separations.* Anal. Chim. Acta, 2013. **772**: p. 93-98.
30. Yu, B., et al., *Novel covalently coated diazo resin/polyvinyl alcohol capillary column for the analysis of proteins by capillary electrophoresis.* Electrophoresis, 2012. **33**(19-20): p. 3066-3072.
31. Yu, B., et al., *A novel diazoresin/polyethylene glycol covalent capillary coating for analysis of proteins by capillary electrophoresis.* RSC Adv., 2013. **3**(43): p. 20010-20015.
32. Castelletti, L., et al., *Quantitative studies on the adsorption of proteins to the bare silica wall in capillary electrophoresis. III: Effects of adsorbed surfactants on quenching the interaction.* J. Chromatogr. A, 2000. **894**(1+2): p. 281-289.
33. Verzola, B., C. Gelfi, and P.G. Righetti, *Quantitative studies on the adsorption of proteins to the bare silica wall in capillary electrophoresis. II. Effects of adsorbed, neutral polymers on quenching the interaction.* J. Chromatogr. A, 2000. **874**(2): p. 293-303.
34. Verzola, B., C. Gelfi, and P.G. Righetti, *Protein adsorption to the bare silica wall in capillary electrophoresis. Quantitative study on the chemical composition of the background electrolyte for minimizing the phenomenon.* J. Chromatogr. A, 2000. **868**(1): p. 85-99.

35. de Jong, S. and S.N. Krylov, *Pressure-Based Approach for the Analysis of Protein Adsorption in Capillary Electrophoresis.* Anal. Chem. (Washington, DC, U. S.), 2012. **84**(1): p. 453-458.
36. Zhu, Z., J.J. Lu, and S. Liu, *Protein separation by capillary gel electrophoresis: A review.* Anal. Chim. Acta, 2012. **709**: p. 21-31.
37. Zhu, G., et al., *On-line amino acid-based capillary isoelectric focusing-ESI-MS/MS for protein digests analysis.* Anal. Chim. Acta, 2012. **750**: p. 207-211.
38. Hutterer, K.M., et al., *Monoclonal antibody disulfide reduction during manufacturing: Untangling process effects from product effects.* MAbs, 2013. **5**(4): p. 608-13.
39. Lu, C., et al., *Characterization of monoclonal antibody size variants containing extra light chains.* MAbs, 2013. **5**(1): p. 102-13.
40. Michels, D.A., M. Parker, and O. Salas-Solano, *Quantitative impurity analysis of monoclonal antibody size heterogeneity by CE-LIF: Example of development and validation through a quality-by-design framework.* Electrophoresis, 2012. **33**(5): p. 815-826.
41. Shi, Y., Z. Li, and J. Lin, *Advantages of CE-SDS over SDS-PAGE in mAb purity analysis.* Anal. Methods, 2012. **4**(6): p. 1637-1642.
42. Cianciulli, C., T. Hahne, and H. Waetzig, *Capillary gel electrophoresis for precise protein quantitation.* Electrophoresis, 2012. **33**(22): p. 3276-3280.
43. Le, M.E., A. Vizel, and K.M. Hutterer, *Automated sample preparation for CE-SDS.* Electrophoresis, 2013. **34**(9-10): p. 1369-1374.
44. Rustandi, R.R., et al., *Qualitative and quantitative evaluation of Simon®, a new CE-based automated Western blot system as applied to vaccine development.* Electrophoresis, 2012. **33**(17): p. 2790-2797.
45. Lu, J.J., et al., *Coupling Sodium Dodecyl Sulfate-Capillary Polyacrylamide Gel Electrophoresis with Matrix-Assisted Laser Desorption Ionization Time-of-Flight Mass Spectrometry via a Poly(tetrafluoroethylene) Membrane.* Anal. Chem. (Washington, DC, U. S.), 2011. **83**(5): p. 1784-1790.
46. Na, D.H., et al., *Characterization of two ricin isoforms by sodium dodecyl sulfate-capillary gel electrophoresis and capillary isoelectric focusing.* Bull. Korean Chem. Soc., 2011. **32**(12): p. 4253-4257.
47. Na, D.H., et al., *Application of Sodium Dodecyl Sulfate-Capillary Gel Electrophoresis to the Characterization of Ricin A-Chain Immunotoxins.* Chromatographia, 2012. **75**(11-12): p. 679-683.
48. Kerekgyarto, M., et al., *Neoglycoproteins as carbohydrate antigens: Synthesis, analysis, and polyclonal antibody response.* Electrophoresis, 2013. **34**(16): p. 2379-2386.
49. Shen, Y., et al., *High-resolution capillary isoelectric focusing of complex protein mixtures from lysates of microorganisms.* Anal. Chem., 1999. **71**(23): p. 5348-5353.
50. Koshel, B.M. and M.J. Wirth, *Trajectory of isoelectric focusing from gels to capillaries to immobilized gradients in capillaries.* Proteomics, 2012. **12**(19-20): p. 2918-2926.
51. Righetti, P.G., R. Sebastiano, and A. Citterio, *Capillary electrophoresis and isoelectric focusing in peptide and protein analysis.* Proteomics, 2013. **13**(2): p. 325-340.
52. Wehr, T., R. Rodriguez-Diaz, and M. Zhu, *Capillary Electrophoresis of Proteins*. Chromatographic Science Series, ed. J. Cazes. Vol. 80. 1998, New York: Marcel Dekker.

53. Anderson, C.L., Y. Wang, and R.R. Rustandi, *Applications of imaged capillary isoelectric focussing technique in development of biopharmaceutical glycoprotein-based products.* Electrophoresis, 2012. **33**(11): p. 1538-1544.
54. Rustandi, R.R., B. Peklansky, and C.L. Anderson, *Use of Imaged Capillary Isoelectric Focusing (icIEF) Technique in Development of Diphtheria Toxin mutant CRM197.* Electrophoresis, 2013.
55. Rustandi, R.R., et al., *Development of imaged capillary isoelectric focusing method and use of capillary zone electrophoresis in hepatitis B vaccine RECOMBIVAX HB.* Electrophoresis, 2013: p. Ahead of Print.
56. Shimura, K., et al., *Estimation of the Deamidation Rates of Major Deamidation Sites in a Fab Fragment of Mouse IgG1-κ by Capillary Isoelectric Focusing of Mutated Fab Fragments.* Anal. Chem. (Washington, DC, U. S.), 2013. **85**(3): p. 1705-1710.
57. Lu, J.J., et al., *Chip-capillary hybrid device for automated transfer of sample preseparated by capillary isoelectric focusing to parallel capillary gel electrophoresis for two-dimensional protein separation.* Anal. Chem. (Washington, DC, U. S.), 2012. **84**(16): p. 7001-7007.
58. Tang, Q., A.K. Harrata, and C.S. Lee, *Capillary isoelectric focusing-electrospray mass spectrometry for protein analysis.* Anal. Chem., 1995. **67**(19): p. 3515-19.
59. Tang, Q., A.K. Harrata, and C.S. Lee, *Comparison of protein separations in capillary zone electrophoresis and capillary isoelectric focusing interfacing with electrospray mass spectrometry.* J. Mass Spectrom., 1996. **31**(11): p. 1284-1290.
60. Foret, F., et al., *Analysis of protein fractions by micropreparative capillary isoelectric focusing and matrix-assisted laser desorption time-of-flight mass spectrometry.* J. Chromatogr. A, 1995. **716**(1 + 2): p. 157-66.
61. Zhang, Z., et al., *Poly(glycidyl methacrylate-divinylbenzene) based immobilized pH gradient capillary isoelectric focusing coupling with MALDI mass spectrometry for enhanced neuropeptide analysis.* Electrophoresis, 2012. **33**(4): p. 661-665.
62. Chingin, K., et al., *Separation of Polypeptides by Isoelectric Point Focusing in Electrospray-Friendly Solution Using a Multiple-Junction Capillary Fractionator.* Anal. Chem. (Washington, DC, U. S.), 2012. **84**(15): p. 6856-6862.
63. Zhong, X., E.J. Maxwell, and D.D.Y. Chen, *Mass Transport in a Micro Flow-Through Vial of a Junction-at-the-Tip Capillary Electrophoresis-Mass Spectrometry Interface.* Anal. Chem. (Washington, DC, U. S.), 2011. **83**(12): p. 4916-4923.
64. Wang, C., et al., *Capillary Isotachophoresis-Nanoelectrospray Ionization-Selected Reaction Monitoring MS via a Novel Sheathless Interface for High Sensitivity Sample Quantification.* Anal. Chem. (Washington, DC, U. S.), 2013. **85**(15): p. 7308-7315.
65. Kuroda, Y., et al., *On-line capillary isoelectric focusing-mass spectrometry for quantitative analysis of peptides and proteins.* J. Pharm. Biomed. Anal., 2005. **37**(3): p. 423-428.
66. Michels, D.A., et al., *Charge Heterogeneity of Monoclonal Antibodies by Multiplexed Imaged Capillary Isoelectric Focusing Immunoassay with Chemiluminescence Detection.* Anal. Chem. (Washington, DC, U. S.), 2012. **84**(12): p. 5380-5386.
67. Fanali, C., G. D'Orazio, and S. Fanali, *Nano-liquid chromatography and capillary electrochromatography hyphenated with mass spectrometry for tryptic digest protein analysis: A comparison.* Electrophoresis, 2012. **33**(16): p. 2553-2560.

68. Nilsson, C., S. Birnbaum, and S. Nilsson, *Nanoparticle-based pseudostationary phases in CEC: A breakthrough in protein analysis?* Electrophoresis, 2011. **32**(10): p. 1141-1147.
69. Gao, J., et al., *Polyamidoamine-grafted silica nanoparticles as pseudostationary phases for capillary electrochromatographic separation of proteins.* J. Sep. Sci., 2013. **36**(9-10): p. 1575-1581.
70. Cheong, W.J., et al., *Comprehensive overview of recent preparation and application trends of various open tubular capillary columns in separation science.* J. Chromatogr. A, 2013. **1308**: p. 1-24.
71. Miksik, I., et al., *Open-tubular capillary electrochromatography with bare gold nanoparticles-based stationary phase applied to separation of trypsin digested native and glycated proteins.* J. Sep. Sci., 2012: p. Ahead of Print.
72. Hamer, M., A. Yone, and I. Rezzano, *Gold nanoparticle-coated capillaries for protein and peptide analysis on open-tubular capillary electrochromatography.* Electrophoresis, 2012. **33**(2): p. 334-339.
73. Qu, Q., C. Gu, and X. Hu, *Capillary Coated with Graphene and Graphene Oxide Sheets as Stationary Phase for Capillary Electrochromatography and Capillary Liquid Chromatography.* Anal. Chem. (Washington, DC, U. S.), 2012. **84**(20): p. 8880-8890.
74. Qu, Q., et al., *Layer-by-layer assembly of polyelectrolyte and graphene oxide for open-tubular capillary electrochromatography.* J. Chromatogr. A, 2013. **1282**: p. 95-101.
75. Liu, H., et al., *An open tubular capillary electrochromatography column with porous inner surface for protein separation.* Anal. Biochem., 2013. **442**(2): p. 186-188.
76. Puangpila, C., T. Nhujak, and R.Z. El, *Investigation of neutral monolithic capillary columns with varying n-alkyl chain lengths in capillary electrochromatography.* Electrophoresis, 2012. **33**(9-10): p. 1431-1442.
77. Wang, Y., et al., *A novel ionic liquid monolithic column and its separation properties in capillary electrochromatography.* Anal. Chim. Acta, 2012. **712**: p. 1-8.
78. Liu, C.-C., et al., *Ionic liquids monolithic columns for protein separation in capillary electrochromatography.* Anal. Chim. Acta, 2013. **804**: p. 313-320.
79. Hempel, G., *Strategies to improve the sensitivity in capillary electrophoresis for the analysis of drugs in biological fluids.* Electrophoresis, 2000. **21**(4): p. 691-698.
80. Swinney, K. and D.J. Bornhop, *Detection in capillary electrophoresis.* Electrophoresis, 2000. **21**(7): p. 1239-1250.
81. de Kort, B.J., G.J. de Jong, and G.W. Somsen, *Profiling of erythropoietin products by capillary electrophoresis with native fluorescence detection.* Electrophoresis, 2012. **33**(19-20): p. 2996-3001.
82. Sarazin, C., et al., *New Avenue for Mid-UV-Range Detection of Underivatized Carbohydrates and Amino Acids in Capillary Electrophoresis.* Anal. Chem. (Washington, DC, U. S.), 2011. **83**(19): p. 7381-7387.
83. de Kort, B.J., G.J. de Jong, and G.W. Somsen, *Native fluorescence detection of biomolecular and pharmaceutical compounds in capillary electrophoresis: Detector designs, performance and applications: A review.* Anal. Chim. Acta, 2013. **766**: p. 13-33.
84. Wang, H., et al., *Immuno-magnetic beads-based extraction-capillary zone electrophoresis-deep UV laser-induced fluorescence analysis of erythropoietin.* J. Chromatogr. A, 2012. **1246**: p. 48-54.
85. Walt, D.R., *Optical Methods for Single Molecule Detection and Analysis.* Anal. Chem. (Washington, DC, U. S.), 2013. **85**(3): p. 1258-1263.

86. Ramsay, L.M., J.A. Dickerson, and N.J. Dovichi, *Attomole protein analysis by CIEF with LIF detection.* Electrophoresis, 2009. **30**(2): p. 297-302.
87. Haselberg, R., G.J. de Jong, and G.W. Somsen, *Capillary electrophoresis - mass spectrometry for the analysis of biopharmaceuticals.* LC GC Asia Pac., 2012. **15**(4): p. 13-18.
88. Pioch, M., S.-C. Bunz, and C. Neusuess, *Capillary electrophoresis/mass spectrometry relevant to pharmaceutical and biotechnological applications.* Electrophoresis, 2012. **33**(11): p. 1517-1530.
89. Haselberg, R., G.J. de Jong, and G.W. Somsen, *CE-MS for the analysis of intact proteins 2010-2012.* Electrophoresis, 2013. **34**(1): p. 99-112.
90. Hommerson, P., et al., *Ionization techniques in capillary electrophoresis-mass spectrometry: Principles, design, and application.* Mass Spectrom. Rev., 2011. **30**(6): p. 1096-1120.
91. Olivares, J.A., et al., *On-line mass spectrometric detection for capillary zone electrophoresis.* Anal. Chem., 1987. **59**(8): p. 1230-2.
92. Taichrib, A., M. Pioch, and C. Neusuess, *Toward a screening method for the analysis of small intact proteins by CE-ESI-TOF MS.* Electrophoresis, 2012. **33**(9-10): p. 1356-1366.
93. Bonvin, G., J. Schappler, and S. Rudaz, *Capillary electrophoresis-electrospray ionization-mass spectrometry interfaces: Fundamental concepts and technical developments.* J. Chromatogr. A, 2012. **1267**: p. 17-31.
94. Moini, M., *Simplifying CE-MS Operation. 2. Interfacing Low-Flow Separation Techniques to Mass Spectrometry Using a Porous Tip.* Anal. Chem. (Washington, DC, U. S.), 2007. **79**(11): p. 4241-4246.
95. Whitt, J.T. and M. Moini, *Capillary Electrophoresis to Mass Spectrometry Interface Using a Porous Junction.* Anal. Chem., 2003. **75**(9): p. 2188-2191.
96. Haselberg, R., et al., *Performance of a sheathless porous tip sprayer for capillary electrophoresis-electrospray ionization-mass spectrometry of intact proteins.* J. Chromatogr. A, 2010. **1217**(48): p. 7605-7611.
97. Haselberg, R., G.J. de Jong, and G.W. Somsen, *Low-Flow Sheathless Capillary Electrophoresis-Mass Spectrometry for Sensitive Glycoform Profiling of Intact Pharmaceutical Proteins.* Anal. Chem. (Washington, DC, U. S.), 2013. **85**(4): p. 2289-2296.
98. Gahoual, R., et al., *Rapid and multi-level characterization of trastuzumab using sheathless capillary electrophoresis-tandem mass spectrometry.* MAbs, 2013. **5**(3).
99. Whitmore, C.D. and L.A. Gennaro, *Capillary electrophoresis-mass spectrometry methods for tryptic peptide mapping of therapeutic antibodies.* Electrophoresis, 2012. **33**(11): p. 1550-1556.
100. Maxwell, E.J., et al., *Decoupling CE and ESI for a more robust interface with MS.* Electrophoresis, 2010. **31**(7): p. 1130-1137.
101. Maxwell, E.J., X. Zhong, and D.D.Y. Chen, *Asymmetrical emitter geometries for increased range of stable electrospray flow rates.* Anal. Chem. (Washington, DC, U. S.), 2010. **82**(20): p. 8377-8381.
102. Zhao, S.S., X. Zhong, and D.D.Y. Chen, *Atmospheric pressure ion lens extends the stable operational region of an electrospray ion source for capillary electrophoresis-mass spectrometry.* Electrophoresis, 2012. **33**(8): p. 1322-1330.

103. Zhong, X., et al., *Flow-Through Microvial Facilitating Interface of Capillary Isoelectric Focusing and Electrospray Ionization Mass Spectrometry.* Anal. Chem. (Washington, DC, U. S.), 2011. **83**(22): p. 8748-8755.
104. Researchmoz.us. *Global and China Monoclonal Antibody Industry Report, 2013 - 2017*. 2013.
105. Rustandi, R.R., C.L. Anderson, and M. Hamm, *Glycosylation Engineering of Biopharmaceuticals*. Methods in Molecular Biology, ed. A. Beck. Vol. 988. 2013, New York: Springer
106. Behne, A., et al., *glyXalign: High-throughput migration time alignment preprocessing of electrophoretic data retrieved via multiplexed capillary gel electrophoresis with laser-induced fluorescence detection-based glycoprofiling.* Electrophoresis, 2013. **34**(16): p. 2311-2315.
107. Wuhrer, M., B.A.R. de, and A.M. Deelder, *Structural glycomics using hydrophilic interaction chromatography (HILIC) with mass spectrometry.* Mass Spectrom. Rev., 2009. **28**(2): p. 192-206.
108. Mittermayr, S., et al., *Multiplexed Analytical Glycomics: Rapid and Confident IgG N-Glycan Structural Elucidation.* J. Proteome Res., 2011. **10**(8): p. 3820-3829.
109. Guttman, A., *Capillary electrophoresis in the N-glycosylation analysis of biopharmaceuticals.* TrAC, Trends Anal. Chem., 2013. **48**: p. 132-143.
110. Mittermayr, S., J. Bones, and A. Guttman, *Unraveling the Glyco-Puzzle: Glycan Structure Identification by Capillary Electrophoresis.* Anal. Chem. (Washington, DC, U. S.), 2013. **85**(9): p. 4228-4238.
111. Kuo, C.-Y., et al., *Application of 2,3-naphthalenediamine in labeling natural carbohydrates for capillary electrophoresis.* Molecules, 2012. **17**: p. 7387-7400.
112. Callewaert, N., et al., *Ultrasensitive profiling and sequencing of N-linked oligosaccharides using standard DNA-sequencing equipment.* Glycobiology, 2001. **11**(4): p. 275-281.
113. Reusch, D., et al., *High-throughput glycosylation analysis of therapeutic immunoglobulin G by capillary gel electrophoresis using a DNA analyzer.* MAbs, 2013. **6**(1).
114. Croset, A., et al., *Differences in the glycosylation of recombinant proteins expressed in HEK and CHO cells.* J. Biotechnol., 2012. **161**(3): p. 336-348.
115. Galili, U., et al., *A unique natural human IgG antibody with anti-α-galactosyl specificity.* J. Exp. Med., 1984. **160**(5): p. 1519-31.
116. Yagi, Y., et al., *Specific detection of N-glycolylneuraminic acid and Galα1-3Gal epitopes of therapeutic antibodies by partial-filling capillary electrophoresis.* Anal. Biochem., 2012. **431**(2): p. 120-126.
117. Maeda, E., et al., *Analysis of Nonhuman N-Glycans as the Minor Constituents in Recombinant Monoclonal Antibody Pharmaceuticals.* Anal. Chem. (Washington, DC, U. S.), 2012. **84**(5): p. 2373-2379.
118. Szabo, Z., et al., *Ultrasensitive Capillary Electrophoretic Analysis of Potentially Immunogenic Carbohydrate Residues in Biologics: Galactose-α-1,3-Galactose Containing Oligosaccharides.* Mol. Pharmaceutics, 2012. **9**(6): p. 1612-1619.
119. Hamm, M., Y. Wang, and R.R. Rustandi, *Characterization of N-linked glycosylation in a monoclonal antibody produced in NS0 cells using Capillary Electrophoresis with Laser-Induced Fluorescence detection.* Pharmaceuticals, 2013. **6**: p. 393-406.

120. Bunz, S.-C., F. Cutillo, and C. Neusuess, *Analysis of native and APTS-labeled N-glycans by capillary electrophoresis/time-of-flight mass spectrometry.* Anal. Bioanal. Chem., 2013. **405**(25): p. 8277-8284.
121. Bunz, S.-C., E. Rapp, and C. Neusuess, *Capillary Electrophoresis/Mass Spectrometry of APTS-Labeled Glycans for the Identification of Unknown Glycan Species in Capillary Electrophoresis/Laser-Induced Fluorescence Systems.* Anal. Chem. (Washington, DC, U. S.), 2013. **85**(21): p. 10218-10224.
122. Wang, Y., M. Santos, and A. Guttman, *Comparative core fucosylation analysis of some major therapeutic antibody N-glycans by direct infusion ESI-MS and CE-LIF detection.* J. Sep. Sci., 2013. **36**(17): p. 2862-2867.
123. Initiative, G.a.B. *Biosimilars marketed in Europe*. 2012.
124. Falconer, R.J., D. Jackson-Matthews, and S.M. Mahler, *Analytical strategies for assessing comparability of biosimilars.* J. Chem. Technol. Biotechnol., 2011. **86**(7): p. 915-922.
125. Beck, A., et al., *Analytical characterization of biosimilar antibodies and Fc-fusion proteins.* TrAC, Trends Anal. Chem., 2013. **48**: p. 81-95.
126. Taichrib, A., M. Pioch, and C. Neusuess, *Multivariate statistics for the differentiation of erythropoietin preparations based on intact glycoforms determined by CE-MS.* Anal. Bioanal. Chem., 2012. **403**(3): p. 797-805.
127. Espinosa-de, l.G.C.E., et al., *Analysis of recombinant monoclonal antibodies by capillary zone electrophoresis.* Electrophoresis, 2013. **34**(8): p. 1133-1140.
128. Visser, J., et al., *Physicochemical and Functional Comparability Between the Proposed Biosimilar Rituximab GP2013 and Originator Rituximab.* BioDrugs, 2013. **27**(5): p. 495-507.
129. Salas-Solano, O., et al., *Robustness of iCIEF methodology for the analysis of monoclonal antibodies: An interlaboratory study.* J. Sep. Sci., 2012. **35**(22): p. 3124-3129.
130. Salas-Solano, O., et al., *Intercompany Study to Evaluate the Robustness of Capillary Isoelectric Focusing Technology for the Analysis of Monoclonal Antibodies.* Chromatographia, 2011. **73**(11-12): p. 1137-1144.
131. Culbertson, C.T., et al., *Micro Total Analysis Systems: Fundamental Advances and Biological Applications.* Anal. Chem. (Washington, DC, U. S.), 2014. **86**(1): p. 95-118.
132. Neuzi, P., et al., *Revisiting lab-on-a-chip technology for drug discovery.* Nat. Rev. Drug Discovery, 2012. **11**(8): p. 620-632.
133. Mitra, I., et al., *Comparative Profiling of N-Glycans Isolated from Serum Samples of Ovarian Cancer Patients and Analyzed by Microchip Electrophoresis.* J. Proteome Res., 2013. **12**(10): p. 4490-4496.
134. Zhuang, Z., et al., *Electrophoretic Analysis of N-Glycans on Microfluidic Devices.* Anal. Chem. (Washington, DC, U. S.), 2007. **79**(18): p. 7170-7175.
135. Han, H., E. Livingston, and X. Chen, *High Throughput Profiling of Charge Heterogeneity in Antibodies by Microchip Electrophoresis.* Anal. Chem. (Washington, DC, U. S.), 2011. **83**(21): p. 8184-8191.
136. Primack, J., G.C. Flynn, and H. Pan, *A high-throughput microchip-based glycan screening assay for antibody cell culture samples.* Electrophoresis, 2011. **32**(10): p. 1129-1132.
137. Chen, X., et al., *Microchip assays for screening monoclonal antibody product quality.* Electrophoresis, 2008. **29**(24): p. 4993-5002.

138. Han, H. and X. Chen, *Microchip electrophoresis-SDS methods with high-resolution and silver stain sensitivity for quality screening and quantitation of protein products.* Electrophoresis, 2012. **33**(5): p. 765-772.
139. Pan, W., W. Chen, and X. Jiang, *Microfluidic Western Blot.* Anal. Chem. (Washington, DC, U. S.), 2010. **82**(10): p. 3974-3976.
140. Jin, S., G.J. Anderson, and R.T. Kennedy, *Western Blotting Using Microchip Electrophoresis Interfaced to a Protein Capture Membrane.* Anal. Chem. (Washington, DC, U. S.), 2013. **85**(12): p. 6073-6079.
141. Kinoshita, M., et al., *Quality assurance of monoclonal antibody pharmaceuticals based on their charge variants using microchip isoelectric focusing method.* J. Chromatogr. A, 2013. **1309**: p. 76-83.
142. Hughes, A.J. and A.E. Herr, *Microfluidic Western blotting.* Proc. Natl. Acad. Sci. U. S. A., 2012. **109**(52): p. 21450-21455, S21450/1-S21450/6.
143. O'Neill, R.A., et al., *Isoelectric focusing technology quantifies protein signaling in 25 cells.* Proc. Natl. Acad. Sci. U. S. A., 2006. **103**(44): p. 16153-16158.
144. He, X., et al., *Recent advances in microchip-mass spectrometry for biological analysis.* TrAC, Trends Anal. Chem., 2014. **53**: p. 84-97.
145. Chambers, A.G., et al., *Monolithic Integration of Two-Dimensional Liquid Chromatography-Capillary Electrophoresis and Electrospray Ionization on a Microfluidic Device.* Anal. Chem. (Washington, DC, U. S.), 2011. **83**(3): p. 842-849.
146. Mellors, J.S., et al., *Hybrid Capillary/Microfluidic System for Comprehensive Online Liquid Chromatography-Capillary Electrophoresis-Electrospray Ionization-Mass Spectrometry.* Anal. Chem. (Washington, DC, U. S.), 2013. **85**(8): p. 4100-4106.